Thermoelectric transport in quantum point contacts and chaotic cavities: thermal effects and fluctuations

Adel Abbout

▶ To cite this version:

Adel Abbout. Thermoelectric transport in quantum point contacts and chaotic cavities: thermal effects and fluctuations. Mesoscopic Systems and Quantum Hall Effect [cond-mat.mes-hall]. Université Pierre et Marie Curie - Paris VI, 2011. English. <tel-00793816>

HAL Id: tel-00793816

https://tel.archives-ouvertes.fr/tel-00793816

Submitted on 23 Feb 2013

Transport thermoélectrique dans des contacts quantiques ponctuels et de cavités chaotiques : Effets thermiques et fluctuations.

Adel Abbout

Directeur de thèse : Jean-Louis PICHARD

Jury :
Doucot BENOIT
Klaus FRAHM
Jean-Louis PICHARD (Directeur de thèse)
Marc SANQUER
Dima SHEPELYANSKY (rapporteur)
Dietmar WEINMANN (rapporteur)

.

.

To my parents

Acknowledgement

I would like to thank my thesis advisor Jean Louis Pichard for all the work achieved together. I record my gratitude to him for his supervision, advice, guidance and specially his presence during all this years. His patience and kindness are well appreciated. I gratefully acknowledge Khandker Abdul Muttalib for our collaboration and for introducing me to random matrix theory. I appreciated all the time working together. A huge thank you goes to Geneviève Fleury for the various advices I benefited from her. I am much indebted to her for reading, correcting my thesis and all her valuable suggestions. I enjoyed all the time we spent together. I thanks all my friends in the SPEC for the interesting discussions and the time we spent together. The team of Rodolfo Jalabert and Dietmar Weinmann are acknowledged for the fruitful collaboration and interesting discussions. I am fully indebted to my family which I thank for being myself. My immense thoughts go to them. I studied equations, languages and gestures but none is sufficient to express what I owe them. For the moment I may just say : to the family, the son is grateful.

Table of contents

résumé

Dans cette thèse, on s'intéresse au transport quantique des électrons dans des nano-systèmes et des cavités chaotiques . En particulier, on apporte dans un premier temps la base théorique qui permet d'expliquer les expériences de microscopie à effet de grille dans des contacts quantiques ponctuels. Dans ces expériences, on étudie la conductance d'un contact quantique ponctuel (QPC).À l'aide d'une pointe chargée d'un AFM, quelques nanomètres au dessus d'un gaz bidimensionnel d'électrons, on crée une région de déplétion de la charge électronique. Cette déplétion modifie la conductance du QPC et permet de tracer en changeant la position de la pointe chargée, des figures de franges d'interférence espacées de la moitié de la longueur d'onde de Fermi. En se basant sur des constatations numériques obtenues à l'aide de programmes écrits en utilisant des algorithmes de fonctions de Green récursives, on propose un modèle simple que l'on résout exactement. Ce modèle, nous permet de mieux comprendre les résultats des expériences et de répondre à toutes les questions que l'on se pose notamment sur la loi de décroissance des franges d'interférence. On trouve que :

– Pour un QPC complètement ouvert pour le premier mode de conduction (premier plateau, $T^\circ = 1$), l'effet de la pointe chargée, décroît rapidement comme $\frac{1}{x^2}$ loin du QPC avec pratiquement pas de franges d'interférence. En plus, la pointe agit toujours par effet négatif en réduisant la conductance du système original.

– Si le QPC est moins ouvert ($T^\circ < 1$), les franges décroissent plus lentement et oscillent autour de zero. Ceci indique que la pointe peut augmenter la conductance du système, ce qui ne peut être, évidement, qu'un effet quantique.

Ce modèle permet aussi de comprendre comment dépendent les résultats de la valeur du potentiel de la pointe.

À la lumière de tous ces résultats, on prévoit un effet très intéressant d'accroissement des franges avec la température. En effet, en partant d'un contact quantique complètement ouvert pour le premier mode de conduction à température nulle, la figure d'interférence qui ne montre quasiment pas de franges, devient, en augmentant la température plus claire avec des franges bien visibles et une amplitude plus grande. Un effet contre-intuitif si l'on rappelle que d'habitude, la température tue les effets quantiques. On établie cet effet avec des expressions simples et on le verifie avec la

simulation numérique.

Dans une deuxième partie, on s'intéresse à la thermoélectricité et plus spécialement au coefficient Seebeck. On propose de refaire sur les mêmes bases, la microscopie à effet de grilles du coefficient Seebeck d'un contact quantique ponctuel. Les figures d'interférence sont obtenues facilement numériquement. Afin d'établir les lois de décroissance des franges, on utilise le même modèle proposé précédemment et on obtient dans la limite de la validité de la loi de Cuttler-Mott le comportement des franges. On trouve les résultats suivants :

– Pour un QPC complètement ouvert pour le premier mode de conduction (premier plateau, $T° = 1$), les franges d'interférence décroissent en $\frac{1}{x}$

– Pour un QPC moins ouvert, les franges décroissent également en $1/x$ mais sur toutes une plage, l'amplitude reste constante sans décroître ! ceci est intéressant vu que le systeme est 2D, et donc on s'attendrait à un décroissement du signal !

Idem pour le coefficient Seebeck, on établie les expressions analytiques, que l'on vérifie numériquement.

La loi de décroissance des franges d'interférence du changement dans le coefficient Seebeck est établie en partant des résultats de la première partie portant sur la conductance. Ceci dit, l'expression des formules de manière simple nécessite l'hypothèse de faibles températures assurant la validité du développement de Sommerfeld et donc la formule de Cutler-Mott. Les expressions finales montrent de manière explicite la dépendance en énergie, en température et en position.

Afin de discuter les fluctuations du coefficient Seebeck, on s'intéresse dans la dernière partie de cette thèse au transport quantique des électrons à travers des cavités chaotiques. L'approche adoptée pour cette étude est basée sur la théorie des matrices aléatoires.

Distribution de probabilité du coefficient Seebeck Dans cette deuxième partie, on adopte un modèle de cavité chaotique connectée à deux réservoirs d'électrons. On s'intéresse uniquement au premier mode de conduction et donc les réservoirs seront modélisés par des leads semi-infinis 1D. La cavité quant à elle est modélisée par un grand nombre de sites connectés aléatoirement entre eux et portés à des potentiels aléatoires aussi. Le grand nombre de degrés de liberté du problème nous oblige

à attaquer, dans une première partie, cette question numériquement. Cette approche est basée sur l'échantillonnage de matrices de manière aléatoire à partir des différents ensembles d'Hamiltoniens. Cette procédure montre très vite que le choix de l'ensemble de matrices à utiliser doit être judicieux. Le transport des électrons à travers la cavité peut être décrit en suivant deux approches différentes : La première approche se base sur l'échantillonnage de l'Hamiltonien H de la cavité alors que la deuxième approche de base plutôt sur l'échantillonnage de la matrice de diffusion S. On commence par considérer des cavités complètement chaotiques au sens des ensembles circulaires de Dyson. En fait, ces ensembles assument des matrices de scattering uniformément distribuées : chaque matrice a la même probabilité d'être choisie. Ce choix apporte une signification mathématique au sens des mots " complètement aléatoire " adopté ici. Une analyse rapide montre que ce choix de la distribution des matrices de scattering impose un choix unique pour la distribution de l'Hamiltonien H : Le Hamiltonien doit être forcément échantillonné parmi l'ensemble des matrices Lorentziennes. De plus, La centre et la largeur de cette distribution doivent être adaptés à l'environnement de la cavité qui est constitué des réservoirs d'électrons. Une fois ce choix adopté, le calcul de la distribution du coefficient Seebeck devient moins difficile. Le résultat des calculs faits dans la limite de demi-remplissage (bande de conduction moitié remplie), puis généralisé à une énergie arbitraire montre une distribution singulière à l'origine et non nulle uniquement pour des valeurs d'un coefficient Seebeck borné. la distribution trouvée est :

$$p(S_k) = \begin{cases} -\frac{a}{\pi} \log(\frac{|aS_k|}{1+\sqrt{1-a^2 S_k^2}}) & \text{if} \quad |S_k| < 1/a \\ \\ 0 & \text{if} \quad |S_k| > 1/a \end{cases}$$

avec $a = (\Gamma/2)^2$. Γ est le taux d'échappement vers les réservoirs.

0.1 Introduction and overlook

Recent technological progress in the fabrication of high quality electronic micro structures brought more attraction to mesoscopic physics. The small scale of the considered systems, generally less than the coherence length, allows the electrons to propagate coherently, keeping the memory of their phase. This leads to the appearance of quantum effects at low temperatures due to interference phenomena. The rich physics of these low dimension systems is subject to intense experimental and theoretical investigations since decades. The confinement of electrons between two sheets heterostructure of GaAs/AlGaAs allowed the achievement of two dimensional electronic gases (2DEG), the basic element of many new electronic components (Quantum Point Contacts, Mac Zender, ...). The quantum transport in these devices shows a fundamental behaviour as the quantification of electronic conductance in multiples of $\frac{e^2}{h}$. known as the quantum of conductance. Thus, the profile of conductance in Quantum Point Contacts showing plateaus are widely obtained and studied experimentally and theoretically.. Playing with disorder, temperature or magnetic field rises a lot of questions which quickly makes this field very wide. In this thesis, we mainly concentrate on systems obtained by means of Quantum point contacts(QPCs): two gates over a 2DEG create a narrow region where electrons could pass. These devices are used in experiments of Scanning Gate Microscopy to image the change in conductance due to the presence of a charged tip over the 2DEG. This kind of setup is the starting point of research in this thesis.
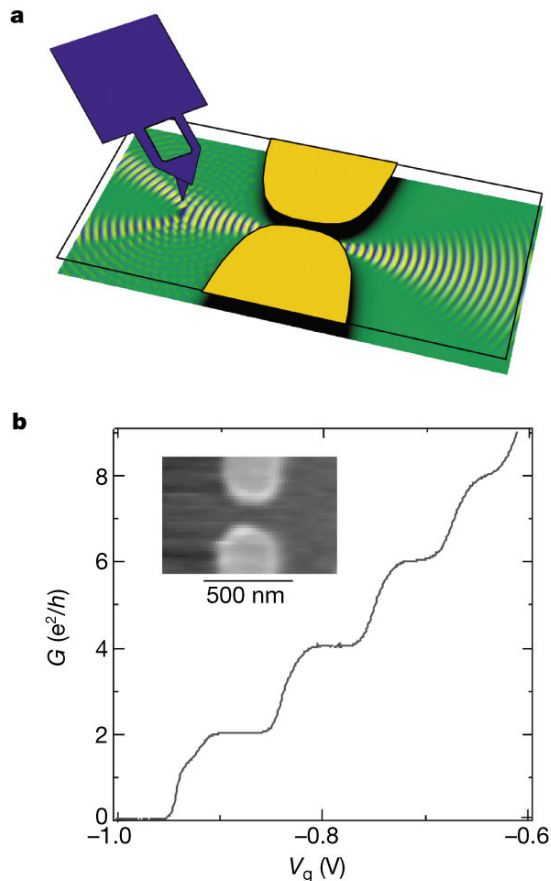
Figure 1: (a) Scanning Gate Microscopy on a Quantum point contact. (b) Conductance quantification.Topinka et al, Nature 2001

0.2 Experimental motivation

Scanning Gate Microscopy is a technique of imaging where by means of an AFM charged tip, we create a depletion region in the electronic charge density of the 2DEG. This variation in the density of charge induces a change in the conductance of the system. Once this change plotted on a 2D graphic as a function of the tip position, we obtain images of interference pattern due to quantum effects. We hope by this technique to shed light on some fundamental aspects of quantum transport and low temperature measurements in high mobility nano-scale devices. This kind of experiments started in the group of Westervelt at Harvard university at Helium liquid temperature in the presence of disorder. Later, they were done in highly clean samples where interesting figures of interference pattern were found. In the first part of this thesis, we study the result of these experiments and give, by means of analytical calculations and numerical simulations, the explanation of these interference patterns. Moreover, new ideas are suggested and tested.

0.3   This thesis

This thesis can be divided on two main parts. The first part concerns quantum transport of electrons through quantum point contacts and the second part concerns the study of transport of electrons through chaotic cavities within the theory of random matrices.

0.3.1   Part one

In this part, we study two very close problems: Scanning Gate Microscopy of the conductance of a quantum point contact (QPC) and in a second time the thermopower of a quantum point contact. The study starts with numerical simulations of realistic models of the QPC and the charged AFM tip. The conclusions of this study claim that, for the zero temperature conductance, the model of both the QPC and the tip are not highly pertinent and therefore much simpler models can be proposed. We therefore propose a simple resonant level model (RLM) that we solve exactly. This model allows us to give the decay law of the fringes in the interference pattern of SGM pictures. These laws are tested on a realistic model and found to be in a good agreement with the numerical simulations. We go further in the study of this model and include temperature. We find an unusual interesting effect: The enhancement of the fringes of the interference pattern with temperature. We give simple formula to explain this phenomena and again test it on a realistic quantum point contact. We study also in this thesis the thermopower of a quantum point contact. We give the figures of the interference pattern of SGM of Seebeck coefficient. Again, we use the resonant level model to obtain the decay law of the fringes of the change in the Seebeck coefficient due to the presence of the tip. The numerical simulations agree well with the analytical formulation of the problem.

0.3.2   Part two

In this part, we continue to study thermopower at low temperature. We choose here, a chaotic cavity and try to find within the theory of random matrices the probability density function of the Seebeck coefficient. We choose for this task two equivalent approaches: The scattering matrix approach and the Hamiltonian approach. We start with an Hamiltonian taken from Gaussian ensembles and prove, in a first time, that this is equivalent, at high degrees of freedom, to taking Hamiltonians from Lorentzian ensembles. These last ensembles are interesting for two things: First, they imply, for an appropriate center and width of the distribution, scattering matrices uniformly distributed according to circular ensembles. The second thing is that they allow to do a decimation-renormalization procedure which lowers the degrees of freedom of the cavity and simplifies a lot the calculations. We succeed in this part to obtain the analytical distribution of the Seebeck coefficient and discuss the energy dependence of this probability.

Chapter 1

Introduction to scanning gate microscopy

Contents

Summary of chapter 1

This chapter is an introduction to Scanning Gate Microscopy (SGM) technique. We first introduce the system to which it is applied in this thesis. We explain how do we obtain quantum point contacts (QPC) in semi-conducting heterostructures and discuss the details of the two dimensional electronic gas 2DEG where the transport happens. Since the QPC is a master piece of this study, we focus on the different models we can define and the precautions we should take to obtain adiabatic opening with a smooth connection to the leads (electron reservoirs). For each model, an analytical description is given and the quantification of the conductance is discussed. We hope after reading this chapter, the reader understands the parameters we need to handle in order to change the conductance of a QPC, to obtain sharp steps in the conductance profile, or to avoid the Fabry-Perot oscillations in the plateaus of conduction. We introduce here, the experiments related to the subject of this thesis and explain how the pictures of the interference pattern of conductance are obtained.

We want to give here, an overlook on the subject of this thesis and specially, the different questions we need to answer or at least make clearer.

1.1 Two dimensional electronic gases (2DEG)

Most of recent electronic devices use two dimensional electronic gases (2DEG). In these components, electrons move freely in a 2D plane with a controlled density of charge. Several methods are used to obtain these systems. Some of them goes to the early 60 such as in thin metallic sheets but the most used systems nowadays are MOSFET (Metal Oxide Semiconductor Field Effect Transistor) supported by the industry of semiconductors. The 2DEG in these MOSFETs is formed in the interface Si/SiO_2 under the effect of an electric field. Even if they are widely used, MOSFETs have an important disadvantage for some quantum experiments: Disorder. Defects on the interface of Si/SiO_2 makes the coherence time short as well as the mean free path, which is not suitable for studying the ballistic and coherent regime. Fortunately, some other growth techniques exist and allow the fabrication of cleaner systems with long mean free path and coherence length. 2DEG in semiconducting heterojunction are made by mean of these techniques and offer samples with very high mobility of carriers.

1.1.1 2DEG in Heterojunctions

2DEG obtained in semiconducting heterojunction could show mobilities 20 times higher than those in MOSFETs which is due to the absence of defects in the interface. In fact, the well-controlled technique of layers growth, makes the fabrication of such samples easier. We will concentrate on samples obtained using the GaAs/AlGaAs heterostructures as used in the group of Westervelt at Harvard university and Goldhaber Gordon at Stanford university to study electronic flow through nano-scale devices.

1.1.2 Fabrication of 2DEG

Making a 2DEG in heterojunction consists on creating a conduction band discontinuity by means of the growth of wide bandgap material over a narrow bandgap material. The choice of gallium arsenide (GaAs) and aluminum arsenide (AlAs)(or intermediate alloy AlGaAs) is explained by the fact that they both have the same crystalline structure and the spacing between atoms is almost identical, leading to minimum of atomic misalignment while fabricating the heterostructure. The process to grow these layers on some substrate is done in ultra high vacuum to avoid defects and impurities. The technique consists on evaporating atoms or molecules with well controlled rate to construct the system atom by atom on a suitable substrate. This technique is called Molecular Beam Epitaxy MBE. To understand how we go from bulk electrons to 2D confined carriers we should know that electrons in GaAs has a smaller conduction band minimum than in AlGaAs. Electrons searching to lower their energy leave this last band to the GaAs one near the heterointerface causing in counterpart an electrical field due to the charged ions (left by their electrons). The balance between these two situations trying to have favorable kinetic or electrical energies leads to the creation of a triangular potential well in the heterointerface which confines electrons in a 2D plane perpendicular to the growth direction but free to move along the interface .

We can understand that at low temperature, only the first level in this quantum well is populated. In fact, the next level is typically around $100K$ far from the fundamental, that is why we say that the electronic gas is 2D which in other words means that quantum mechanically, the electrons are confined in the heterostructure growth direction. Now we come to the question of the electrons populating the 2DEG. The number of electrons directly given by the layer AlGaAs and the few impurities existing in it is small. So, we need to dope with donors atoms to increase the number of electrons populating the 2DEG (with Silicium atoms for example). On the other hand this operation brings defects on the crystal and changes badly its conduction properties. To solve this problem, we let in practice a clean region between the GaAs and the doped layer of AlGaAs as shown in figure . This region of wide d is called *spacer*. This kind of engineering allows to reach very high mobilities ($\mu > 10^6 cm^2/Vs$ with density $10^{11} cm^{-2}$) and obtain very clean sample with almost no impurities. A very important thing we can notice from this is that the 2DEG is underneath the surface of the sample at a distance around $50nm$ (such as the samples used at Harvard in SGM experiments). Of course, the concentration in donors fixes the concentration of carriers in the 2DEG but the most convenient way to manage [1] this concentration is to use a top gate on the surface of the sample and

---

1. Other methods for changing the carriers density could be applayed: Shining light onto the sample increases the
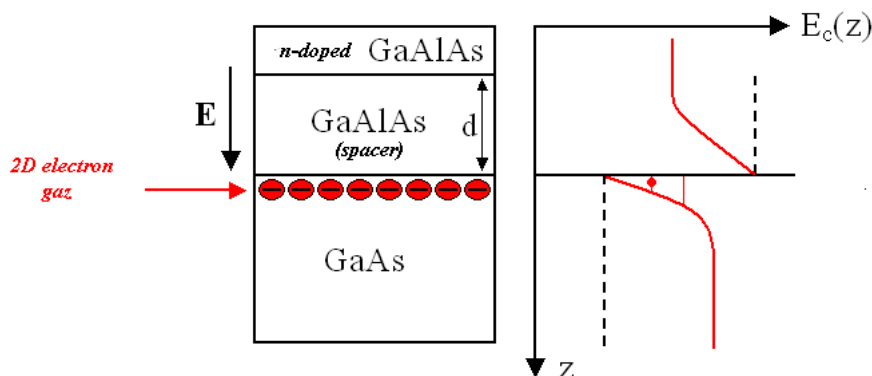
Figure 1.1: Engineering $2D$ electronic gaz. The confinement in the z direction, at the heterointerface, ensures a 2D density of states for the electrons.

play electrically to fix this concentration of electrons. It may be sometimes interesting to study the transport of holes instead of electrons. For such task, we can fabricate a two dimensional hole gas 2DHG in the same way but the kind of doping atoms which is different(p-type donors: Berillium for example). To improve the carriers confinement in the quantum well at the heterointerface, we want to get higher potential barrier. For this task, the 2DEG is obtained solving the Shrodinger's wave equation self consistently with the Poisson's equation [3]. Tools such as TCAD and 1D Poisson solver exist for this analysis.

1.1.3   Density of states

It may be interesting to recall some basic results on the density of states of 2D-systems. Starting from the relation of dispersion of free electrons in 2D systems which reads:

$$E = \frac{\hbar^2 k^2}{2m}$$

we can use the definition of the density of states per unit of area and energy [2]:

$$D(E) = 2g_v 2\pi k \frac{dk}{dE}$$

The factors 2 and g_v are respectively for spin and valley degeneracy and m is the effective mass of the carriers .
Straightforward simplifications show that the density of states of a 2D-system is constant and equal to:

$$D(E) = \frac{g_v m}{\pi \hbar^2}$$

At zero temperatures, all the states below the Fermi energy are occupied and therefore the number of states per unit area is given by:

$$N_s = \frac{g_v m}{\pi \hbar^2} E_F$$

This relation is useful to relate the density of carriers and the wave number at the Fermi energy (or the wavelength). In fact, using again the relation of dispersion we can arrive to the result

$$k_F = (2\pi N_s / g_v)^{1/2}$$

1.1.4   advantages of 2DEG

What makes the 2DEG interesting ? Beside the fact that these systems are 2D which makes them quantum mechanically interesting, they offer very high mobilities and very clean samples to

---

carriers density and enhancing the hydrostatic pressure do the contrary.
    2. In the wave vector space, the density of states per unit of area reads:$1/(2\pi)^2$

engineer good quantum electronic interferometers (Mach-Zender for example). Using electrically charged gates, we can fabricate 2D systems(Quantum Point Contacts), 1D (Quantum wire), 0D (Quantum dot) which are the most common systems used in mesoscopic physics to study fundamental phenomena related to electronic confinement. In this thesis, we shall focus on Quantum Point Contacts (QPC) to study scanning gate microscopy to shed light on quantum transport in these mesoscopic systems. Experiments studying electronic flow (mainly those in Harvard, Stanford and Grenoble) in QPCs, used as quantum interferometers, will be the main references to compare our results and conclusions.

1.2 Quantum Point Contact in 2DEG
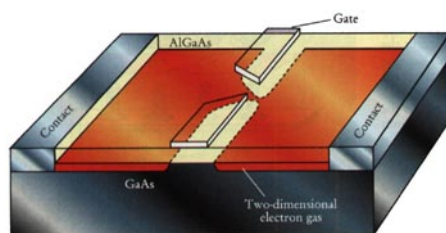
Figure 1.2: Negatively biased gates deplete locally the electron gas and form a narrow constriction called Quantum point contact. Van Houten et al [2]

Quantum Point Contacts (QPC) are devices obtained using 2DEG [3] and controlled by charged gates. It consists on narrow constriction where electrons could pass from an electron reservoir to another one. This narrow region could be thought as a short quasi 1D wire. To understand this general description for the QPC, let us see in details how it can be obtained. The 2DEG situated at around $50-80nm$ beneath the surface of an heterostructure could be electrostatically depleted using charged top gates with suitable shape. The narrow region, wide about the electron wavelength, is delimited by two negatively biased gates as shown in figure 1.2. This is the split-gate technique initiated by the group of Michael Pepper[4] at Cambridge and Daniel Tsui[5] at Princeton .

1.2.1 Conductance quantization

Studying electronic transport through quantum point contacts shows interesting and fundamental behaviour. The conductance of such systems shows quantified plateaus in units of the quantum of conduction: $G_0 = 2\frac{e^2}{h}$ (where e is the electron charge and h is the Planck constant) as reported for the first time in 1988 by the the Delft-Philips and Cambridge groups .

The plateaus are due to a quantized momentum along the transverse direction in the quantum point contact region analogous to the modes in a waveguide. The number of these conducting modes is roughly given by the ratio between the width W of the narrow constriction and the half Fermi wavelength $\lambda_F/2$, the width itself being controlled by the potential of the gates. Yet, the step-like profile of the conductance starts to wash out with temperature as it can be seen on figure 1.3. The regular step-like profile of the conductance means that each mode conducts the same quantum of conductance (each time a mode is open) even in the case of no impurity! This fundamental quantity is well understood as related to the matching of small number of modes in the QPC to a huge number of conducting modes in the leads (reservoirs). For more details, someone could refers to early papers by Glazman [6] or Beenakker [7].

1.2.2 0.7 anomaly

As it can be seen in figure 1.3 or better in figure 1.4 by Cronenwett et al, there is a shoulder-like feature in the first conduction plateau. In fact, the conductance is reduced to something like $0.7 \times 2\frac{e^2}{h}$ when temperature is increased. This strange phenomenological behaviour, with a

---

3. can also be realized in a break-junctions
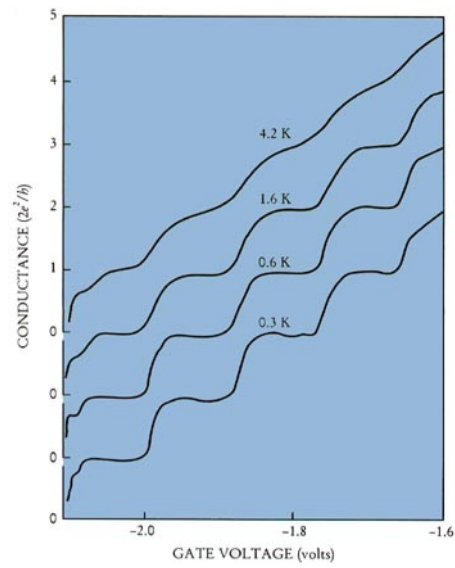
Figure 1.3: Conductance quantization in a quantum point contact in units of $2\frac{e^2}{h}$ for different temperatures. Van Houten et al [2]
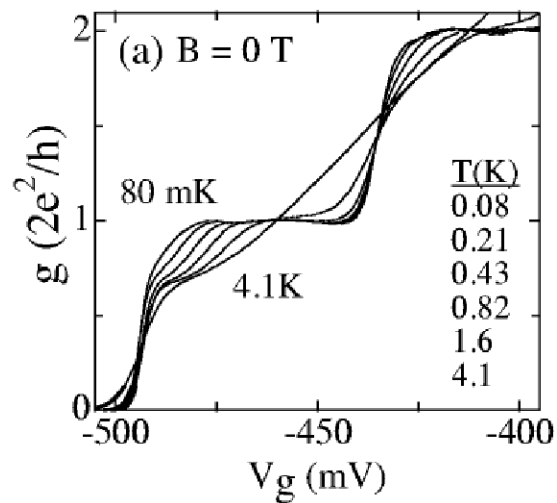
Figure 1.4: Experimental data showing reduced conductance when temperature is increased for the first plateau of conduction obtained using quantum point contacts.

magnitude varying depending on samples can not be explained with a non-interacting Landauer-Buttiker theory although a lot of work on this subject has been published. Among these various works, some tried to explain it with Kondo effect [8]or in term of quasi-localized states inside the QPC[9] but none of all the theories gave a fully accepted explanation. Nevertheless, a lot of people are almost convinced that it has something to do with spin degree of freedom.

1.3 Models for quantum point contacts
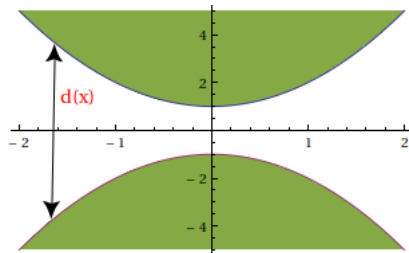
Figure 1.5: Quantum Point Contact: the transverse width varies with x and has a minimum d_0 in the middle of the QPC.

Quantum point contact is the centerpiece in Scanning Gate Microscopy which will be the subject of this thesis. Thus, it worths to be well studied to explain all the results related to it as a function of its parameters specially its geometry and smoothness.

The first question may be related to the quantization of conductance and the number of modes transmitted by the QPC. If we take the case of a QPC defined with a potential having hard-wall boundary conditions, the wave function ψ, solution of the Schrödinger equation verifies:

$$-\frac{\hbar^2}{2m}\Delta\psi = E\psi, \qquad \psi[y = \pm d(x)/2] = 0 \tag{1.1}$$

$d(x)$ is the function specifying the width of the QPC as a function of the position x.

The solution of such equation could be searched in the form [10][6]: $\psi = \psi(x)\phi_x(y)$, where [4]

$$\phi_x(y) = [2/d(x)]^{1/2}\sin\left(\pi n[2y + d(x)]/d(x)\right), \quad \text{n is integer} \tag{1.2}$$

$$-\frac{\hbar^2}{2m}\frac{d^2\psi}{dx^2} + \epsilon_n(x)\psi = E\psi, \qquad \epsilon_n(x) = \frac{\pi^2 n^2 \hbar^2}{2md^2(x)} \tag{1.3}$$

We can see now that the problem is reduced to solving the 1D Schrödinger equation in an effective x-dependent potential made by the eigenergies $\epsilon_n(x)$ of the transverse direction. The solution for such equation could be written in a formal way using the semi-classical definition of the momentum $p(x) = \sqrt{2m[E - \epsilon_n(x)]}$ as follows :

$$\psi_n(x) \propto \exp(\frac{i}{\hbar}\int_0^x p_n(x')dx') \tag{1.4}$$

A propagating mode turns out to be directly related to its semi-classical momentum since when it is complex, the wave function becomes exponentially decaying and therefore corresponds to an evanescent mode. This condition which should be verified for the narrowest region in the QPC (The corresponding width is referred as d_0), fixes the number of propagating modes through the QPC. Using Eq. (1.3), the number of conducting modes reads,

$$n_{max} = [\frac{kd_0}{\pi}] \tag{1.5}$$

---

4. ϕ_x is the solution of the 1D Schrödinger equation for a fixed position x

Here [...] means the integer part function. This relation could be also written using the Fermi wavelength to state that the number of conducting modes is the ratio of the width of the QPC (The narrowest region) to the half Fermi wavelength as it was already mentioned..

What we can understand from relations (1.5) is that each mode conducts a quantum $2\frac{e^2}{h}$ and therefore the profile of conductance versus the Fermi energy or the gates voltages is a step-like function. Now, looking to how exact is this quantization, which as we saw, comes from a semi-classical justification which is correct only in the QPC region(and not in the leads), it turns out to be important to ask the question about the attachment of the leads to the QPC and how this accommodation region affects the step-like profile of the zero-temperature conductance.

Taking into account the curvature of the constriction, it can be shown [6] that the shape of the step-function at low temperature reads:

$$\delta G(z) = \frac{e^2}{\pi\hbar}[1 + exp(-z\pi^2\sqrt{2R/d})]^{-1}, \qquad z = \frac{k_F d}{\pi} - n \qquad (1.6)$$

where R refers to the radius of curvature of the constriction.

A quick analysis of Eq. (1.6) gives the condition for which the steps become sharper:

$$\pi^2\sqrt{2R/d} > 1 \qquad (1.7)$$

This factor affects in an exponential way the sharpness of the steps, and seems to be more important than the index n. This analysis is valid for low temperatures $T < n\hbar^2/m(2Rd^3)^{1/3}$. Otherwise, the factor $\pi^2\sqrt{2R/d}$ should be replaced by $\hbar^2\pi^2 n/md^2 T$.

1.3.1   Adiabatic constriction

The expression "Adiabatic constriction" so often used in literature but most of the time not well understood either for its signification or its implication on quantum transport needs to be clarified. As was previously stated, the smooth variation of the transverse dimension of the constriction is the key for observing the quantization, highly sensitive to the geometry of the QPC. Hence, we start to speak about adiabatic constriction when the splitting of the wave function to transverse and longitudinal function becomes possible as done in Eq. (1.2). The condition stated above ensures sharper steps and the absence of intra-mode conduction. In practice, a very long QPC with small curvature ensures adiabatic quantum transport.

1.3.2   Saddle-point constriction

In the previous study, we looked at a potential with hard-wall boundary condition and we discussed the role of the confinement in the transverse direction to obtain conductance quantization with well abrupt steps. In this section, we shall discuss another type of potential, widely considered in literature for its simplicity: Saddle point constriction. Indeed, the split gates forming the QPC induces a bottleneck potential in a form of a saddle. Thus, this potential expanded in terms of the appropriate variable x and y reads [11] :

$$V(x,y) = V_0 - \frac{1}{2}m\omega_x^2 x^2 + \frac{1}{2}m\omega_y^2 y^2. \qquad (1.8)$$

Where, V_0 is the electrostatic potential at the saddle and the parameters ω_x, ω_y are directly related to the curvature of the saddle. The solution of the Schrödinger equation with this quadratic form of the potential is performed using the same method of the previous section, i.e , we solve the Schrödinger equation for the wave function corresponding to motion along x in an effective potential associated with the energies of the transverse wave function. These eigenenergies are of the form $\hbar\omega_y(n+\frac{1}{2})$ where $n = 0, 1, 2, 3, \ldots$. Hence, a semi-classical point of view suggests that the channels with a threshold energy

$$E_n = V_0 + \hbar\omega_y(n + \frac{1}{2}) \qquad (1.9)$$
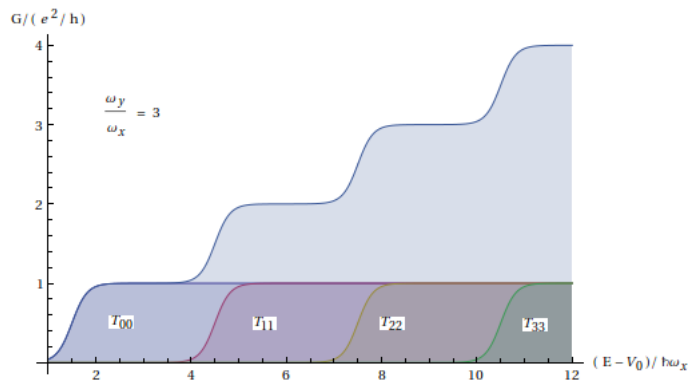
Figure 1.6: Transmission probabilities through a saddle point potential. The total transmission is obtained by summing over all the conducting channels. $T = \sum_n T_{nn}$ (No channels mixing). Adapted from [11]

below the Fermi energy are open (conducting channels) and those with threshold energies above the Fermi energy are closed. Obviously, this picture is false in quantum mechanics since a channel could be neither completely open nor completely closed. In this case, the transmission probability T_{mn} between the modes m and n is simply expressed as follows:

$$T_{mn} = \delta_{mn} \frac{1}{1 + e^{-\pi \epsilon_n}}. \tag{1.10}$$

where we used here the variable ϵ_n defined as:

$$\epsilon_n = 2[E - \hbar\omega_y(n + \frac{1}{2}) - V_0]/\hbar\omega_x \tag{1.11}$$

Two important things could be extracted from Eq. (1.10). First, the picture of good quantization with step-like profile for the conductance is accurate to an exponentially small correction. The second remark is that there is no channels mixing and the transport through the quantum point is globally adiabatic.

If we look carefully to Eq. (1.10), we note that the width of the transition region from nearly closed QPC to an almost open one is given by the energy scale $\hbar\omega_x$. This has to be compared to the distance between modes $\hbar\omega_y$. For instance, a well-pronounced steps are obtained if :

$$\omega_y > \omega_x \tag{1.12}$$

This condition means that the sharpness of the steps is solely determined by the ration of the frequencies ω_y/ω_x without taking too much care to the attachment of the QPC as long as it is not abrupt and follows some smoothness. We shall see in the next section that this is not true for all the models. In fig. (1.6), we can see how does the profile of the conductance depend on this ratio and notice that we can go from a well pronounced steps to a completely no steps with few factors of that ratio (typically 5).

1.3.3 Hyperbolic model

In what follows, we will look at a different model for the QPC and try to obtain the condition under which well pronounced steps occur. The merit of this model is that it describes both the central region of the QPC and the lead to which it is attached. The model is introduced using the hyperbolic variables (α, β) related to the usual variables x, y as follows:

$$x = c\sinh(\alpha)\sin(\beta), \qquad y = c\cosh(\alpha)\cos(\beta) \tag{1.13}$$

where c is a scale factor and the variables α and β verify: $\alpha \in]-\infty, \infty[, \quad \beta \in [0, \pi]$. The constriction, delimited by two hyperbola, will be defined with hard wall boundary condition using a potential :

$$V(\alpha, \beta) = 0, if \ \ \beta \in [\beta_0, \pi - \beta_0], \ and \ \infty \ elsewhere \tag{1.14}$$

β_0 and $\pi - \beta_0$ correspond to the two hyperbola limiting the QPC. The Schrödinger equation defined in terms of the variables α and β and using the potential defined above reads [12]:

$$-\frac{\hbar}{2m} \frac{1}{c^2(\cosh^2 \alpha - \cos^2 \beta)} \left(\frac{\partial^2 \Psi}{\partial \alpha^2} - \frac{\partial^2 \Psi}{\partial \beta^2} \right) + V\Psi = E\Psi. \tag{1.15}$$

Again, we search solution $\Psi = \psi(\alpha)\chi(\beta)$ which should verify the following 1D-Schrödinger equation:

$$\frac{d\psi}{d\alpha^2} - (b - s\cosh^2 \alpha)\psi = 0 \tag{1.16}$$

$$\frac{d\chi}{d\beta^2} + (b - s\cos^2 \beta)\chi = 0 \tag{1.17}$$

The dimensionless constants are $s = 2mc^2 E/\hbar^2$ and $b = 2mc^2 \lambda/\hbar^2$.

These 1D Schrödinger equations have as a solution even Mathieu's functions. The transverse energy λ_n fixes the amount of energy left for longitudinal movement through the QPC and plays the role of an effective potential and allows to write the longitudinal Schrödinger equation as:

$$\frac{1}{c^2} \frac{d^2\psi}{d\alpha^2} + \frac{2m}{h^2} [E_F - (\lambda_n - E_F \alpha^2)]]\psi = 0 \tag{1.18}$$

for which, the transmission probability is already expressed and given by:

$$T_n = \frac{1}{1 + e^{-\pi \epsilon_n}} \tag{1.19}$$

and here $\epsilon_n = [s - b_n(s)]/s^{1/2}$

Using the characteristics of Mathieu's functions, we can extract more information from these equations and results. The most important conclusions we can address concerning the shape effects of the constriction are(for more details see [12]):

  – The number of conducting channels depends not only on the width of the constriction but also on the slope of the hyperbola (think about β_0).
  – Large β_0 ensures well pronounced steps and good quantization(this corresponds to long constriction with a smooth variation).
  – Although the smoothness of the constriction is required for observing a step-like profile for the conductance, this condition is not a strict one.

From the different QPC models presented here, we can learn some general information about quantum transport through quantum point contacts. The first idea is that the eigenenergies related to the transverse confinement in the QPC affect highly the shape of the conductance profile and this is true whatever is the potential since only the form of these eigenenergies changes but the main results remain similar. Thus, in all cases the attachment to the leads seems to be important that is why some smoothness is required to not destroy quantization. Even if people believe that quantization is sensitive to the shape of the constriction, we can summary in few words the QPCs we should construct to see good quantization without taking too much care to which model well describes it, as follows: Long QPC with smooth variation and attachment to the leads.

1.3.4   Wide-Narrow-Wide model

I would like to present here a simple model for the QPC with which I played a lot during my first steps in this subject and which has the merit of being simple to implement numerically and at the same time shows some results of the previous discussion. The model is of the type wide-narrow-wide wave guide[13], which means it considers an abrupt connection of the central system to the leads.

The central region has a constant width which in some way satisfies the condition of smoothness and although the connection to the leads is brutal and shows some discontinuities in the shape of the constriction, the formula giving the number of conducting modes $N = 2W/\lambda_F$, is good and
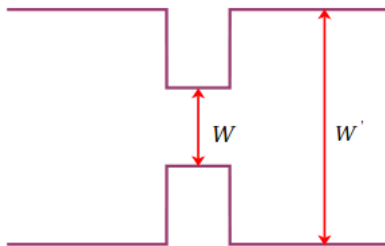
Figure 1.7: Wide-narrow-wide model: the attachment of the central region to the leads is abrupt.
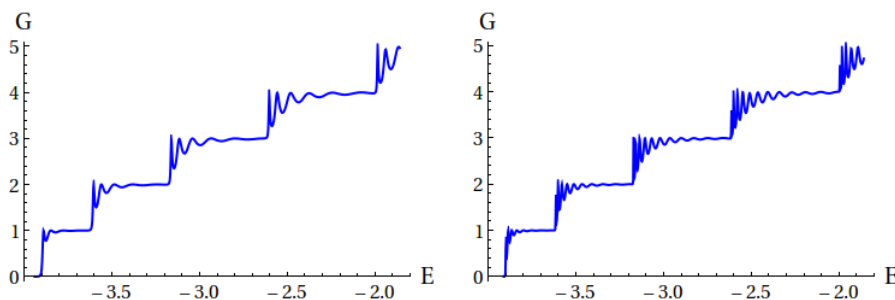
Figure 1.8: Transmission profile for a wide-narrow-wide model.In the right Fig, the length of the constriction is twice the length of the constriction which gave the left Fig. In both figures Fabry-Perot oscillations are visible. The bottom of the conduction band is taken at -4 (units of t_h). The conductance is expressed in units of the quantum $2e^2/h$

remains roughly valid . However, the quantization is not good and we get plateaus altered with some oscillations clearly appearing in the Fig. (1.8) . The number of oscillations increases for longer constrictions and at the same time the step of the plateaus become sharper. The explanation of these oscillations is simple: the quantization of the wave number in the leads and in the constriction is different. In fact, in the constriction, k_F is a multiple of $\frac{\pi}{W}$ while in the leads it is multiple of $\frac{\pi}{W'}$. Knowing that $W' \gg 1$, it appears that the leads could be considered, for large width, as a continuum. Because of this difference of quantization in the lead and in the constriction, the oscillations appear as if you think of the optic analogy where each time light passes from a media with an index of refraction n to another with an index n' we obtain reflection and because we have here two of these separations (Lead-constriction and constriction-lead) we have a kind of a Fabry-Perot interferences which appear in the conductance profile as oscillations. In Fig. (1.8), we plotted the profile of the transmission as a function of the Fermi energy of the electrons. We notice that because of the abrupt connection to the leads, Fabry-Perot oscillations occur on the plateaus of conduction. As these oscillations are induced by the interference of the electron wave function reflected by the two ends of the narrow region , their number depends on the length of this constriction as it can be seen while comparing the two figures in (Fig 1.8) obtained for different lengths. A smearing of the resonances occurs at non-zero temperatures[13].

This shows that we need to avoid abrupt coupling to the reservoirs in order to obtain plateaus of conduction of a good quality.

1.4 Scanning Gate Microscopy

Scanning Gate Microscopy (SGM) is a technique widely used in the last decade to study systems at the nano-scale. By means of a charged tip of an atomic force microscope, capacitively coupled to the electrons in the nano device, we map the local effect it induces on the physical observables related to the electronic density in the structure such as quantum conductance or thermopower. Thus, electronic flow or conductance changes, while the tip moves, could be obtained by recording the output as a function of the tip position and plotting them in a data-image. This way, a variety of systems have been explored to extract some fundamental results on quantum transport in the
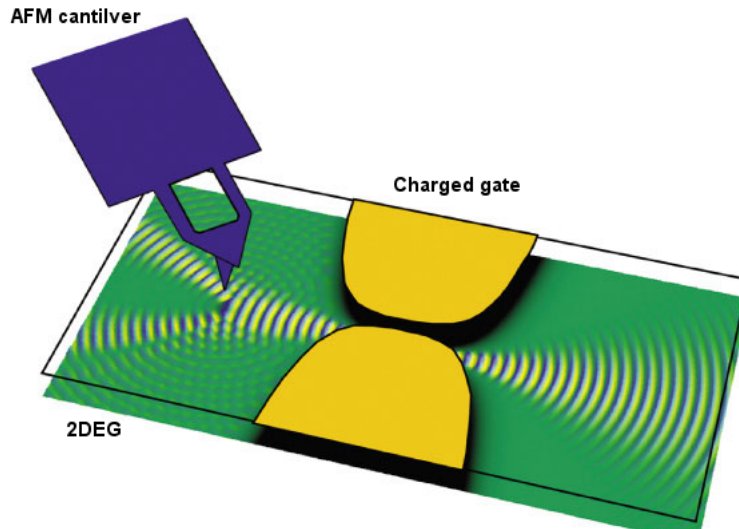
Figure 1.9: In a quantum point contact, open for few modes of conduction, an AFM charged tip depletes the charge density beneath it and changes the conductance of the system.

ballistic and coherent regime. A wide range of systems were probed using this technique either 2D like Quantum point contacts (QPC), 1D like quantum wires and quantum rings[14] or 0D systems such as GaAs-based quantum dots and graphene quantum dots[16].

1.4.1   SGM on Quantum Point Contacts

In this thesis, we will be more interested in the experiments using SGM to probe the transport of electrons through Quantum Point Contacts. The setup for this kind of experiments is summarized in Fig. (1.9). The charged tip, altering the local electron density of the 2DEG, changes its conductance which when reported on a 2D graph, shows a fringes pattern. This system acting like a quantum electronic interferometer, is mostly studied at very low temperatures and in very clean samples with ultra high mobilities. Actually, very low temperatures ensure large electrons mean free path and coherence length, which enable to look at the ballistic and coherent regime for electrons transport. We know also that temperature averages the quantum quantities over a range of energy in the order of $k_b T$ and therefore some details could be washed out. However, the first works on the subject[1] considered QPCs in the presence of disorder and studied electronic flow through the constriction at around liquid Helium 4 temperature. Interesting results on small angle scattering were obtained leading to the appearance of narrow branches and a focusing effect nearby the impurities. The interference fringes, due to quantum effects on conductance, are visible for very long distances, even longer than the thermal length l_t .

As was previously stated, experiments on cleaner samples were considered particularly in the group of Stanford (Goldhaber Gordon) where the mobilities of the samples were very high. In fact, in these experiments, there were no defects in the 2DEG and therefor the setup works as a simple interferometer since the electrons are scattered solely by the QPC or the charged tip. In this thesis only these kind of samples would be considered and as we will be see along the next chapters, although the simplicity of the system, there is too much information we can extract and a lot of physics to learn.

In the theoretical study we will start soon to introduce, electronic interactions would be neglected. In fact, we quickly understood that there is too many things too say and to understand before we consider interactions. At the same time, considering no interactions could be justified when we consider systems with electrons density quiet high the keep the screening effect of electrons but at the same time, this density should not be very high that some unexpected and unwanted effects (such as lattice effects in some model).
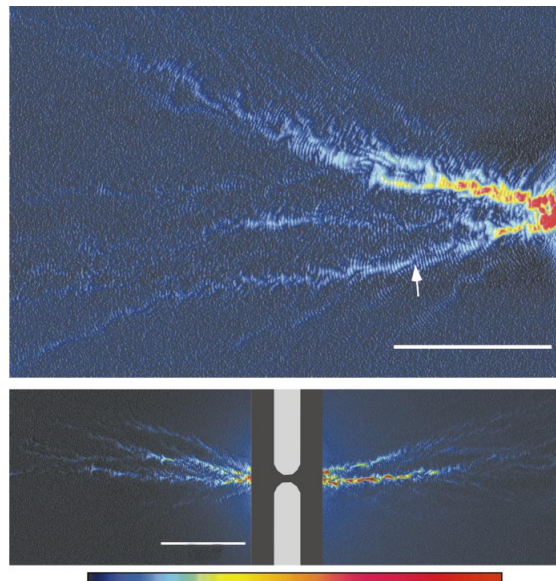
Figure 1.10: Experimental results on conductance changes with SGM technique. An interference pattern of $\lambda_f/2$ fringes is obtained. We notice small angle scattering and branching strands for the electronic flow. the temperature in this experiments is 1.7 K . TopinKa et al [1].

1.4.2 The charged Tip in SGM techniques

To continue the introduction of the device which will be the main system studied in this thesis using SGM techniques, it is very useful to study how does work the charged tip and look at its effects on the 2DEG or directly on the physical observables it may alters. The role of the charged tip is to deplete the charge density below it and backscatter the electrons. In fact, each time the depletion is in a region of intense electrons flow, the backscattering reduces significantly the quantum conductance. Plotting these changes in a 2D graph translates the flow differences between the 2DEG regions. It seems as discussed in [17] that depleting the 2DEG (and not only bumping it) is important to see significant changes. For this reason, the tip is biased negatively to -3 volt and positioned at typically 20 nm above the sample surface (remember that the 2DEG is around 60 nm below the surface). Higher tip or less biased one may lead to absence of relevant changes in the conductance. It seems that these conditions ensures also good resolution for the acquired images. For more technical details and good illustrations, reference [17] is recommended.

1.4.3 Modelization of the charged tip

It is important to know in details the effect of the tip on the 2DEG and to have an idea on the potential it creates either for experiments or for theoretical models. The depletion acts like a potential seen by electrons. In [], the tip was modeled as a sphere at the end of cone, and its effect was simulated using a 3D Poisson Simulator. The results obtained by simulation were confirmed by experiment searching the condition to have significant output for the change in conductance. In other works, the effect of the tip induces a circularly symmetric Lorentzian bump with parameters depending on the tip: the hight of the Lorentzian depends on the voltage of the AFM tip and its width depends on how far is the 2DEG from the tip . It follows that a good model and complete one have to take in consideration all these results but sometimes it seems that simpler models with less conditions allow to obtain the main results with simple formulas and clear results as we can see it in the next chapters.

1.4.4 Questions on experiment

The experiments we are particularly interested in are done in the group of Goldhaber Gordon at Stanford university. In these experiments[18], the SGM technique is applied on Quantum Point

Contacts built in very clean samples with very high mobilities ($density = 1.5 \times 10^{11} cm^{-2}$ and mobility of $4.4 \times 10^6 cm^2/V$ at 4.2 K). Taking advantage from the wavelike nature of electrons, this device acts like an electron interferometer and offers direct visualization of a fringes pattern due to the different paths coherently interfering in the system.

The temperatures considered in these experiments were very low, but as was shown by the recorded images for conductance changes, it seemed that 1.7 K of temperature was too hot to see the fringes in these samples (with very low density of impurities) . To put this in contrast, let us remind that experiments on samples with disorder[1] were carried out at 4.2 K and that the fringes were visible beyond the thermal length !
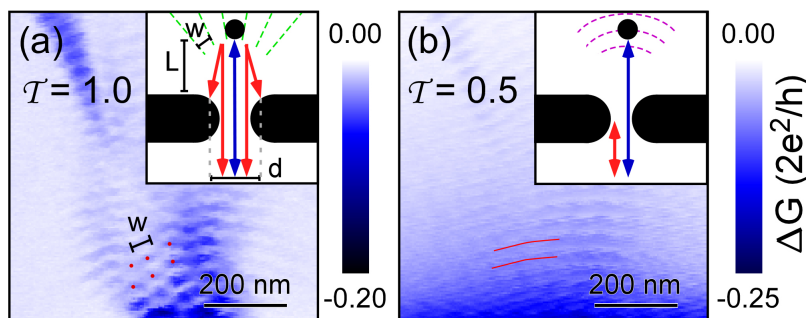
Figure 1.11: Imaging conductance changes by SGM technique for different opening of the QPC. In the case of $\mathcal{T} = 1$ a checkerboard pattern of interference is visible whereas for less transmissions ($\mathcal{T} = 0.5$) the picture shows ring pattern. From [18]

At lower temperatures, typically 350mk, the interferences in the very clean samples are visible and the acquired images of conductance changes due to the presence of the charged tip shows fringes spaced by half the Fermi wavelength $\lambda_F/2$. Thus, the thermal averaging limits how far from a coherent source interference effects can be observed.

To make more precisions on those experiments, we can mention that two different cases were considered depending whether the system without the charged tip is fully transparent for some modes or almost pinched off. Fig. (1.11) shows the kind of pictures obtained for fully open QPC (Fig a) and half opened one (Fig b).

The aim of this thesis is to study this experiment in details and to look at the electronic quantum transport in general. A lot of questions could be raised and we may list some of the pertinent effects we should either understand or shed light on them:

1. The main question we try to answer is: What is the law decay of the fringes in SGM experiments?

2. How does is it depend on the opening of the QPC ?

3. what is the angle dependence of the electronic current flow (focusing effect)?

4. what do we image and map using this technique? Is it density of charge, density of states, electronic current flow or may be nothing about these observables?

5. what is the role of the charged tip in this pictures? how does the effect depend on its voltage?

6. How does the effect depend on the QPC shape?

7. What is the role of temperature in this effect and how does it affects the pictures of interference pattern?

8. How could we understand the results using a wave function interpretation?

9. what is the minimal model and the simplest one to reproduce the behavior of the QPC to obtain the pictures of interference pattern?

To answer these questions we need to study the quantum transport in quantum point contacts. The easiest and convenient way to do it is to use numerical simulations using suitable programs. This will be the topic of the next chapter

Chapter 2

Numerical tools for quantum transport

Contents

Summary of chapter 2

In this chapter, we will introduce the quantum transport of electrons and the different tools of numerical simulations. First we introduce the different length scales and the regimes they define. We will be interested particularly in the conductance of a nano-system in the ballistic regime. The different ways to express this transport coefficient are listed and explained briefly. The most important relation we will use all over this thesis is the Fisher-Lee formula expressing the conductance of a system:

$$G(E) = \frac{2e^2}{h} \times \text{Tr}[\Gamma^l G \Gamma^r G^\dagger]$$

This expression uses the Green's function G of the system and the left and right coupling matrix Γ. This Green's function is the major tool of this thesis. Its calculation is obtained recursively in order to save time and computer memory. The recursive algorithms are obtained using the Dyson equation. The use of these algorithm requires the introduction of the concept of the self energy in order to take into account the leads which have infinite size. The algorithm is applied to calculate the conductance of a quantum point contact defined with tight binding Hamiltonian model on a lattice. After that, the algorithm is managed to take into account the effect of an external tip which changes the conductance of the system. The way the tip is taken into a count depends on the considered partition of the system:

– The system is considered as a central region (QPC+ the region containing the tip) coupled to perfect leads. This method implies long time of calculation since each time we change the position of the tip, we compute a new Green's function of the scattering region.

– The system is considered as a central region (QPC) connected to leads. The leads here are imperfect in a sens they contain the tip. This method is much easier since the scattering region remains the same while the self energy of the lead is updated for each new position of the tip. This procedure is very easy.

This method is seen as a generalized Fisher-Lee formula.

Beyond the simplification this method introduces in the algorithms, it will be the basic tool which makes the analytical formulation of this problem possible. It is very important to see the system as the same scattering region and only the self energies of the leads change.

We also define in this chapter the dispersion relation in this system. We will adopt in all this thesis a symmetrized conduction band:

$$E \in [-4t_h, 4t_h]$$

The hopping term in the lead t_h will be taken equal to one ($t_h = 1$) all over this thesis.

2.1 Quantum transport

Recent electronic devices become smaller and smaller thanks to the huge improvements in nano-scale manufacturing. This suggests to consider a new physics for the electrons transport different from the Drude theory, taking into account the quantum effects due to the small size of the studied systems. Adding to this the fact that most recent experiments, looking to fundamental physics in nano-structures, consider very low temperatures and therefore degenerate electronic gases, quantum transport seems to be unavoidable to interpret the results.

2.1.1 Characteristic lengths

To introduce the field of quantum transport, some length scales should be introduced to be considered when we study nano-structures.

Electron wavelength:

The wavelength of a free electron λ, known as the De Broglie wavelength is related to its momentum simply by :

$$\lambda = \frac{h}{p} = \frac{2\pi}{k}$$

where p is the typical electron momentum. This relation reads for the case of a single filled 2DEG:

$$\lambda = \frac{2\pi}{k} = \sqrt{\frac{2\pi}{n_s}}$$

Here n_s represents the sheet density.

We so often compare typical lengths to the electrons wavelength which is due to the wave nature of the electrons. The most important example which concerns the topic of this thesis may be the number of transmitted modes which is given as the ratio of the QPC width to the half of the electrons wavelength (eq 1.5).
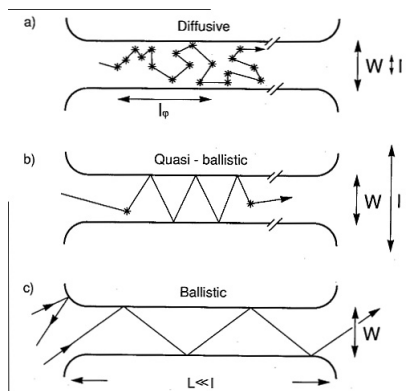
Figure 2.1: The different lengths defining the different regimes of electrons transport.

Electron mean free path l_e:

defined as the average distance between successive collisions. It can be calculated using the relation

$$l_e = v\tau_{tr}$$

v is the typical velocity while τ_{tr} is the transport relaxation time, related to the scattering as follows:

$$\frac{1}{\tau_{tr}} \propto \int d\theta \sin(\theta) W(\theta)(1 - \cos(\theta))$$

Here, θ is the scattering angle and $W(\theta)$ is the scattering probability.

Since samples are most of the time characterized by their mobility μ, we can link this quantity to the transport relaxation time using the relation :

$$\mu = \frac{e\tau_{tr}}{m}$$

The mobility relates the drift velocity of electrons v_d to the electrical field inducing this motion. We can simply write:

$$v_d = \mu E$$

Phase-relaxation length l_ϕ:
This scale is defined as the distance an electron can propagate without loosing its phase memory. All quantum phenomena related to interferences effects can only prevail if l_ϕ is larger than any other relevant length scale. The relaxation time τ_ϕ due to scattering is related to the phase relaxation by the relation

$$l_\phi = \sqrt{D\tau_\phi}$$

Where D is the diffusion constant.
It is interesting to know that collision with static scatterers, having no internal degree of freedom, do not influence the phase coherence. Only inelastic scattering processes, like electron-electron or electron-phonon interactions do reduce the phase relaxation length [19].
Thermal length:
We know that thermal averaging limits how far from a coherent source interference effects can be observed. The distance after which the interference fringe intensity fades is the thermal wavelength. In fact, the propagation of electrons having close energy (in a window $k_b T$) averages the fringes pattern and makes it fade after a distance l_T.
The thermal wavelength is given by the following relation:

$$l_T = \sqrt{\hbar D/k_b T}$$

Noticing that for the scale of energy $k_b T$ we can associate a scale of time $\tau = \hbar/kT$, the thermal wavelength could be interpreted as the distance traveled by the electrons at the Fermi energy in a time τ. Other expressions could be found in literature. We can mention for example:

$$l_T = h^2/2\pi m \lambda_F k_b T$$

λ_F is the Fermi wavelength and m is the effective electron mass. It is very important to have in mind all these scale lengths when we study a mesoscopic system in order to understand the quantum effects which could occur.
A system is said to be diffusive if its size $L \gg l_e$. The other situation ($L \ll l_e$), where electrons propagate freely without collision with any static scatterer is known as the ballistic regime. If in addition, the system size is smaller than the phase-relaxation wavelength, the transport of careers is said to be coherent and quantum effects related to interferences phenomena can occur. We will be interested in the transport of electrons through quantum point contacts in the coherent and ballistic regime.

2.1.2   Quantum transport and scattering matrix

For mesoscopic systems, the conductance is not expressed by Ohm's law any more. We need to use a formalism adapted to coherent ballistic transport taking into account the quantum effects. In particular, the wave nature of the electrons should be taken into account and the physical observables should be calculated solving the Schrödinger equation or an equivalent formalism.
In the system of interest (QPC), the electron reservoirs (left and right) inject the careers in the system (constriction) which scatters them in the different available conducting modes. The Amplitudes of the incoming waves are related to the outgoing waves amplitude by means of a $2M \times 2M$ matrix called the scattering matrix and noted S:

$$\begin{pmatrix} O \\ O' \end{pmatrix} = S \begin{pmatrix} I \\ I' \end{pmatrix} \tag{2.1}$$

M is the number of conducting modes in the leads (reservoirs). I and I' are vectors containing the amplitudes of the incoming waves respectively from left and right whereas O and O' represent the amplitudes of the outgoing waves respectively from left and right.
The matrix S has to be unitary because of current conservation. We can therefore write $S^\dagger = S^{-1}$. This matrix has a block structure and can be written as follows

$$S = \begin{pmatrix} r & t' \\ t & r' \end{pmatrix} \tag{2.2}$$

where t, t' are $M \times M$ matrices describing the transmission amplitudes from left to right and from right to left respectively whereas r, r' describe reflection from left to left and right to right respectively [1]. Sometimes, we prefer to express the right probability amplitudes as function of the left ones rather than the outgoing as function of the incoming probability amplitudes. This is done by means of the transfer matrix T:

$$\begin{pmatrix} I \\ O \end{pmatrix} = T \begin{pmatrix} O' \\ I' \end{pmatrix} \tag{2.3}$$

This formulation is very useful when we consider systems with disorder or many systems in series. In fact, the transfer matrix of the whole system expressed in terms of the transfer matrix of subsystems in series composing it, is very simple and reads:

$$T = T_1 T_2 \ldots T_n \tag{2.4}$$

Here T_k represents the transfer matrix of the kth subsystem.
The use of the transfer matrix to express the conductance of mesoscopic systems is of great importance and widely used is random matrix theory [22][23]

2.1.3 Quantum conductance

Within the linear response theory, the conductance of the system when a small voltage difference between source and drain is imposed can be obtained by the following expression:

$$G = \frac{2e^2}{h} \int_0^\infty d\epsilon (-\frac{\partial f}{\partial \epsilon}) \text{Tr}(tt^\dagger). \tag{2.5}$$

where e is the electron charge, h plank constant and the factor 2 is for spin degeneracy. The energy dependent function f is the Fermi-Dirac distribution

$$f = \frac{1}{1 + e^{\frac{\epsilon - \mu}{k_b T}}} \tag{2.6}$$

μ is the chemical potential and k_b is the Boltzmann constant.
Using 2.5, we can compute the zero temperature conductance and write the following useful formula known as Landauer formula:

$$G = \frac{2e^2}{h} \text{Tr}[t(\epsilon_F)t^\dagger(\epsilon_F)] \tag{2.7}$$

We should note that this relation was first established for non-interacting electrons. Nevertheless, it remains correct and exact for electrons transport through an interacting region (electronic interactions) as it was proved in [20]. The zero-temperature conductance, obtained using relation 2.7, is the sum over the transmission coefficients from the left lead modes to the right lead modes as can be shown in the details of relation 2.7:

$$G = \frac{2e^2}{h} \sum_{mn} |t_{mn}|^2 \tag{2.8}$$

The transmission coefficients t_{mn} are taken at the Fermi energy.
When the system involves multiple reservoirs, the transmission from one lead to another could be obtained the same way, that is to say the sum over the transmission probabilities:

$$G_{pq} = \frac{2e^2}{h} \sum_{mn} |t_{mn}^{pq}|^2 \tag{2.9}$$

---

1. If the number of modes in the two leads (right and left) are different the S matrix reads

$$S = \begin{pmatrix} r_{n \times n} & t'_{n \times m} \\ t_{m \times n} & r'_{m \times m} \end{pmatrix}$$

t_{mn}^{pq} is the probability amplitude of an electron injected by reservoir p through the channel m to be scattered in the channel n of the lead q.

In the absence of magnetic field, we have the following relation :

$$\sum_p G_{pq} = \sum_p G_{qp} \tag{2.10}$$

which is valid regardless to the detailed physics. It interprets the fact that if all the reservoirs were put to the same voltage, the current should vanish [2]

In the presence of a magnetic field, we do not have time reversal symmetry anymore and the relation above becomes:

$$\sum_p G_{pq}(+B) = \sum_p G_{qp}(-B) \tag{2.11}$$

In the absence of magnetic field, transport equations have time reversal symmetry and thus the transmission of the system for a wave coming from left and scattered by the system is the same to the case of the same wave coming from right. Once the magnetic field is applied, this property is not true any more.

For some problems, it is more useful to express the conductance using the eigenvalues of the product $tt^\dagger$, where t represents the transmission matrix. If we denote T_n these eigenvalues we can write :

$$G = \frac{2e^2}{h} \sum_n T_n \tag{2.12}$$

Each one of these different ways to express conductance is suitable for some formalism and for others it may appear less convenient. So far, they all need to express the scattering matrix or at least the transmission matrix t (which is still a submatrix of S). The scattering matrix approach is difficult to use since it requires solving Schrödinger equation to get the transmission and reflection amplitudes. Moreover, it is not easy to implement numerically to do simulations to obtain the quantum transport observables. We will introduce a new formalism based on Green's functions rather than the scattering matrix, which is more convenient to the task of calculating the conductance of complicated systems.

2.1.4   The Green's function formalism

Instead of using a scattering approach which seems not suitable for numerical calculation, we introduce an alternative approach, based on the Hamiltonian matrix and the Green function of the system. This task starts by a discretization of the system by well known procedures of derivative approximation and lattice formulation of the Schrödinger equation or the system Hamiltonian. Considering only the nearest neighbors in the discretization procedure, we obtain an Hamiltonian in the tight-binding approximation.

$$H = -\sum_{mn} [t_{mn}^x |n+1, m\rangle\langle n, m| + t_{nm}^y |n, m+1\rangle\langle n, m| + hc] \tag{2.13}$$

$$+ \sum_{nm} \epsilon_{nm} |n, m\rangle\langle n, m| \tag{2.14}$$

This Hamiltonian contains a hopping term describing an electron jumping from a site to its neighbors with hopping factors t_{mn}^x, t_{mn}^y [3] and a term containing the on-site energies:

$$\epsilon_{nm} = 4t + V_{nm} \tag{2.15}$$

V_{nm} is the on-site potential.

The reservoirs of electrons are generally taken to be translational invariant with a constant on-site

---

2. The current flowing from lead p is: $I_p = \sum_q [G_{qp} V_p - G_{pq} V_q]$

3. In the absence of magnetic field, we do have $t_{mn}^x = t_{mn}^y = t = \frac{\hbar^2}{2ma^2}$

potential and hopping factors.

Under this considerations, the relation of dispersion for free electrons reads [4]:

$$\epsilon = 2t(2 - \cos k_x a - \cos k_y a) \tag{2.16}$$

This relation defines the band of conduction which is of length $8t$. Sometimes this band is shifted by $4t$ to obtain a symmetric interval of energies ranging from $-4t$ to $4t$ (ie $\epsilon \in [-4t, 4t]$). In this case, the middle of the band at $\epsilon = 0$, is called the half filling limit. In deed, half of the sites are occupied and therefore there is a symmetry between the transport of electrons and holes. However, in this limit, the tight-binding model suffers from the approximations we did and the relation of dispersion recedes from the 2D relation in continuum. Consequently, some unusual phenomena related to lattice effects are expected to be found. Another interesting limit is the continuum one obtained for Fermi energies belonging to the bottom of the energy band, around $-4t$ [5]. Indeed, the wave numbers at this limit verify $k_x a \ll 1$ and $k_y a \ll 1$ (a is the lattice spacing) allowing to do an approximation in relation 2.16 to recover the parabolic relation of dispersion of the continuum. This limit corresponds to the case of an electron wavelength too big (compared to a) to see the details of the lattice.

Green's function

After we introduced how to write the Hamiltonian of the system in a lattice form represented by its matrix H, we move to the very important concept of Green's function. The direct definition of this quantity is:

$$G(E) = \frac{1}{E - H} \tag{2.17}$$

where $G(E)$ and H are respectively the matrices representation of the Green's function and the Hamiltonian operators.

Expressing this in the position representation, we obtain the following expression:

$$G(r, r', E) = \langle r | G(E) | r' \rangle \tag{2.18}$$

which is solution of the Schrödinger equation with a delta excitation source:

$$[E - H(r)]G(r, r', E) = \delta(r - r') \tag{2.19}$$

From Eq. (2.19), we can understand the Green's function as the answer at a position r to an impulse excitation at position $r\prime$ of the system. Of course, having this information for all the sites allows to understand the physics of the system and to get the transport observables.

Eq. (2.17) is meaningful provided the matrix $E - H$ is nonsingular to let the inversion possible for all the energies out of the spectrum. The discrete eigenenergies of the Hamiltonian are the poles of the Green function whereas the continuous spectrum represents a cut. To avoid these real [6] singularities, we introduce the retarded and advanced Green functions as follows [7]:

$$G^r(E) = \frac{1}{E - H + i\eta}, \qquad G^a(E) = \frac{1}{E - H - i\eta} \tag{2.20}$$

η is a small real number and the limit $\eta \to 0^+$ is implicitly meant in those expressions. The retarded and advanced Green function correspond in the position representation to an outgoing and incoming wave respectively. It is easy to notice that they are related by the following relation:

$$G^a(E) = G^{r\dagger}(E) \tag{2.21}$$

---

4. we take generally the lattice spacing $a = 1$

5. for the shifted band which corresponds to the neighborhood of zero in the real case

6. When the Hamiltonian is Hermitian, the spectrum of H is real

7. So far, The Green function we introduced is energy dependent. it is related to the time dependent Green function via Fourier transform:

$$G^r(E) = \int_{-\infty}^{+\infty} G(t) e^{i(E+i\eta)t} dt$$
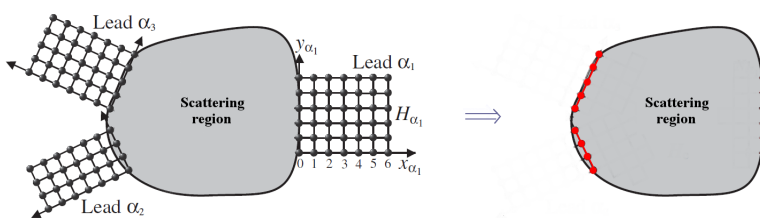
Figure 2.2: The size of the problem is reduced by changing the leads by their self energy. The red points symbolize the effect of the lead, contained in the self energy

Partition of the Hamiltonian

The Hamiltonian describing the quantum transport in the system we may study, could partitioned to three main parts as follows:

$$H = H_s + H_L + H_c \tag{2.22}$$

H_s represents the scattering region and contains all the information on the on-site potentials and the hopping terms between them. It may be seen as a closed system of finite size. We refer to it as the Hamiltonian of the central system or the scattering region.

H_L is the Hamiltonian of the leads (Left and right). It describes the reservoirs of electrons. Its matrix has an infinite dimension.

H_c is the coupling Hamiltonian which describes how the system is connected to the leads.

Studying transport and electrons scattering by potential involves open systems described by infinite dimension Hamiltonians. To avoid the impossible task of inverting this Hamiltonian to obtain the Green function (using Eq. (2.20)), we proceed to this partition of the Hamiltonian to get rid of the huge parts composed by the leads and the coupling matrices. In fact, we do not need the Green's function of the whole system, only the scattering region matters. The way this is done, as we shall see, is exact. The effect of the leads is not omitted. It is taken into account via its effect on the central system, this effect is contained in what we call the self-energy. This quantity will be introduced in details later.

We can explain this operation as follows: let us take the simple case of a system connected to one lead. The coupling matrix will be denoted τ. The Green's function reads:

$$\left(\begin{array}{c|c} G_l & G_{ls} \\ \hline G_{sl} & G_s \end{array} \right) = \left(\begin{array}{c|c} E - H_l & \tau \\ \hline \tau^T & H_s \end{array} \right)^{-1} \tag{2.23}$$

As we can see the Green's function has the same partition as the Hamiltonian one. Using the fact that $[E - H]G = 1$ leads after straightforward manipulations to the following result for the Green's function submatrix of interest G_s:

$$G_s = \frac{1}{E - H_s - \Sigma} \tag{2.24}$$

and the self energy Σ is given by [8] :

$$\Sigma = \tau^\dagger \frac{1}{E - H_l} \tau \tag{2.25}$$

This self energy characterizes the lead and how it is connected to the central system.

We can summarize the main results of this operation as follows :

– The size of the problem is reduced to the one of central system Hamiltonian.
– Only a the submatrix G_s is for interest to get transport coefficients. It has finite size (the same as H_s, the scattering region)

---

8. A small imaginary part is added to E. It is positive for the retarded self energy and negative for the advanced one. We should note that we do not need to do this for G_s since Σ is complex

– To get G_s, all what we need is to replace the H_s by an effective complex Hamiltonian. $H_s \to H_{\text{eff}} = H_s + \Sigma$. Moreover, The effective Hamiltonian is energy dependent.
– The self energy Σ has finite size (The same as H_s). It is a complex matrix, and contains all the "effect" of the lead on the central system.
– In case of several leads, we can show that the total self energy is the sum of all the self energies of each lead.

The self energy

As we saw, the self energy is the key to reduce the infinite size of the Hamiltonian. This complex matrix can be obtained by several methods for the case of uniform 2D leads. We can find in appendix C a general method for non conventional uniform lattices.
A uniform 2d lead has a self energy matrix given by:

$$\Sigma(i,j) = \frac{2t_c^2}{N+1} \sum_{m=1}^{n=N} \sin(\frac{m\pi}{N+1}i) \sin(\frac{m\pi}{N+1}j) \zeta(E_m, m) \tag{2.26}$$

and the function $\zeta(E_j, m)$ is:

$$\zeta(E_m, m) = \frac{1}{2t_l^2}(E_m - i\sqrt{4t_l^2 - E_m^2}), \; if \; |E_m| < 2t_l \tag{2.27}$$

and

$$\zeta(E_m, m) = \frac{1}{2t_l^2}(E_m - s\sqrt{E_m^2 - 4t_l^2}), \; if \; |E_m| > 2t_l \tag{2.28}$$

Here, we put $s = sign(E_m)$, t_l the hopping term in the lead and the coupling matrix is proportional to the identity matrix :

$$\tau = t_c I$$

$E_m = E + 2\cos(\frac{m\pi}{N+1})$, is the energy left for the longitudinal motion [9].
In general, the Self energy matrix is complex. In fact, the complex elements of Σ describe the conducting channels in the lead whereas the real elements describe the evanescent modes. The ratio between the closed channels to the open ones is fixed by the Fermi energy. As we may simply understand, the channels are completely closed at the bottom of the band and completely open at the middle of the band (The half filling limit). Because of the dispersion relation of the discretized model, increasing energy beyond the middle of the band will start to close the channels.
The self energy is related to the surface Green's function of the lead. That is to say, it gives the Green's function elements of the sites connected to the closed system at the surface of lead.
After we did define the retarded and advanced self energies, let us introduce the broadening function or linewidth operator. For the lead p we associate the matrix:

$$\Gamma_p = i(\Sigma_p - \Sigma_p^\dagger) \tag{2.29}$$

It is a real matrix which contains the imaginary part of the retarded self energy (up to a factor 2).

Fisher-Lee Formula

We already expressed the conductance of a system using the transmission matrix obtained directly from the scattering matrix Eq. (2.7). The importance of the Green's function formalism is to reduce the size of the system to only the size of the scattering region. The zero-temperature conductance within this formalism is given by the Fisher-Lee formula [21] based on the matrix defined in the previous section. The transmission from lead p to lead q reads:

$$T_{pq} = \text{Tr}[\Gamma_p G_{pq} \Gamma_q G_{pq}^\dagger] \tag{2.30}$$

---

9. the eigenenergies for the transversal confinement is :

$$\epsilon_m = -2\cos(\frac{m\pi}{n+1})$$

Γ_p, Γ_q are the broadening matrices of the two leads and G_{pq} a submatrix of the Green's function matrix. This last contains the Green's function elements between the sites of the surfaces p and q. Comparing this relation (with only left and right leads) to Eq (2.7) , we deduce the transmission matrix t:

$$t = \sqrt{\Gamma_L} G_{LR} \sqrt{\Gamma_R} \tag{2.31}$$

L, R refer to respectively left and right.
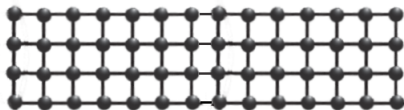
Figure 2.3: A uniform quasi-1D system. Any slice can be considered as the scattering region and what remain as the left and right leads.(the longitudinal size is ∞)

2.1.5 Application to quasi 1D wire

It may be interesting to apply the relations we introduced so far in a simple example: A uniform quasi-1D system. The system as shown in Fig. (2.3), is a quasi-1D lead obtained by connecting finite size slices. The scattering region we consider here in this example will be the central slice (containing N sites). The hopping term t_h is taken constant and equal to one everywhere($t_h = 1$). In this case, the matrix τ which couples each lead to the system is the identity matrix. The Green's function of the system (central region) is given by :

$$G = \frac{1}{E - H - 2\Sigma^r} \tag{2.32}$$

The factor 2 is due to the fact that the left and right self energies are added to the same sites in the central system(and of course $\Sigma_L = \Sigma_R$). As it can be noticed in Fig. (2.4), the transmission is quantized and equal to the number of open channels (step-like profile). The same curve could be obtained by imposing that the imaginary part of the self energy is not zero ($\Rightarrow \Gamma \neq 0$). This condition is verified if:

$$|E + 2\cos(\frac{m\pi}{n+1})| < 2 \tag{2.33}$$

Each mode indexed by m verifying this relation is a conducting mode and therefore , the transmission of the system is directly given by the biggest mode index. We can notice that the transmission
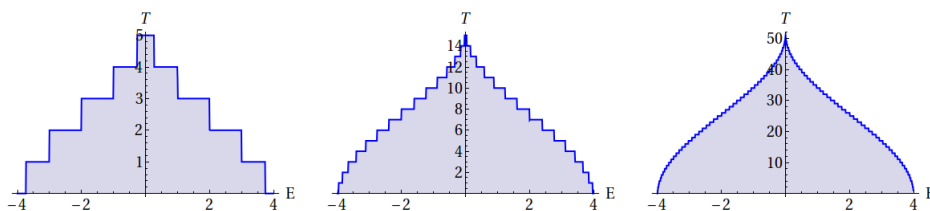
Figure 2.4: Transmission of a uniform quasi-1D system of wide (respectively from left to right) 5, 15, 51 sites. At the middle of the band (half-filling limit) all the channels are open. The conducting band is $[-4, 4]$ where $t_l = 1$ is considered.

of the system doesn't increase with energy on the whole band. In fact, after the half filling limit, channels starts to close. This is of course due to the discrete nature of the model which makes the dispersion relation different from the continuum limit [10]. Fig. (2.4) shows symmetric profile for the transmission which means that the transport of holes is similar to the conduction of electrons. The profile of transmission for wide systems converges to the following function:

$$\frac{T}{M} = \frac{1}{\pi} \arccos(\frac{-2 + |E|}{2}) \tag{2.34}$$

M is the total number of modes.
This function could be simply deduced from the condition (2.33). However, it is solely valid for this kind of confinement (uniform transverse confinement). For other type of confinements (parabolic for example) we only need to change the eigenenergy $-2\cos(m\pi/(n+1))$ with the corresponding relation for the new confinement in rel 2.33.

2.2 Dyson equation and recursive Green's function

Although we reduced the size of the problem of electrons transport to the size of the scattering region, it is still hard to get its Green's function by direct matrix inversion. Moreover, we only need the Green's function submatrix of the sites on the surfaces connected to the leads, and all the other elements all useless to the conductance calculation. For this reason, we proceed recursively and construct the scattering region slice by slice (or sometimes site by site. See[25]). The tool to do this recursion is based on the Dyson equation.

2.2.1 Dyson equation
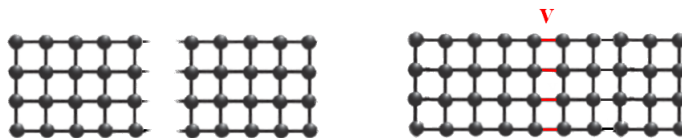
Figure 2.5: The whole system is constructed by gluing disconnected parts. The calculation of the Green's function is easily obtained using the Dyson equation in a recursive algorithm

The purpose of this part is to express the Green's function of a system starting from the knowledge of the disconnected subsystems Green's function. The Dyson equation states that if two disconnected subsystems are "glued together" via the coupling matrix V, the Green's function G of the whole system is related to the Green's function g of the disjoint subsystems via the following important relation:

$$G = g + gVG \tag{2.35}$$

To understand better this equation, the example illustrated in Fig. (2.5) shows the situation this relation is applied to. In fact the Green's function g of the subsystems is block diagonal since there is no communication between them. Each block represents the Green's function of each subsystem.

$$g = \begin{pmatrix} g_{11} & 0 \\ 0 & g_{22} \end{pmatrix} \tag{2.36}$$

---

10. In this discrete model, increasing the wavenumber enhances the energy in the first half of the conduction band and lowers energy in the second half of the band

after being connected, the new Green's function for the "glued systems" has the following form:

$$G = \left(\begin{array}{c|c} G_{11} & G_{12} \\ \hline G_{21} & G_{22} \end{array} \right) \tag{2.37}$$

As we can see, G is a full matrix and contains all the elements of the Green's function between all the sites of the scattering system. Calculating all these terms seems to be hard task for programs needing this matrix at different energies(huge time of calculation and memory size). Fortunately, we only need the surface Green's function elements to express the conductance using the Landauer-Butticker formula. Restricting the calculation on these elements can reduce the time of calculation by factor which can exceed 1000.

2.2.2   Recursive Green's function

The way these elements are obtained is by projecting the Dyson equation Eq. (2.35) between the slices 1 and N [24]
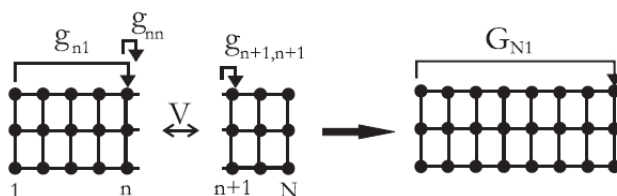
Figure 2.6: The different Green's function submatrices before and after connection. The Green's function is obtained recursively while the system is constructed slice by slice using the Dyson equation [24]

$$\begin{align} G_{N1} &= \langle N|G|1\rangle \tag{2.38} \\ &= \langle N|g|1\rangle + \sum_{\alpha\beta}\langle N|g|\alpha\rangle\langle\alpha|V|\beta\rangle\langle\beta|G|1\rangle \tag{2.39} \\ &= \langle N|g|n\rangle\langle n|V|n+1\rangle\langle n+1|G|1\rangle \tag{2.40} \\ &= g_{Nn}V_{n,n+1}G_{n+1,1} \tag{2.41} \end{align}$$

In this calculation, the Green's function between disconnected parts is zero and therefore $g_{N1} = 0$. More, the hopping matrix V has nonzero elements only between columns n and $n+1$ that is why the sum in (2.40) is reduced to only one term. Of course, the work is not finished yet since the final relation (2.41) contains the unknown matrix $G_{n+1,1}$. To obtain this matrix we proceed again and do the appropriate projection of the Dyson's equation. This procedure can be continued again until we obtain a closed set of equations. The result here reads:

$$\begin{align} G_{n+1,1} &= g_{n+1,n+1}V_{n+1,n}G_{n1} \tag{2.42} \\ G_{n1} &= g_{n1} + g_{nn}V_{n,n+1}G_{n+1,1} \tag{2.43} \end{align}$$

Handling together these equations, we can write the following matrix:

$$G_{n+1,1} = [1 - g_{n+1,n+1}V_{n+1,n}g_{nn}V_{n,n+1}]^{-1}g_{n+1,n+1}V_{n+1,n}g_{n1} \tag{2.44}$$

From Eq. (2.41) and Eq. (2.44) we obtain the wanted submatrix G_{1N} in terms of the isolated parts Green's function. [11] Now we can understand how to build our system and get the necessary

---

11. In the recursive procedure to obtain the submatrix G_{1N} a lot of elements have to be used. Nevertheless, this operation uses only product and inverse of matrices of a small size which is an operation lighter than the hard task of inverting the matrix of the whole system.

quantities to compute the conductance. It appears as follows: We first start by the left semi-infinite lead whom the self energy is already known. We attach a first slice and compute the new Green's function elements. We do it again and again (attaching new slices from right) until we reach the right semi-infinite lead. Of course, the slice we add each time is different since it contains the on-site potential at that position. At the end, the ensemble of all the slices shows the picture of the whole potential defining the scattering region (the QPC in our case). More details with example could be found in appendix B.

2.3 Including the charged tip
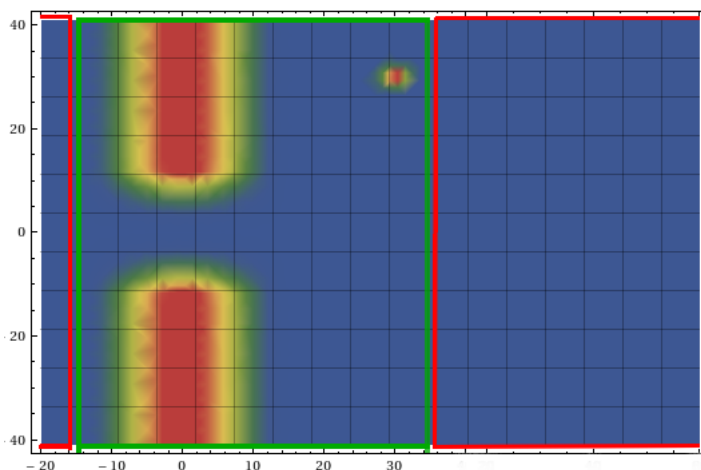
Figure 2.7: In the presence of the tip, we can consider the QPC+Tip as the new scattering region(Green box). In this case the attached leads are perfect(red boxes) since the tip is taken into account in the scattering region. In this figure, red color refers to regions of high potential.

In the Scanning Gate Microscopy, a charged tip, $50-80$ nm above the 2DEG, creates a region of depletion in the electronic charge density. We mimic this effect by means of a short range potential in the right lead. In fact, putting a potential on some sites with a Lorentzian, Gaussian or any others forms and changing its position reproduces the figures of the interference pattern with the same inter-fringes distance as the experiments (Half the Fermi wavelength).

The procedure to include the effect of this diffusion potential in the Green's function recursive algorithm is very simple. We only need to consider a new scattering region ranging from the end of the left lead to the slices containing the tip as explained in Fig. (2.7). The way we compute the Green's function is the same as explained in the previous section and in the appendix. Nevertheless, This method suffers from the fact that for each position, the Green's function of the scattering region needs to be computed again. If we add to this the need of doing this procedures at different energies (to include temperature for example) and that for every new position of the tip (in the longitudinal direction) the size of the scattering region becomes bigger, we quickly face very long time of calculation and huge amount of memory use. We can always improve such procedure to avoid the calculation of the Green's function from the beginning but still not enough and the algorithms are not the easiest we can do.

Method using imperfect leads

This thesis owes too much to the method we will present here. Not only to the time it allowed us to save or the algorithms complexity we avoided but to the better understanding of the physical phenomenon in SGM experiments and the analytical formulation of the problems with their solution. Moreover, it helped us a lot to foresee unexpected interesting phenomena. This method is easy to be understood and to be implemented numerically. We remind that in the previous method, as
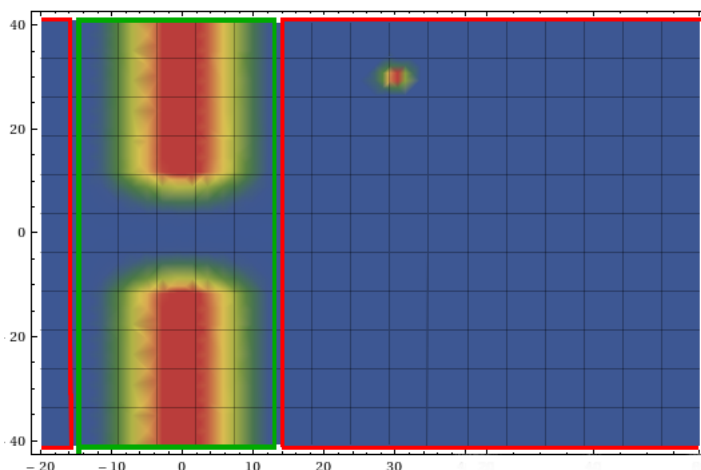
Figure 2.8: Here we consider a scattering region formed by the QPC (Green box) and the tip is included within the right lead (refer to it as imperfect lead) red box .

explained previously, the leads are always perfect (semi-infinite perfect lead) and the scattering region changes each time the tip is moved. Here, we do things the other way: We keep the same scattering region (only the potential region forming the QPC, see Fig. (2.8) to which we need to attach imperfect leads. By "imperfect" we refer to the presence of the tip in the lead. In fact, taking into account the effect of the tip on the right semi-infinite lead affects the right self energy Σ_r and the right broadening matrix Γ_r. These new quantities are very easy to obtain thanks to Dyson equations. The procedure to compute the Green's function with this method is pretty simple: We start the recursive algorithm from left (including the self energy of the left lead) and add slices one after one from the right to construct the central region (QPC) and do this until the last slice where we need to include the right self energy. The quantities obtained so far, remain the same for all the tip positions, only the last step will change: in fact for each tip position the right self energy we include is different and needs to be updated. This task is also very easy if we do it the following way:

Because of the semi-infinite nature of the lead, adding a perfect slice from left is equivalent to moving the tip one step to the right(see Fig 2.9). Of course this is valid for all the transverse positions of the tip.
If we note the self energy with the tip at position (x, y) as $\Sigma(x, y)$ then we can write the following relation expressing the new self energy when the tip is moved one step to the right :

$$\Sigma(x + 1, y) = \frac{1}{E - H_0 - \Sigma(x, y)} \qquad (2.45)$$

H_0 is the Hamiltonian matrix of a perfect slice.
In this relation, you can notice that the hopping factor in the lead is taken to be equal to one $(t_h = 1)$ so that the coupling matrix between slices is the identity matrix. Of course, the coupling matrix to the central system could be different: all what we need is to multiply the Eq. (2.45) by the correct coupling matrix and its transpose from right and left respectively.
To start using the recursive relation 2.45, we need the first element. This is obtained from a perfect semi-infinite lead to which we add a slice containing the tip. The self energy after doing this step is obtained as follows:

$$\Sigma = \frac{1}{E - H_0 - V - \Sigma_{\text{perfect}}} \qquad (2.46)$$

V is a sparse matrix which contains only one non-zero element : $V_{ij} = v\delta_{ip}\delta_{jp}$. P is the ordinate of the tip and v is its potential. Σ_{perfect} refers to the self energy of a semi-infinite perfect lead [27]
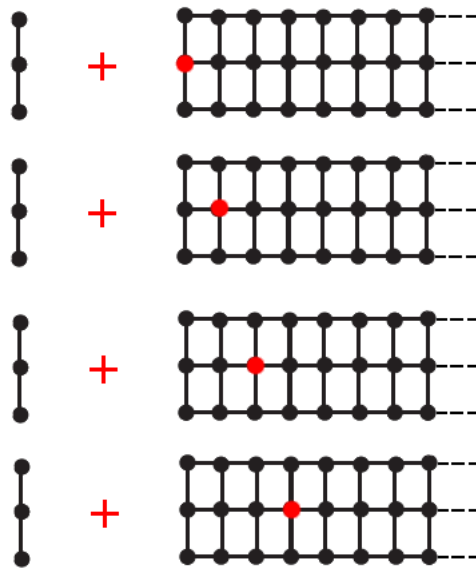
Figure 2.9: Each time we add a perfect slice to a semi-infinite lead from the left, the situation is equivalent to moving the charged tip (Red color) one step to the right

[28].
You can notice that the procedure as explained above works for a single site potential (for the tip). Fortunately, only few changes are needed to apply the previous procedure to the case of an extended tip: All what we need is to add many slices to define the potential of the tip. In fact, each slice should contain the right potential on the right site such that after adding few slices the profile of the potential is completely "painted". The way we change the position of the extended tip is the same as for the single site tip. All what we do is to add perfect slices.

Generalized Fisher-Lee Formula

The method detailed above, explaining the easiest way to compute the conductance in the presence of the charged tip, can be seen as a generalized Fisher-Lee Formula (see Eq. 2.30). In fact, the general form of the formula remains unchanged and expressed using Green's function and a broadening matrix. Thus, it considers the general case of scattering region connected to non-ballistic leads. This generalized relation is expressed as follows [26]:

$$G = \frac{2e^2}{h}\text{Tr}(\tilde{\Gamma}_l G \tilde{\Gamma}_r G^{\dagger}) \tag{2.47}$$

By non-ballistic, we refer to non-uniform leads, leads with disorder, or the case of leads with tip. The tilde ˜ in this formula can be omitted since it is only to remind that the leads could be non-ballistic and therefore different from the usual case we consider in the simple Fisher-Lee formula. The broadening matrix $\tilde{\Gamma}$ is always defined using the self energy of the lead :

$$\tilde{\Gamma} = -i(\tilde{\Sigma} - \tilde{\Sigma}^{\dagger}) \tag{2.48}$$

With all the tools introduced so far, we are ready to run efficient programs to compute the conductance of nano-systems of different shapes and different kind of scattering potentials. The effect of the charged tip on the conductance can be obtained at the same time. In the next section we will comment the figures of the interference pattern obtained by this technique of Scanning Gate Microscopy.

Chapter 3

Quantum transport and numerical simulation

Contents

Summary of chapter 3

After introducing the tools of numerical simulations and the recursive Green's function algorithms in the previous chapter we start here to analyze the results of these algorithms. This chapter is important for the analytical treatment of the SGM problem. It will provide the justifications of the simplifications adopted to obtain a solvable model. We first look at different realistic QPC models and compare their results. We find that, qualitatively, for the same QPC opening, it does not matter which QPC model we do take. They all exhibit more or less the same interference pattern of fringes spaced by $\lambda_F/2$ (of course with slightly different oscillating amplitude). The figures of the change ΔG as a function of the tip position, show the existence of two regimes at zero temperature:

  – **Case of completely open QPC,** $T^\circ \sim 1$: In this case, the tip always reduces the conductance of the QPC ($\Delta G < 0$) with a quick decay of the fringes amplitude.
  – **Case of less opened QPC,** $T^\circ < 1$: In this case, ΔG oscillates between positive and negative values with a slower decay law for the fringes.

These results are obtained assuming realistic models on a lattice, where the leads are taken as wide as possible to avoid the backscattering from the borders of the leads.
We focus in this thesis on the first mode of conduction (first plateau), but we give the numerical simulation of the second plateau as an example of the application of our algorithms to higher modes of conduction.
After discussing the different models of the QPC, we switch to the different models of the landscape induced by the tip in the 2DEG. We show that the tip, capacitively coupled to the 2DEG induces an extended charge density, well fitted by a Lorentzian curve. However, the numerical simulations assuming a Dirac delta function as a model for the tip exhibit more or less, the same interference pattern and position dependence of ΔG. Moreover, the dependence on the tip voltage, shows the same kind of resonances and the curves of $\Delta G(v_{tip})$ are very similar. This discussion concerns the tips with a small extension, less than the electrons wavelength. This conclusion helps us in a sense that the use of delta tip models saves a lot of time and is much more simpler to simulate than realistic models. A simpler model for the QPC and the tip makes the description of the fringes much more easier and leads to much more clear conclusions.
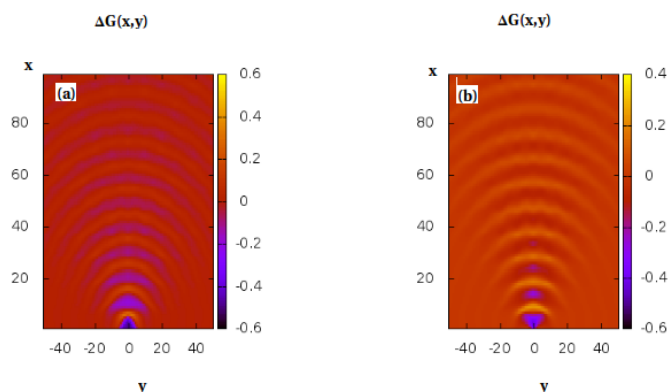
Figure 3.1: Spatial map of the zero temperature conductance change $\Delta G(x, y)$ in units of the quantum conductance $\frac{2e^2}{h}$ for two different models of the QPC. (a) a Wide-narrow-wide model shown in Fig (1.7). (b) Potential $V(x, y)$ defined with Eq. (3.1). The effect of the tip on the 2DEG is modeled with an on-site potential at position (x, y).

3.1 Zero temperature conductance change

The algorithms we use to calculate the conductance are very easy to implement: The new method of expressing the conductance by means of the Green's function using leads with tip(See previous chapter), uses simple mathematical operations, restricted to inverse and product of matrices of a small size. The way the recursive procedure is fulfilled to spatially map the zero-temperature conductance change shows no complexity and doesn't necessitate neither huge amount of memory nor long time of calculation, if the procedures detailed in the previous chapter and in the appendix B are followed.

3.1.1 Comparing different QPC models

In Fig. (3.1), we applied the method of recursive Green's function to two different QPC models: Figure (a) shows the change in the zero-temperature conductance for a wide-narrow-wide model(see Fig 1.7). Figure (b) gives the same quantity with a more realistic model, where the QPC is given by the following potential[32]:

$$V(x, y) = \begin{cases} a\frac{1}{2}y^2(1 - 3(\frac{2x}{l})^2 - 2|\frac{2x}{l}|^3)^2 & \text{if} \quad |2x| < l \\ 0 & \text{if} \quad |2x| > l \end{cases} \tag{3.1}$$

a is a constant which, for a given Fermi energy E_F, gives the number N of conducting modes in the QPC as follows:

$$a = \frac{E_f^2}{2(N - \frac{1}{2})^2} \tag{3.2}$$

l is a parameter which determines the length of the QPC.

The two models are obviously quiet different: The first one has uniform parts, assumes hard wall boundary conditions and the coupling of the QPC to the leads is abrupt. The second model is chosen to be more realistic and approaches better the adiabatic limit. The transverse potential in this model is chosen parabolic to allow an analytic treatment for the Schrödinger equation as a 1D wave function in an effective potential(see Chapter 1 or the references [6] and [11]). At the ends of the QPC ($|x| = l$), the potential V vanishes in a smooth way to avoid electrons reflection due to abrupt changes in the potential between the lead and the QPC. This potential has another advantage: The number of modes is controllable via the formula Eq. (3.2) which facilitates the verification of the numerical program.

Conclusions from comparing the different QPC models

First, we note that these programs reproduce the experimental results of Scanning Gate Microscopy done on very clean samples [18] with very high mobilities. Indeed, we obtain an interference pattern of fringes spaced by half the Fermi wavelength $\frac{\lambda_F}{2}$. We can see from the numerical values of ΔG that the effect of the charged tip on the conductance can be positive as it can be negative: Indeed, the tip reduces the conductance of the system because the electrons crossing the QPC are backscattered by the potential induced by the tip. Nevertheless, at some positions, the tip effects is to enhance the conductance which can be explained only within the quantum mechanics theory as an interference effect: An electron injected by the left reservoir can either be reflected by the QPC or crosses the scattering region to be, probably, reflected back later by the tip. The two probability amplitudes for these two coherent paths can interfere constructively to increase the conductance of the whole system. It is clear that this situation depends on the position of the tip and thus the positive and negative effects of the tip alternate spatially to reproduce fringes of interference. The conclusion from this explanation of the interference pattern is that the system acts like a 2D Fabry-Perot interferometer.

The analysis of the two Fig 3.1 (a) and (b) shows that, qualitatively, the two QPC models give, more or less, the same pattern and that the effect of the tip on the zero-temperature conductance does not depend too much on the details of the QPC. Eventually, the numerical results show a difference in the effect amplitude and there may be a phase difference too. Of course, we do not expect them to be exactly the same. All here, we compare two models having the same(or at least close) conductance in the absence of the tip. The key to understand why different models can exhibit the same tip effect is temperature: We claim that the details of the QPC do not matter too much in the SGM pictures only at zero-temperature. In fact, at zero temperature, the conductance is given by:

$$G = \frac{2e^2}{h} \sum_{i=1} T_i(E_F)$$

Where $T_i(E_F)$ are the different modes of transmission at the Fermi energy. That is to say, only electrons at the Fermi energy fixes the conductance. Since a QPC can be interpreted with its scattering matrix, and at zero temperature, this scattering matrix is needed only at Fermi energy, different QPC models can have the same S matrix at E_F even though they are different at other energies and therefore the details of the model which gives this S-matrix are irrelevant.

If the temperature is not zero, the conductance reads:

$$G = \frac{2e^2}{h} \int_0^\infty (-\frac{\partial f}{\partial \epsilon}) T(\epsilon) d\epsilon \tag{3.3}$$

f is the Fermi-Dirac distribution.

We understand from this equation that not only the electrons at the Fermi energy are important but all the electrons with an energy $k_b \mathcal{T}$ far from the Fermi energy have a considerable weight to fix the conductance. Now, since different models can have the same transmission at a given energy but not the same profile at other energies, it is clear that the effect of the tip in each model is not expected to be the same in general.

We already mentioned that the system QPC-Tip acts like a Fabry-Perot interferometer. In our case, the tip reflects only a small amount of the electronic flow and this amount decreases at large distances from the QPC because of the 2D nature of the electronic gas. That is way it is better to call it "Open" Fabry-Perot interferometer. The decay law of the tip effect with distance is one of the important questions we want to answer in the coming chapters.

3.1.2   Conductance change as a function of the tip position

We focused the discussion on the comparison of the results for different QPC models without taking into account the details of the model itself. Here, we discuss the results for the potential model $V(x, y)$ defined previously in Eq. (3.1)

For each picture we obtain, we need to specify the conductance of the system in the absence of the tip noted generally G°. Of course, we need to study the effect of the tip for different values of G° that is to say, for different QPC openings.
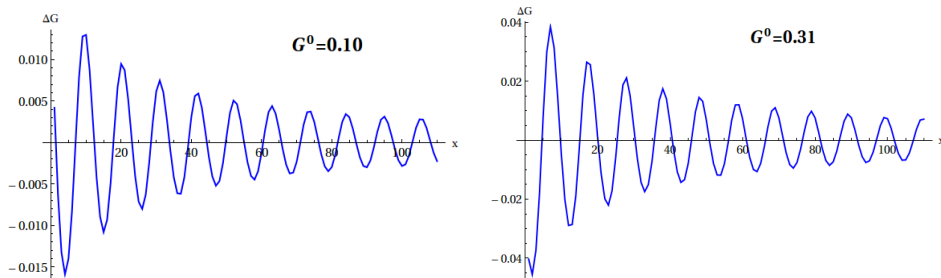
Figure 3.2: ΔG as a function of the tip position for a pinched off QPC
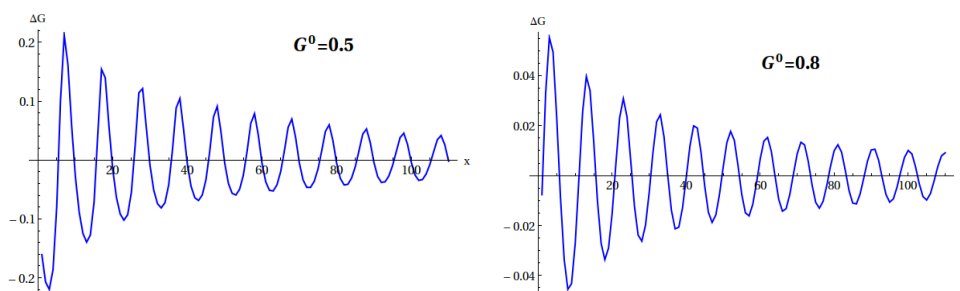
Figure 3.3: The effect of the tip along the central axis of the system for the first mode of conduction. The figures are given for different cases of the QPC opening. The conductance is expressed in units of $\frac{2e^2}{h}$. Lead width $N = 2001a$.The tip is a Dirac delta function (on-site potential)
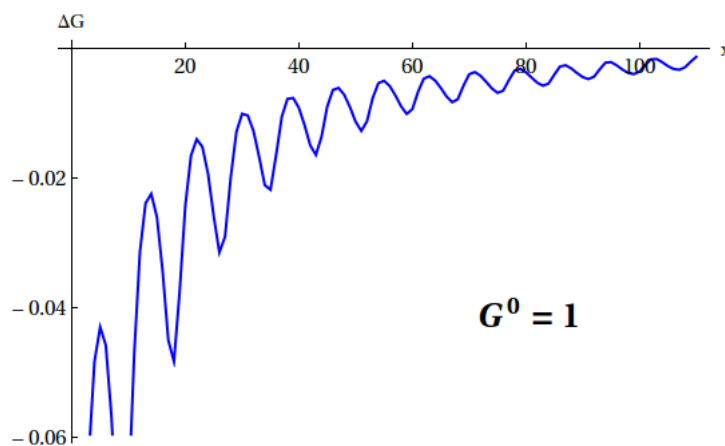
Figure 3.4: The conductance change ΔG as a function of the tip position.Case of a transparent QPC (first plateau, $G^\circ = 1$). The position of the tip is restrained to the axis $y = 0$. The effect of the tip is generally to reduce the conductance ($\Delta G < 0$). The simulation is done assuming an on-site tip potential. The electron wavelength $\lambda_F = 16a$ and the leads are very large: $N = 2001a$ (a is the lattice step). The conductance is in units of $\frac{2e^2}{h}$. The QPC potential is $V(x,y)$ defined with Eq. (3.1).

We remind that the quantity we are looking to is defined as :

$$\Delta G(x,y) = G - G^\circ$$

We show in Fig. (3.2), (3.3) and (3.4) the results of the numerical simulations on the potential $V(x,y)$ defined above[1] where the data are restrained to the central axis of the QPC. The figures

---

1. For optimization, the potential is cut when it exceeds few times the Fermi energy.

are obtained for different values of the QPC opening G°.

First, we notice that the profile of $\Delta G(x)$ (we took $y = 0$) is an oscillating function with a decaying amplitude and a pseudo-period equal to half the Fermi wavelength $\frac{\lambda_F}{2}$. The interesting thing we notice is that the effect takes both signs for pinched off QPC whereas it is always negative at full transmission ($T^\circ = 1$). We already explained why the tip can enhance the conductance of the system: It is an interference effect, that is why figures such as for Fig. (3.2) can show an effect oscillating around zero. However, systems with high transparency ($G^\circ \simeq 1 \times \frac{2e^2}{h}$) have a different behavior: The effect of the tip on the zero-temperature conductance of the system begins to be more negative then positive when we approaches full transmission. It becomes completely negative on the first plateau of conduction ($G^\circ = 1 \times \frac{2e^2}{h}$) which means that the charged tip reduces the transmission even though the transport of electrons still obeys to quantum mechanics and the paths of the careers are still coherent. The explanation of this situation is not complex: The system without tip is completely transparent for the first mode of conduction and therefore the presence of the tip can not enhance the transparency of this mode (because it is completely open) and obviously can not open a new mode because it is far away at higher Fermi energies. In conclusion, the tip can only reduce the conductance($\rightarrow \Delta G < 0$) at full transparency. In addition, the decay law of the effect is quite different than the case of less opened QPC. The fringes decay faster and have a very small amplitude.

Effect of the charged tip on the higher conducting modes

In this discussion, we mainly talked about the first mode of conduction. It is easy to understand that most of the arguments apply for the higher modes. However, the 2D maps of the conduction changes have a different angular dependence. For example, Fig. (3.5) shows the results of numerical simulation for the zero-temperature conductance change of the SGM of the second conducting mode. The system without tip is transparent for the two first modes of conduction (second plateau). We still obtain an interference pattern of fringes spaced by half the Fermi wavelength. Moreover, the effect of the tip is mostly to reduce the conductance ($\Delta G < 0$) because we can not open a new mode. Nevertheless, the effect of the tip on the second plateau of conduction is different from the first plateau as it can be seen just by comparing the two Fig. (3.5) and (3.1 b): Two relevant directions seem to emerge in the case of two modes of conduction: $\pm 45°$. In the direction of these two angles, the effect of the tip is higher than in other directions. This behaviour is similar to what was obtained experimentally in [33]. We can do the same, just by changing the parameters of the potential in Eq. (3.1) [2], to obtain the zero-temperature change for the third plateau of conduction or even for higher modes. Finally, may be we should remind that the figures obtained so far are the simulation of SGM experiments using an on-site potential for the tip. This means that the tip is less than a short range potential: it is only non-zero on a unique site. This is not a bad approximation and the numerical results seem pretty good and enough to explain all the physical aspects of the experiments. In fact, this assumption is valid since the wavelength of the electrons (around 37 nm) is bigger than the range of the potential induced by the charged tip. In other words, the electron do not see the details of lengths smaller than half the Fermi wavelength that is way the tip of small range can be considered as an on-site delta potential. I present more details on the effect of the tip in the following section.

3.2   The charged tip effect

In SGM experiments, an AFM charged tip induces a potential landscape in the 2DEG due to the capacitive coupling of the tip to the electrons which are displaced. This change in the density of charge modifies the physical quantities of the system such as the conductance. This technique using an AFM charged tip is widely applied to scan different type of systems: Quantum rings [34][35][14], quantum point contacts [18] [33] and carbon nanotubes [36]. In all those experiments, the effect of the tip on the system is the key to understand the physics behind the acquired data. In our case, the QPC is obtained using 2DEG, and what we should know is that the gas of electrons is around

---

2. We can keep the same parameters and change the Fermi energy to get smaller Fermi wavelength. Numerically, at higher energies, the discrete nature of the lattice gives a dispersion relation different from the continuum and therefore some lattice effect can occur.
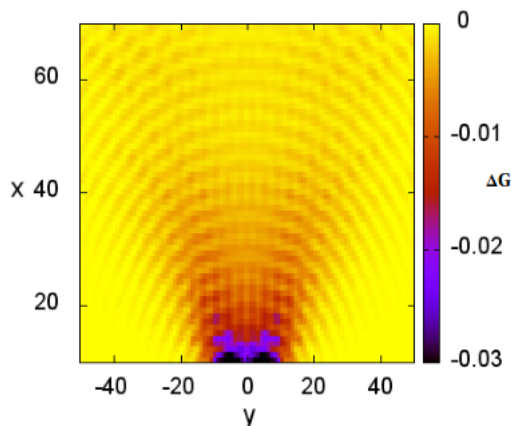
Figure 3.5: The map of the zero-temperature conductance change for the second plateau of conduction($G° \simeq 2$). The effect of the tip is mostly visible in the directions $\pm45°$. The tip model is a delta function potential.

50 nm beneath the surface and the AFM tip moves at around 30 nm above the same surface as simplified in schematic in Fig. (3.6). Because of this, we expect the density of charge to be depleted over a long range region and the potential induced by the tip to have an extended profile centered around its position. It is important to know the profile of this potential in order to use the correct form when doing numerical simulations.

Before talking about the simulation techniques and the models of the tip we use, we need to understand some aspects about the experimental issues when we use an AFM charged tip to scan the change in conductance of electrons through nano-constrictions. The theses of Brian James LeRoy [17] and Mark Topinka [37] are highly recommended for more details on the experimental work.

Electronic charge depletion requirement

In most experimental setups, the tip is biased negatively in order to chase away the electrons and deplete the charge density. We dispose of two parameters to change the size of the depleted region: The hight and the voltage of the tip. The images of scanning gate microscopy of conductance changes are obtained because the tip backscatters some of the electrons flow towards the QPC. This means that the requirement to acquire a signal of a change in the conductance is obviously to have a depletion region which is the origin of the electrons backscattering. Therefore, if the potential of the tip is not strong enough to deplete the charge density beneath the sample surface, no image of significant change in the conductance can be obtained. In [38] [17], The experimental team acquired several images of the conductance change scan for different values of the tip voltage going from -1.5 V to -4V and noticed that no change in the pattern profile is noticeable for small tip voltages and it is only when the voltage reaches -2.5V that a significant change is registered. This means that the small values of the tip voltage do not deplete the charge density in the 2DEG and its effect is no more than creating a small bump which is not enough to backscatter the electrons. It was also signaled [39] that when they change the potential voltage they do not acquire significant signal for some range of the potential and at some value they quickly start to see a good picture of conductance change. This means that $\frac{d(\Delta G)}{dV_{Tip}}$ is very big at this value and the change is fast.

Another way to show the importance of creating a depletion region in the 2DEG is to compare different pictures of the change in conductance obtained for different tip heights and at fixed voltage. Fig. (3.7), shows the spatial change in conductance at different heights of the charged tip [17]. This
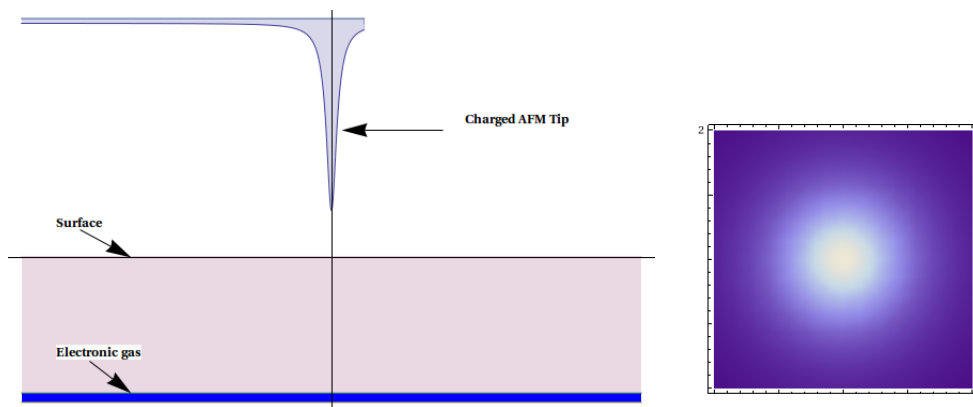
Figure 3.6: left figure: AFM tip above a semiconducting heterostructure. The 2D electronic gas (2DEG) is around 50 nm beneath the surface and the tip is around 30nm above this surface. The electronic gas is depleted because of the capacitive coupling (electrostatic repulsion) to the tip. This depletion in the electronic gas (right figure) acts like a potential with a circular symmetry and decaying from the center.
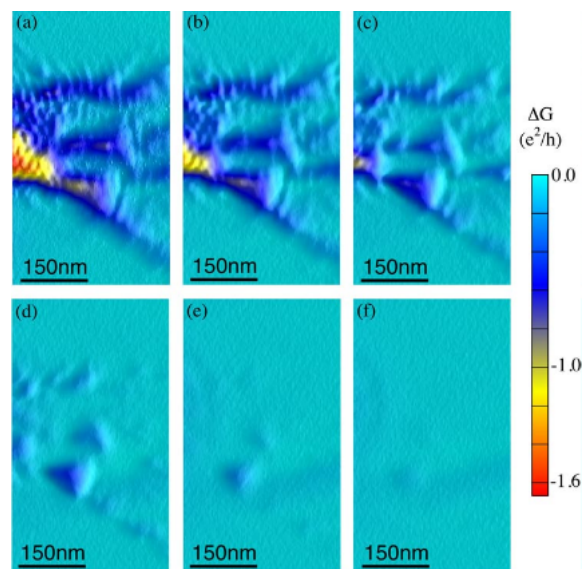
Figure 3.7: 2D scan of the conductance change for increasing heights of the tip above the surface of the sample:(a) 10 nm, (b) 15 nm,(c) 20 nm, (d) 25 nm, (e) 30 nm, (f) 35 nm. The tip has no effect for heights above 20 nm: It does no longer make a depletion region. Picture from [17].
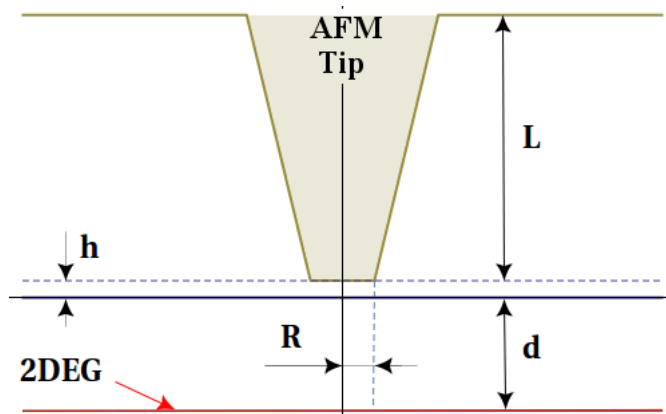
Figure 3.8: Geometry used in Poisson-3D simulation. adapted from [37]

last is biased at a fixed voltage and for each picture, it scanned the sample at a given height. We notice that in figures (d), (e), (f), the tip has almost no effect on the system conductance. This means that the tip did not deplete the charge density beneath the surface, and all what it did is to create a small bump which is not high enough to backscatter the electrons towards the QPC. On the contrary, when the tip is closer to the sample surface, as in Fig. (3.7 (a), (b) and (c)), for heights less than 20 nm, the tip induces a significant change in the system conductance and a beautiful pattern is obtained. In this case, since the tip is closer to the surface and therefore to the 2DEG, it creates an important depletion region which induces a potential so high that it backscatters the electrons towards the QPC and the effect is more important each time the tip is above a region of high electronic flow.

The creation of the depletion region, where the potential induced by the charged AFM tip is higher than the Fermi energy makes this region classically forbidden for the electrons. Thus, the resolution of pictures is very high and even less than the distance between the Tip and the 2DEG. In fact, the distance between fringes is $\frac{\lambda_F}{2}$ (λ_F is around 37 nm for the energies chosen in most experiments) and the distance between the tip and the 2DEG is around 80 nm.

Depletion region profile

The depletion region is a perturbation of the 2DEG induced by the charged tip positioned above the sample's surface. The theoretical investigation of this perturbation is an electrostatic problem since the tip is capacitively coupled to the gas of electrons. This 2DEG is assumed to be an equipotential before it undergoes the effect of the tip. This situation is numerically modeled using a 3D-Poisson solver [37]. In the simulation, a tip situated 67 nm above the 2DEG is considered. The end of the tip has a radius of $R = 40$ nm. The tip itself is a big piece of height $L = 2$ μm (see Fig. (3.8)). The result of the numerical simulation assuming a density of electrons in the 2DEG $n = 4.2 \, 10^{11} e/cm^2$ is shown in Fig. (3.9). The charge induced by the tip is centered at the position of the tip and has a large extension. This simulation uses a realistic model for the tip, nevertheless, a model where the tip is assumed as a charged point at the same height gives the same result with an accuracy around 1% [37].

The triangular shape of the profile of the induced charge can lead someone to think about a Lorentzian curve to model the potential induced by the tip:

$$V_{Tip}(x,y) = \frac{V}{\pi} \frac{\frac{1}{2}\Gamma}{x^2 + y^2 + (\frac{1}{2}\Gamma)^2} \tag{3.4}$$

Γ is a parameter specifying the width of the function and V specifies the height.

Indeed, the experimental observations [40] agree with this kind of induced charge and their numerical simulations are well fitted with a Lorentzian distribution. The height of the Lorentzian is controlled with the AFM tip voltage and the half-width is equal to the distance of the tip to the 2DEG [32] [40]. This distribution is considered as the most realistic model for the tip effect on the
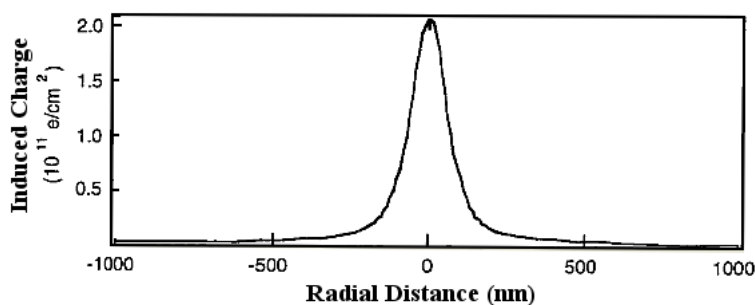
Figure 3.9: Profile of the charge induced by the tip on a 2DEG of density $n = 4.2\ 10^{11}e/cm^2$ obtained by numerical simulation. The tip is 10nm above the sample surface . Adapted from [37]
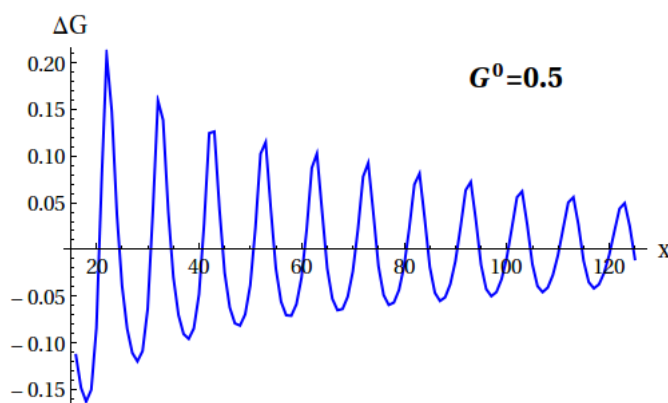
Figure 3.10: Change in the conductance (in units of $\frac{2e^2}{h}$) as a function of the tip position. The tip is Lorentzian and the QPC realistic. The conductance of the systems without tip is $G^\circ = 0.5$. The position x is in units of the the lattice step a. The effect has both signs: negative and positive.

2DEG density charge and this potential was considered in several works [34] [32] [41], nevertheless, other models were considered too with very satisfactory results such as a Gaussian potential [41] which was compared to the Lorentzian model and found to be weakly affecting the results and therefore the shape of the perturbation induced by the tip is not highly pertinent. We can mention also more simpler models where the potential is taken as a Dirac delta function. Surprisingly, the numerical simulations explain nicely the experimental observations [42] [43].

Numerical simulations using a Lorentzian tip model

In the previous sections, we used our algorithm based on recursive Green's function formalism to obtain the change in conductance $\Delta G = G(\text{Tip}) - G^\circ$. The results of the effect of the tip along the central axis of the QPC ($y = 0$) are given in Fig. (3.2), Fig. (3.3) and Fig. (3.4). However, if the potential chosen to model the QPC was realistic Eq. (3.1), the tip model was not: In those simulations, the tip was modeled with a Dirac delta potential.
Here, we will show the numerical simulation results of SGM considering a realistic model (Lorentzian) for the AFM tip. The QPC model also is realistic Eq. (3.1) with a smooth opening and a good connection to the semi-infinite leads. We restrict the tip on the central axis in order to have an idea on the decay law of the fringes. In the simulation which gives Fig. (3.10) and Fig. (3.11), the QPC has a length of $63a$ (a is the step of the lattice) and the leads are very large ($W = 2001a$) in order to neglect the reflection from the borders. The tip is modeled with a Lorentzian occupying 31×31 sites with a half-width of 7 sites. The maximum of the potential tip is taken equal to $\frac{2}{\pi}$. It is important that the highest value of this potential be small to avoid some effects due to resonances that I will explain in the next section. The first remark we do when we see Fig. (3.11)
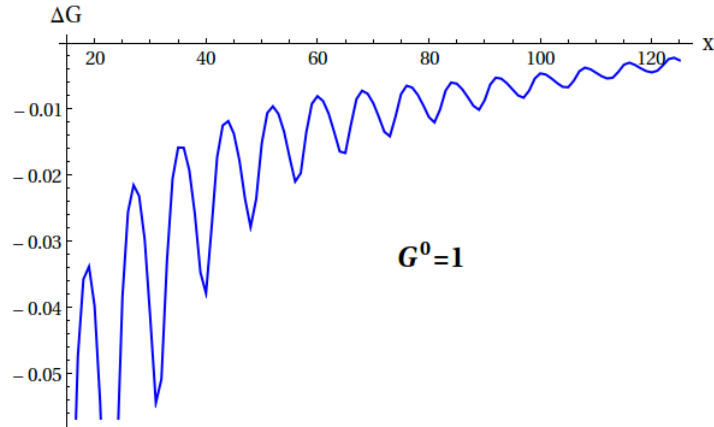
Figure 3.11: Change in the conductance (in units of $\frac{2e^2}{h}$) as a function of the tip position. The tip is Lorentzian and the QPC realistic. The conductance of the systems without tip is $G^\circ = 1$ (First plateau of conduction). We notice that the effect is always negative.
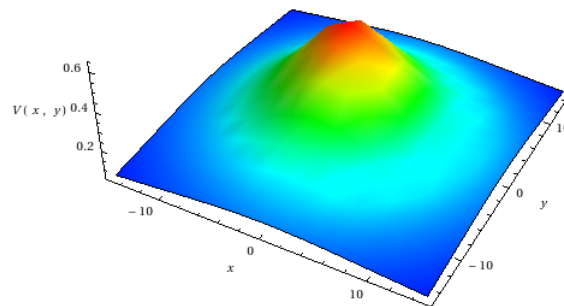
Figure 3.12: The form of the Lorentzian potential used in the simulation of SGM in quantum point contact.

and Fig. (3.10) is that they are very similar to the figures obtained previously(Figs 3.3 and 3.4) using a Dirac Delta function as a model for the tip. This means that the shape of the tip is not highly pertinent to study the qualitative behavior and effect of the tip on the system quantum conductance. This comes to strengthen the assumption claimed in [41] when they compared the Lorentzian model to the Gaussian one to find that the shape of the tip model is weakly affecting the results. This is an important conclusion since, obviously, using the Dirac delta model is much simpler for numerical simulations.

Again, we find that the effect of the tip is always to reduce the conductance ($\Delta G < 0$) for the first plateau of conduction ($G^\circ = 1 \times \frac{2e^2}{h}$) whereas for less opened QPC (Fig (3.10))it oscillates around zero which means that the conductance can be enhanced. This is of course a quantum effect. We mention that in order to obtain an effect clearly negative for the first plateau of conduction, we need to have a long QPC because this leads to good quantization and long pronounced plateau. Otherwise, at some distance from the QPC, the results starts to achieve small positive values. It is also recommended to consider very large leads because short widths have a visible effect at long distances from the QPC. This is due to electron reflection from the borders of the leads. Of course, this leads to larger time of calculation because the recursive Green's function algorithm inverts larger matrices. So, we need to search an optimum width which ensures short time of calculation without destroying the figures of the tip effect. Later, we will give a very fast program which uses matrix product instead of matrix inversion but needs the tip to be Dirac delta function.

3.2.1   Dirac delta potential tip model

The comparison of the figures of interference pattern obtained with realistic models both for the QPC and the tip with the figures obtained using a simpler model for the charged AFM tip suggests that it is enough to consider the Dirac delta function when we do not seek a very good precision in the numerical results. Indeed, if only the behavior behind the physics of the experiment is needed, the simpler model for the tip reproduces the main results and explains well the quantum effects induced in Scanning Gate Microscopy (SGM) experiments.

The Dirac delta function modeling the tip is a perturbation which is non-zero only on one site:

$$V(x,y) = V_{tip}|x_0,y_0\rangle\langle x_0,y_0| \tag{3.5}$$

Where x_0 and y_0 are the coordinates of the tip and V_{tip} is the value of the scattering potential.

The advantage of using the local on-site scatterer is to avoid the task of inverting matrices in the algorithm of recursive Green's function. In fact, the Dyson equation expressing the Green's function G of the system with the tip using the the Green's function G° of the system without the tip reads:

$$G = G^\circ + G^\circ V G \tag{3.6}$$

Taking this Dyson equation between the slice number 1 and N gives:

$$G_{1N} = G^\circ_{1N} + G^\circ_{1n}V_{nn}(1 + V_{nn}G^\circ_{nn})^{-1}G^\circ_{nN} \tag{3.7}$$

n is the index of the slice containing the tip and V_{nn} is the matrix containing the perturbation of the Dirac delta tip. This matrix is sparse and has only one non-zero element. Because of this, the inversion $(1 + V_{nn}G^\circ_{nn})^{-1}$ boils down to the inversion of a scalar and therefore Eq. (3.7) uses only product of matrices which is an easier operation than the matrix inversion. The other advantage of using a Dirac delta function for the tip model is to allow an analytic expression for the change it induces in the Green's function and therefore in the transmission of the system. For more details you can read [42]. The analytic expressions of the Green's function will be an important chapter of this thesis.

The resonance of a Dirac delta tip

The response of the system to a local tip perturbation modeled with a Dirac delta function is the starting point to understand the effect of an extended tip and how the conductance is affected with the value of the tip voltage.

We study in this section the same system described previously where the QPC is realistic, modeled
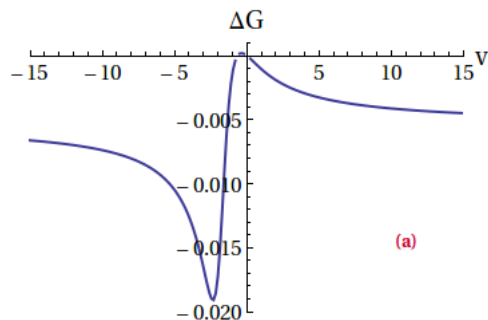
Figure 3.13: Numerical simulation for ΔG vs the tip potential for Dirac delta model and completely open first mode . The tip is positioned at $x = 40a$ far from the QPC. The effect is always negative and show a resonance at some negative potential value. (ΔG in units of $\frac{2e^2}{h}$ and 'a' is the step of the lattice).
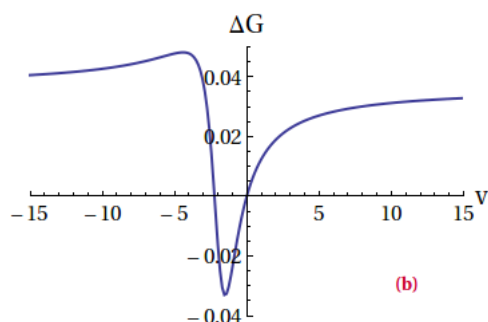
Figure 3.14: Numerical simulation for ΔG vs the tip potential for Dirac delta model and half opened first mode. The tip is positioned at $x = 40a$ far from the QPC.The resonance is a local extremum. (ΔG in units of $\frac{2e^2}{h}$ and 'a' is the step of the lattice).

with a potential $V(x, y)$, but the tip is considered local, with a Dirac delta model. We will focus on the tip potential value: The tip is situated at a given position, and we plot the change in the conductance of the QPC as the potential induced by the tip varies. Small values of the potential refer to a weak effect of the tip as long as it only makes a small bump in the 2DEG density charge and not really a depletion region whereas huge values of the potential correspond to deep depletion region of high potential. This big value of the potential means that the region is classically forbidden for electrons and in the numerical simulation, this means that this site (where is put the Dirac delta function) is like excluded from the lattice.

Fig. (3.13) and Fig. (3.14) show the numerical simulation of the change in the conductance ΔG as a function of the tip potential value. The tip position in both figures is $x = 40a$ and the model chosen is a Dirac delta tip. We considered here two situations: A full open QPC completely transparent for the first mode of conduction (First plateau), this is the case of Fig (a), and the situation of an almost closed QPC which is closed for half of the first mode ($G^{\circ} = 0.5 \times \frac{2e^2}{h}$). We can see in Fig. (3.13) that the effect of the tip is always to reduce the conductance on the first plateau and this is true for all the values of the tip potential[3]. We notice also the presence of a resonance at a negative value of the tip potential ($V_{tip} \sim -2.5$) where the effect on the conductance is maximum. At high absolute values of the potential the curve converges quickly to the same limit[4] for positive and negative values of the tip potential, which means that the site just below the tip becomes quickly forbidden for electrons which do not have enough energy to cross it.

---

3. We already mentioned that the effect of the tip on an open QPC (transparent for a mode) is to reduce the conductance for all the tip positions

4. We prove that the limit is the same for positive and negative tip potential values in the next chapter where an analytical solution is proposed

Now, if we slightly close the QPC without the tip to $G° = 0.5 \times \frac{2e^2}{h}$, and we maintain the tip at the same position ($x = 40a$) we obtain the curve in Fig. (3.14). This time, the effect of the tip can be either negative or positive (conductance can be enhanced). Again, there is a resonance at a negative value of the potential, thus it does not correspond necessarily to the maximum effect [5] of the tip: Indeed, higher absolute value of the tip potential could induce a bigger effect than at the resonance. This depends on the position x of the tip and the Fermi energy of electrons. In fact, we will show that it actually depends on the on-site Green's function (which is a position and energy dependent quantity) at the tip position. At large distances from the QPC, the position dependence tends to disappear.

The Lorentzian tip vs the Dirac delta tip

We have already compared the results obtained with a realistic Lorentzian model to what was obtained using the Dirac delta model. We concluded that the behavior of the change in the conductance is almost the same for both of the two models and this is true for different QPC opening. Here, we try to understand what precautions we should take when we use a long range potential such us the Lorentzian model. We know that any function can be written as the sum over delta functions as follows:

$$V(x,y) = \iint V(x_0, y_0)\delta(x - x_0, y - y_0)dx_0 dy_0. \tag{3.8}$$

This integral relation will be approximated to a sum, which can be easily used in a simulation based on Tight Binding Model on a lattice: Each site around the position of the tip is put to a potential in a way that the whole sites landscape exhibits the form of the wanted tip model, a Lorentzian for instance. Accordingly, the characteristics of a single Dirac delta tip should be taken into account, namely the resonance implications. In fact, if we consider a Lorentzian with a maximum in the origin V_{max} bigger than V_{res} of a Delta potential (see Fig 3.13), then since the potential decays from V_{max} at the center of the Lorentzian to vanish far away, necessarily there is some sites at a distance R from the center where the potential is equal to the value of resonance V_{res} of a single Delta function. Therefore, these sites (they represent a ring of radius R) have more effect than the center of the Lorentzian (because they correspond to a resonance) and therefore, the tip acts like a ring rather than a centered potential. This situation induces irregularities in the curves of the conductance change as a function of the position of the tip, and of course we do not expect to obtain the figure 3.11. To simplify, We can summarize this effect in two statements:

1. A Lorentzian is modeled numerically with many Dirac delta potentials making together a Lorentzian shaped landscape.

2. If $V_1 > V_2$, that does not mean that V_1 backscatter more electrons than V_2.

To simplify things, we can say: we should take a Lorentzian with a small height.

Finally, we may mention that extended models for the tip effect on the 2DEG density of charge raise also another problem which concerns the bound states. If the Fermi energy is close to the energy bound state of the tip, we expect to have some anomalies in the figures of the interference pattern.

So far, we compared the results of a Dirac delta tip and extended models, to come with the conclusion that when there is no anomalies related to resonances and bound states, the Dirac delta model is, in general, quite enough to reproduce the same effect of the tip on the conductance of Quantum Point Contact. Nevertheless, we need to put more analytic justification and come out with physically comprehensive conditions. This will be the topic of the next section.

3.3   Short range impurity

There is no doubt that scattering problems are more simplified when we consider Dirac Delta impurities. Nevertheless, it may be a non trivial task and a lot of care is needed in the definition of the Delta function (see M. Ya Azbel [44] [45] [46]). The scattering of electrons by such delta potentials in confined systems was successfully studied in the low energy regime (The first mode

---

5. When we talk about the effect of the tip, we mean the biggest change in the conductance with absolute value.
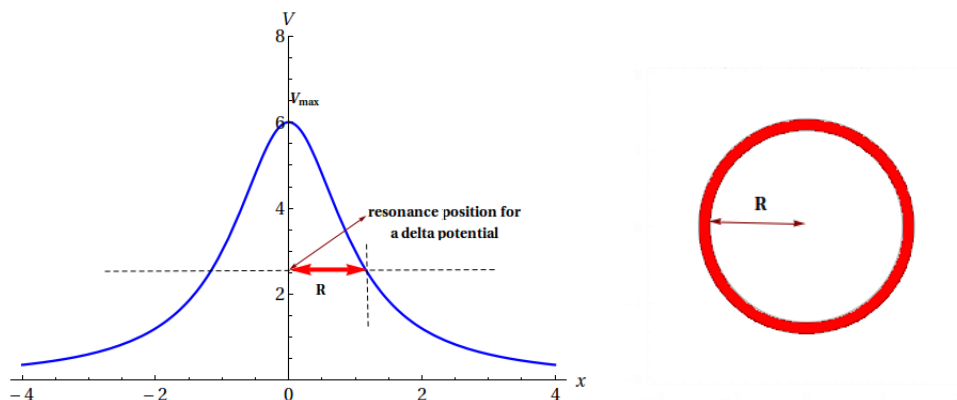
Figure 3.15: A Lorentzian shape of the potential induced by the tip. If $V_{max} > V_{res}$ (here $V_{res} \approx 2.5$ (absolute value, see Fig. (3.13)), then at a distance $x = R$, the value of the Lorentzian is equal to the resonance value of a Dirac potential (see Fig. (3.13)). Because the Tip effect is circular, these sites are situated on a ring (right Fig) and have more effect than the center of the Lorentzian. This means that the tip seems like not centered on one site and therefore some anomalies could appear in the curves of $\Delta G(x)$.

of conduction is dominant) such as to describe the transmission of graded bent orifice [47] or the conductance near threshold energy in quasi 1D systems [48]. The effect of delta impurities on the conductance and how it is affected when the defect is situated near the surface of quasi 1D wire is studied in [49]. Also, the semiclassical approach was applied to study the resonant reflection and transmission in a conducting channel with a single impurity [50]. Here, we will be interested in the scattering by short-range impurities (Not delta potential) in two dimensional conducting channel, and we will focus on the work by Levinson, Lubin and Sukhorokov [51] to find the conditions where the short range potential can be approximated by a Dirac delta potential.

If a quantum point contact is defined by the potential $V(r)$, $r = (x, y)$, and a short range scatterer with the potential $U(r)$ (with amplitude U_0 and range of interaction ρ), then the Schrödinger equation for the wave function reads:

$$\left(-\frac{\hbar^2}{2m} \Delta + V(r) + U(r) \right) \psi(r) = E \psi(r) \tag{3.9}$$

The solution of this equation has the form of:

$$\psi = \psi^0 + \psi'$$

where ψ^0 is the asymptotic wave function in the absence of the impurity and ψ' is an outgoing wave function. If we assume that the impurity is at $r = 0$ and the energy $E = 0$ to correspond to $V(0) = 0$, then we can seek to simplify the problem by considering the impurity as a short range scatterer. This means, we need:

$$k\rho \ll 1, \qquad E \ll |U_0|.$$

where $E = \frac{\hbar^2 k^2}{2m}$.

The first condition means that the range of the impurity is smaller than the Fermi wave length and the second condition means that the electrons have a very low energy compared to the height of the scatterer. The implication of these conditions is that the the s wave dominates and the solution of the Schrödinger equation for $\rho < r < \lambda$ is :

$$\psi(r) = C \ln(\frac{r}{a}) \tag{3.10}$$

where a is a scattering length.

Far from the impurity, the scattered wave reads:

$$\psi' = A\, G_E(r, 0) \tag{3.11}$$

$$= \frac{A}{2\pi} \ln\left(\frac{h_E(r)}{r} \right). \tag{3.12}$$

Where G is the 2D Green's function and $h_E(r)$ is a length depending on the confinement potential $V(r)$.

The presence of the impurity in the center of the QPC leads to a change ΔG in the conductance of the system:

$$\Delta G = \sum_n t^2(\epsilon_n)[Re(A_{nn}) + \exp(-\pi\epsilon_n)Im(A_{nn}]$$ (3.13)

where A_{nn} is the amplitude of the outgoing wave modes. and $t(\epsilon_n)$ are the transmission amplitudes:

$$t(\epsilon_n) = [1 + \exp(\epsilon_n)]^{-1/2}$$

ϵ_n are the threshold energies.

The study of the characteristics of the correction to the conductance [51] due to the impurity in the center of the QPC shows that the impurity enhances the transmission of the threshold mode below the threshold and suppresses the transmission above the threshold which means additional smearing of the threshold.

Now, using all the conclusions we obtained from the comparison of different models for the QPC and for the tip, we wish to understand better the results of scanning gate microscopy and to put analytical formula on the decay law of the fringes in the interference pattern for different case of the QPC opening (different plateau of conduction). To fulfill this task, we need to do some simplifications which make the analytical formulation of the problem possible but do not affect the main results of the problem. In the next chapter, assuming a justified toy model, we try to give the most important answers that the problem of electrons transport through nano-constrictions rises.

Chapter 4

Resonant level model and analytical solution for electron transport through nanoconstrictions

Contents

Summary of chapter 4

Here, we propose, in the light of the numerical simulation conclusions of the previous chapter, a simple model to answer the questions concerning the decay law of the fringes in a scanning gate microscopy of a QPC conductance. This resonant level model (RLM), is easily solved and reproduces the main figures of interference pattern obtained by a realistic QPC. We first express the dependence of the lead self energy on the tip position. This task is accomplished using the method of mirror images, and the results are well verified by simulation. Once this done, we obtain the change in the conductance due to the tip, as an expansion in terms of the change in the real and imaginary parts of the self energy. This expansion gives the following main results:

  – For a completely open system, the first order of the expansion is suppressed and the change in the conductance ΔG is therefore, obtained by the second order, decaying like $\frac{1}{x^2}$ with no oscillating amplitude (Almost no fringes).
  – For less opened systems, the first order of the expansion is sufficient to express the change ΔG. We find that the fringes decay as $\frac{1}{x}$.
  – The dependence of ΔG on the tip voltage v is proportional to $\mathcal{A} = |\frac{v}{1-vG^\circ}|$ if the system is less opened whereas for a fully open system it is proportional to $\mathcal{A}^2$

On the basis of these results, we predict an unusual interesting effect: Thermal enhancement of the fringes using temperature.

A QPC, fully open in the edge of the first plateau, exhibits almost no fringes at zero-temperature and the effect of the tip decays like $\frac{1}{x^2}$. Rising temperature, shows a new oscillating term in the expansion of ΔG proportional to $(k_b \mathcal{T})^2$ and decaying slowly (like $1/x$). This occurs in the figures of interference pattern as an enhancement of the fringes when temperature is slightly increased from zero. This behaviour is counterintuitive since the general idea we get from quantum mechanics is that quantum effects disappear with temperature and generally the fringes are averaged and reduced. This result is well verified by the analytical calculation obtained from the temperature dependent conductance of the RLM.

Most of the results obtained here are first deduced from the analytical solution of the resonant level model. However, they are all tested later on quantum point contacts with different realistic models either for the QPC itself or the tip (extended tip). Beyond the important results this model provides, what do we intend to take away from this chapter is the simplicity of the model we propose and its efficiency in reproducing realistic QPC results. It also helps to predict other unexpected results. We will have faith in this model to study the thermopower of a QPC in the next chapter.

The numerical simulation gives the correction to the conductance of a quantum point contact due to a charged tip with a very good precision for all the situations we look at. This task is done easily what ever is the complexity of the system we look at. On the contrary, the analytical formulation is very hard and sometimes impossible. In order to make the problem simpler, we need to assume less complex models without loosing the same behaviour of electrons transmitted through the quantum point contact QPC. We need also a tip model simpler than the extended Lorentzian realistic model and at the same time ensures the same effect. A lot of effort has been devoted in the previous chapter to investigate in details the properties of the system in study, and the different models we can assume for both the QPC and the charged AFM tip. The aim in this chapter is to propose a justified toy model, based on the conclusions we obtained after comparing the different results of the numerical simulations. The solution of this model should be simple, verified with the numerical simulation and should agree with the physical intuitions and the experimental observations.

4.0.1 The conclusions of numerical simulations

The first conclusion we obtained after comparing the results of the numerical simulations concerns the model of the quantum point contact (QPC). Indeed, we found that the figures of the interference pattern are almost the same for different QPC models having the same opening (the same conductance G^0 without the tip). This means that for the interference pattern and the decay law of the fringes, we solely need a system which has the same transmission as the QPC and we can take it as simple as possible as long as it has the same transmission at zero-temperature. We should remind that the behavior at non-zero-temperature may be more affected with this simplification since the quantum transport deals with electrons at different energies around the Fermi energy(For more details see the previous chapter).

The second simplification concerns the tip and the model we choose to mimic the effect it produces in the 2DEG charge density. Again, after comparing the different numerical results, namely the Lorentzian model with the Dirac delta tip(See Fig 3.3 3.4 and 3.10 3.11), it seems that it is enough to take a Dirac delta potential for the tip since it reproduces the same behavior and that only the amplitude and the phase of the conductance change $\Delta G(x)$ can change with the Lorentzian Tip.

4.0.2 Toy Model: 2D resonant level model

In what follows, we will be more interested in the first mode of conduction since it is the most studied one [18]. We propose a simple model capable of reproducing the one mode transmission in nanoconstrictions in the presence of the tip. The most important thing is to be able to do analytical formulation of the problem and to obtain simple expressions for the decay law of the fringes. We seek a model which implies the use of scalars in the conductance expression rather than the usual matrix formulation based on the Green's matrices.

The model which gathers all the requirements listed so far looks like Fig. (4.1): One site biased at potential V_g and connected to two semi-infinite 2D leads via the coupling elements t_c. The hopping term in the leads is t_h which will be taken all over this chapter equal to one ($t_h = 1$). Also, the potential in the lead sites is taken equal to zero since it is just a reference to all the energies of the problem. The conductance of the system can be controlled via the voltage gate V_g which in some way mimics the potential of the quantum point contact: It closes the system at high absolute values of V_g and completely opens it near certain Fermi energy. The coupling term t_c can also fix the conductance of the system as usually do the coupling of scattering region (QPC) to the leads in the realistic model. The leads, being infinite (length and width) represent a continuum of energies whereas the central region, with a small size (one site in this model), has discrete energies (here,only one level). This problem of electron conduction through nanoconstrictions is the same as what was studied by Fano [52] (discrete state in configuration interaction with a continuum).

Transmission of the toy model

We remind that the zero-temperature conductance and the transmission are related by the Landauer formula:

$$G(E) = \frac{2e^2}{h} T(E)$$
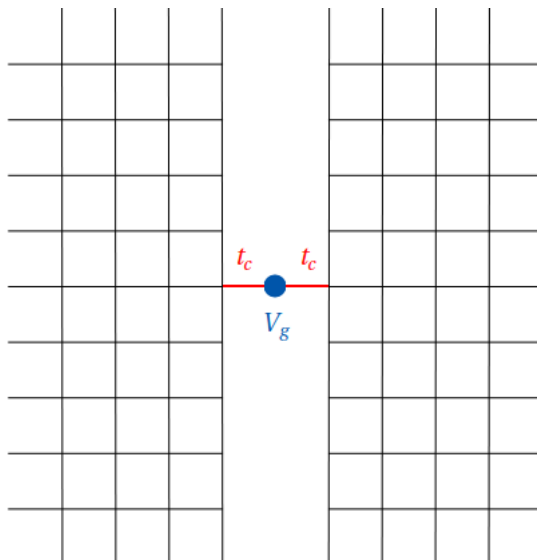
Figure 4.1: Toy Model to mimic transport through nanoconstrictions: One site biased to potential V_g and connected to two semi-infinite 2D leads via the coupling elements t_c. V_g and t_c both control the conductance of the system.

This means that the transmission represents the zero-temperature conductance of the system in units of the quantum of conductance $\frac{2e^2}{h}$. The transmission of the system can be expressed using the Fisher-Lee formula:

$$T(E) = \text{Tr}(G\Gamma^l G^\dagger \Gamma^r)$$

where G is the Green's function of the central region and Γ^l, Γ^r represent respectively the left and right broadening elements.

Since the central region in the toy model contains only one site, G, Γ and Γ^r are scalars and therefore we can omit the trace:

$$T(E) = G\Gamma^l G^\dagger \Gamma^r \tag{4.1}$$

The Green function is easily obtained:

$$G = \frac{1}{E - V_g - 2\Sigma} \tag{4.2}$$

Σ is the self energy of one lead. In the absence of the tip, the left and right lead have the same self energy. Therefore, the linewidth elements are also the same

$$\Gamma^l = \Gamma^r = \Gamma = -2\Im(\Sigma) \tag{4.3}$$

We remind that the self energy translates the effect of the lead on the central system and contains the information on the kind of the lead and how it is coupled to the central region. It is important to know that the self energy is proportional to the square of the coupling term t_c [1]:

$$\Sigma \propto t_c^2 \tag{4.4}$$

We so often talk about weakly or strongly coupled leads by referring to the coupling elements t_c. This is equivalent to large or small self energy.

---

1. The self energy is a function of the Fermi energy. Most of the time we do not exhibit this explicitly, but we should not forget it.
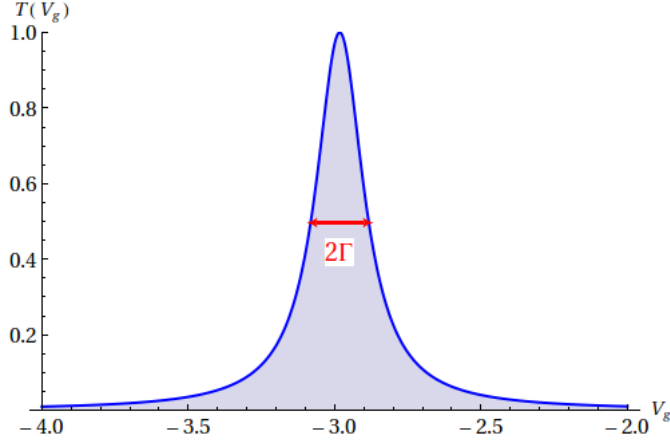
Figure 4.2: Transmission of the toy model as a function of the gate voltage V_g. The curve is a Lorentzian centered at $E - 2\Re\Sigma$ and full width at half maximum 2Γ. This curve is obtained for the Fermi energy $E = -3.8$ and the coupling $t_c = 1$.

With all these elements, we can express the transmission of the toy model as follows [2]:

$$T(E, V_g) = \frac{1}{1 + \left(\frac{E - V_g - 2\Re(\Sigma)}{\Gamma}\right)^2} \tag{4.5}$$

This relation shows that the transmission, as a function of the gate voltage V_g, is a Lorentzian curve centered at the position $E - 2\Re(\Sigma)$ and with full width at half maximum equal to 2Γ (Fig 4.2).

It is necessary to fix some conventions which lighten the expressions without altering the final results and conclusions:

The conduction band is fixed by the leads (electron reservoirs) via the dispersion relation (Rel 2.16). We prefer to shift the conduction band and make it symmetric. In our case (2D leads), this reads:

$$E \in [-4t_h, 4t_h] \tag{4.6}$$

Moreover, the hopping term in the lead t_h, will be taken as reference and therefore can be fixed to one: $t_h = 1$. All the energies will be in units of t_h. The middle of the band, $E = 0$, is the half-filling limit (Particle-hole symmetry) and the bottom of the band at energies E near -4 is the continuum limit where the dispersion relation of the lattice is well approximated by the dispersion relation of the continuum. Most of the time , we will assume this limit to describe the quantum transport in our systems. In Fig (4.2), we plotted the profile of the transmission at a Fermi energy $E_F = -3.8$ as a function of the gate voltage V_g. We can notice a clear Lorentzian resonance. The presence of this single resonance, related to the eigenenergy of the central region (One site), lead us to call this model : **Resonant Level Model RLM**. It is important to notice that the resonance is not at the Fermi energy but at position $V_g = E_F - 2\Re(\Sigma)$. The shift is due to the real part of the self energy of the leads which is generally neglected in literature. Indeed, most of publications assume the wide band limit which neglects the energy dependence of the self energy. Thus, the real and imaginary part of the self energy are related by the Kramers-Kronig relations which automatically shows that the self energy is pure imaginary if the energy independence is assumed. We will show along this chapter, that the role of the real part of the self energy is more important than solely shifting the resonance energies. In Fig (4.3), we obtained the profile of the resonant level model transmission for different coupling constant t_c. Indeed, the resonance becomes very narrow for weakly coupled system and closer to the Fermi energy since the shift $2\Re(\Sigma)$ becomes smaller. At the resonance, the system is completely open for one mode of transmission. Indeed, the value of the maximum at the resonance is $T = 1$.

---

2. $\Sigma = \Re(\Sigma) - i\frac{\Gamma}{2}$
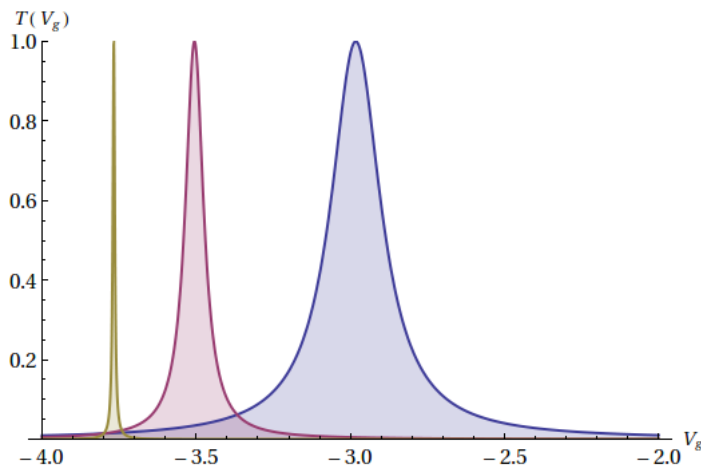
Figure 4.3: Resonant level model (RLM) transmission profiles for different coupling constant t_c. $tc = 1$ blue curve, $t_c = 0.6$ purple curve, $t_c = 0.2$ green curve. the Fermi energy is the same for all the curves ($E_F = -3.8$).

The first remark we can do is that this system seems different from the quantum point contact ! The profile of the transmission is a resonance while for a QPC it is a plateau. Moreover, the transmission of this system can never exceed $T = 1$ at all the Fermi energies and for all the gate voltages while in the case of a QPC, several modes could be transmitted! To clarify the situation, we need to remind that our aim is to study the interference pattern for first mode of conduction and not the other modes. In fact, the first mode is the most studied and we have experimental results [18] to which we can refer for comparison. Including the other modes, brings unnecessary complications that we want to avoid since we are looking only at the first mode of conduction. The second remark concerning the presence of a resonance instead of a plateau is actually not important because the interference pattern depends only on the zero-temperature conductance at the Fermi energy and not on the whole profile of the transmission. For people for whom an explanation with hand is not enough, we can point out that the profiles in Fig (4.3), are obtained with a gate voltage varying linearly and of course there is no reason to be that way. Thus if someone chooses to change $V_g \rightarrow V_{res}(e^{-V_g/V_{res}} + 1)$, with V_{res} the voltage at the resonance, we recover a profile with a plateau of conduction. All this argumentation is good, but there is no better than a direct comparison with a realistic model results: We need to compare the profile of the conductance change as a function of the tip position in both models, the realistic and RLM. In figures (4.4, left and right) we give the result of numerical simulation on the resonant level model RLM for two different opening of the QPC: In left figure, the QPC [3] is fully opened with a transmission without the tip $T^0 = 1$. The effect of the tip is always to reduce the conductance [4] since we can not open a new mode. We clearly recognize the behavior of the change in conductance of a realistic fully open QPC (first mode of conduction) (see Fig (3.4)). In right figure (4.4), the QPC is half closed and the behaviour of the change in transmission is similar to what happens in a realistic QPC (see Fig 3.3). We conclude from this comparison, that the RLM is the a sufficient minimal model which allows us to study the transport through QPC and to understand the law decay of the fringes in scanning gate microscopy. In what follows, we adopt this model (RLM) and try to provide the decay law of the fringes.

4.1 The 2D lead self energy in the absence of the charged tip

4.1.1 Presentation of the lattice model

The presence of the tip changes the transmission of the system, and precisely it is the self energy of the lead which changes. For this reason, we need to study in details the self energy of the lead

---

3. We continue to apply the name QPC to the central region of the RLM
4. I remind that $\Delta T = T - T^0$, and T^0 is the transmission without the tip
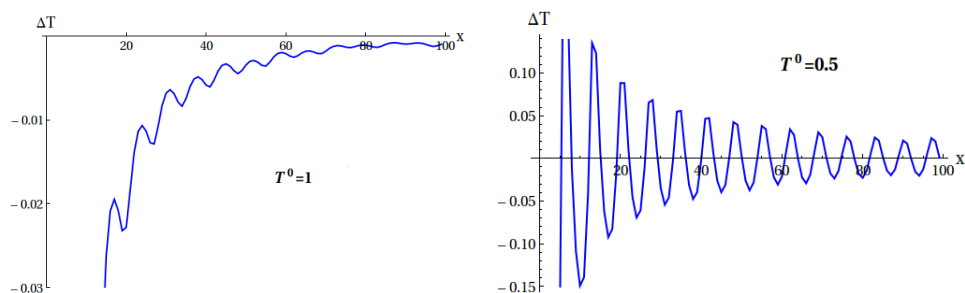
Figure 4.4: The transmission change $\Delta T(x) = T - T^\circ$ of the RLM for two different opening of the system. In left figure, the transmission without the tip is $T^0 = 1$ and the effect of the tip is always negative. In right figure, the system is half closed $T^0 = 0.5$. The effect of the tip alternates the sign. The Fermi energy for in both cases is $E_F = -3.8$ (the bottom of the conduction band is at $E = -4$). The leads are 2D with a width N=1201 sites. The figures are obtained in the central axis of the lead $y = 0$
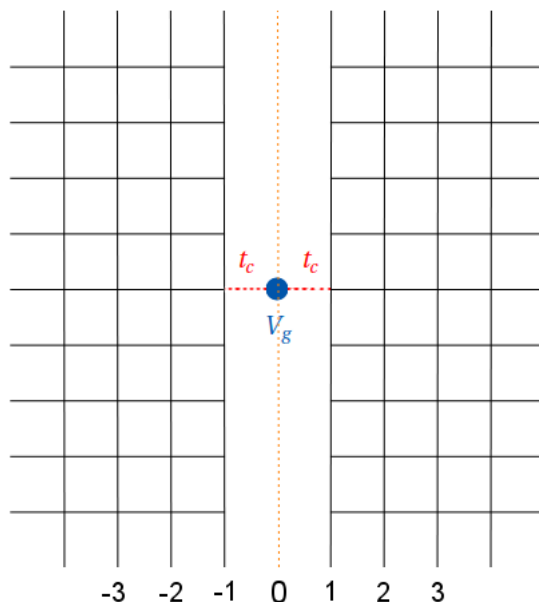
Figure 4.5: Left (from -1 to $-\infty$) and right (from 1 to infinite $+\infty$ semi-infinite 2D leads. The point (0,0) is the place of the site biased to potential V_g. This picture helps to find the Green's function of a 2D semi-infinite lead from the Green's function of an infinite 2D lattice by the method of mirror images.

and to get its energy dependence.

The lead is a 2D semi-infinite system with a width we manage to take as bigger as possible in numerical simulations [5] to be considered as infinite. This means that the lead, indeed, occupy a half-space. The lead, considered as an electron reservoir, fixes the dispersion relation and provides the conduction band of electrons. For a 2D semi-infinite lead, the symmetrized conduction band is:

$$E \in [-4t_h, +4t_h] \tag{4.7}$$

To obtain the self energy of the semi-infinite lead, we use the Green's function of an infinite 2D uniform lattice and the method of mirror images [6] to deduce the Green's function expression of a semi-infinite lead.

4.1.2   Method of mirror images and self energy of a semi-infinite lead

We use here the method of mirror images to find the Green's function of a semi-infinite lattice from the Green's function of an infinite one. We know that the differential equation verified by the Green's function is the same in both cases and only the boundary conditions differs. We know also that any linear combination of two solutions is still a solution. Therefore, we need just to combine linearly, two solutions of the differential equation verified by the Green's function of an infinite lattice, in a way that this solution verifies the boundary conditions of a semi-infinite lattice: The Green's function vanishes at the edge of the semi-infinite lattice.

Let us call the Green's function between any point (x, y) and the origin $(0,0)$ of an infinite lattice: $G(x, y)$. To express the self energy we need the on-site green function $G^{\frac{1}{2}}$ of the semi-infinite lattice between the positions $x = d$ and $x' = d$ This can be given using the method of mirror images as :

$$G^{\frac{1}{2}}_{d,d} = G_{d,d} - G_{d,-d} \tag{4.8}$$

$G_{d,d}$ is the on-site Green function of infinite lattice. Because of the translational invariance we have $G_{d,d} = G_{0,0} = G(0, y)$. The Green's function of interest is $G^{\frac{1}{2}}_{1,1} = G_{1,1} - G_{1,-1}$ at $y = 0$. We can write this using the notation $G(x, y)$ as follows: $G^{\frac{1}{2}}_{1,1} = G(0,0) - G(2,0)$ The self energy we want to obtain is the surface Green's function $G^{\frac{1}{2}}_{1,1}$ on the site connected to the central system multiplied by the factor t_c^2. We first do the calculation for $t_c = 1$ and easily get the result for different coupling. We start by writing [7]:

$$\Sigma(E) \quad = \quad G(0,0) - G(2,0) \tag{4.9}$$

We use the results known for the Green function[55][54] and simplify the result:

$$\Sigma(E) \quad = \quad G(0,0) - G(2,0) \tag{4.10}$$
$$= \quad G(0,0) - [EG(1,0) - G(0,0) - 2G(1,1)] \tag{4.11}$$

We use the following relations[54][55] to simplify more:

$$G(1,0) = \frac{1}{4}[EG(0,0) - 1] \tag{4.12}$$

The relation we get after the simplification is:

$$\Sigma(E) = (2 - \frac{E^2}{4})G(0,0) + 2G(1,1) + \frac{E}{4} \tag{4.13}$$

At this step, we want to replace the two quantities $G(0,0)$ and $G(1,1)$, known in literature and expressed using the complete elliptic integrals of the first and the second order $\mathcal{K}$, $\mathcal{E}$, as follows:

$$G(0,0) \quad = \quad \frac{2}{\pi E}\mathcal{K}(\frac{4}{E}) \tag{4.14}$$

$$G(1,1) \quad = \quad \frac{2}{\pi E}[(\frac{E^2}{8} - 1)\mathcal{K}(\frac{4}{E}) - \frac{E^2}{8}\mathcal{E}(\frac{4}{E})] \tag{4.15}$$

---

5. Of course, this implies larger computing time.

6. A lot of people know this method in potential theory or in quantum mechanic to solve the Schrödinger equation but do not expect it elsewhere. In fact, this method is more general and apply even for probability theory. Actually, it is related to linear differential equations

7. The self energy is obtained using the Green's function between the point (x,y)=(1,0) and $(x', y') = (1, 0)$. So, we need $G(x - x', y - y') = G(0,0)$
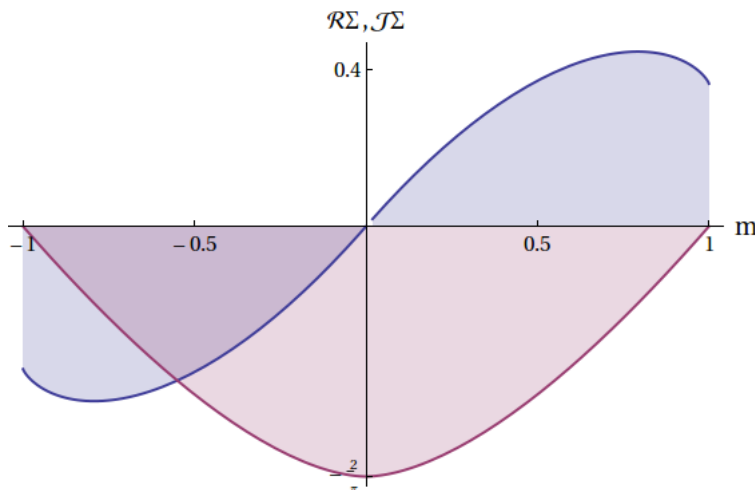
Figure 4.6: Energy dependence of the real (Blue curve) and imaginary part(Red curve) of the self energy. The variable used here is the normalized energy $m = \frac{E}{4}$. The imaginary part is always negative(True for the retarded self energy).

We obtain the following simple interesting result:

$$\Sigma(E) = -\frac{E}{2\pi}\mathcal{E}(\frac{4}{E}) + \frac{E}{4}. \tag{4.16}$$

This important relation, gives the energy dependence of the self energy of a 2D lead connected in the middle as in Fig(4.5). In this relation, the energy E has a small complex part: $E \to E + i\epsilon$ and the function is generalized to the whole complex space by analytic continuation. This remark helps us to find the expression of the real and the imaginary parts of the self energy. Indeed, the complete elliptic integrals of the second order has the following property:

$$\mathcal{E}(\frac{1}{m}) = \frac{1}{m}[s(\mathcal{E}(m) - m'^2\mathcal{K}(m)) + i(\mathcal{E}(m') - m^2\mathcal{K}(m'))] \tag{4.17}$$

with $m^2 + m'^2 = 1$ and $m = \frac{E}{4}$. $s = \text{sign}(m)$
This relation helps to give the explicit expression of the real and imaginary parts. We can write the self energy as a function of the normalized energy $m = \frac{E}{4}$:

$$\Re\Sigma(m) = m - \frac{2}{\pi}[s(\mathcal{E}(m) - m'^2\mathcal{K}(m)] \tag{4.18}$$

$$\Im\Sigma(m) = -\frac{2}{\pi}[\mathcal{E}(m') - m^2\mathcal{K}(m')] \tag{4.19}$$

Most of the time, we will keep using the variable m instead of the energy E in order to lighten the expressions. We need just to keep in mind that $m = \frac{E}{4}$ and that the number 4 refers to the half width of the conduction band of 2D systems. The plot of the real and imaginary parts of the self energy is given in Fig(4.6).

We notice that the imaginary part is always negative which reminds us to precise that we are talking about the retarded self energy. This will be always the case unless otherwise mentioned. This part is negative because of causality. The advanced self energy, when needed, can be obtained by taking the complex conjugate. It is interesting to have formula Eq(4.19) for all the energy spectrum, nevertheless, only two cases are worth being pointed out: The first one is the half-filling limit $E = 0$, where we have a symmetry between the transport of electrons and holes.Here, the dispersion relation is far from the one of the continuum and lattice effects are expected to be found in the physics of this limit. The second interesting limit is the continuum limit, near the bottom of the conduction band ($E \sim -4$, or $m \sim -1$).

4.1.3 Expansion of the self energy in the continuum limit

Although the complete elliptic integrals of the first and the second kind are well documented and provided by programs [8] of formal calculations [56], it may be preferable to give the expansion of the self energy to see how is the dependence near the continuum. To do this task, we need the expansion of the special functions $\mathcal{K}$, and $\mathcal{E}$ [57]:

$$\mathcal{K}(m) = \log 4 - \frac{1}{2}\log(1 - m^2) + O(|(1 - m^2)\log(1 - m^2)|) \tag{4.20}$$

$$\mathcal{E}(m) = 1 + \frac{1}{2}[\log 4 - \frac{1}{2}\log(1 - m^2) - \frac{1}{2}](1 - m^2) \tag{4.21}$$

$$+O(|(1 - m^2)^2 \log(1 - m^2)|) \tag{4.22}$$

Applying this expansions on the expressions of the real and the imaginary parts of self energy, we obtain the following interesting relations:

$$\Re\Sigma \sim a + b(1 + m) + \frac{1}{\pi}(1 + m)\log(1 + m) \tag{4.23}$$

with a and b are:

$$a = -1 + \frac{2}{\pi}$$

$$b = 1 - \frac{3\log 2 + 1}{\pi}$$

The imaginary part expansion, near $m = -1$, reads:

$$\Im\Sigma \sim -(1 + m) + \frac{1}{4}(1 + m)^2 \tag{4.24}$$

With all the relations provided so far, we are able to study analytically the transmission of the RLM with Eq(4.5) and the energy dependence of the transmission becomes now completely mastered.

4.2 Self energy of a 2D semi-infinite lead in the presence of a charged tip

To study the decay law of fringes in Scanning Gate microscopy, using a resonant level model, we need to express the self energy of the 2D semi-infinite lead in the presence of the tip. Indeed, the transmission of the system is expressed using the real and imaginary parts of the lead self energy. The presence of the tip, in the lead makes a change in its self energy. To obtain the analytical form of this change, we need first to express the Green's function position dependence in a 2D semi-infinite lead. Again, we use the method of images combined with the Dyson equation to make this task possible. We first start by writing the Hamiltonian of a 2D semi-infinite lead in the presence of a tip bias at potential v. This Hamiltonian, written in a tight binding representation reads:

$$H = H_0 + V \tag{4.25}$$

H_0 is the Hamiltonian of a 2D perfect lead (in the absence of the tip) which can be given as follows:

$$H_0 = -t_h \sum_{x,y} |x, y\rangle\langle x + 1, y| + |x, y\rangle\langle x, y + 1| + hc \tag{4.26}$$

x takes values from 1 to $+\infty$ and y from $-\infty$ to $+\infty$.
The perturbation V due to the presence of the tip is:

$$V = v|x_0, y_0\rangle\langle x_0, y_0| \tag{4.27}$$

---

8. I highly recommend Wolfram Mathematica program.

x_0, y_0 are the coordinates of the tip position.

The first step consists in the use of the Dyson equation to take into account the tip. I remind that Dyson equation reads:

$$\begin{aligned} \mathcal{G} &= \mathcal{G}^0 + \mathcal{G}^0 V \mathcal{G} && (4.28) \\ &= \mathcal{G}^0 + \mathcal{G}^0 V (1 - V \mathcal{G}^0)^{-1} \mathcal{G}^0 && (4.29) \end{aligned}$$

The index 0 reminds that this quantity is for the perfect semi-infinite lattice. We do not need the Green's function between all the sites of the lattice. Indeed, we only need it between the site of the lead connected to the central scattering potential and the site where is positioned the tip. Thus, we express the submatrix containing this element by sandwiching Eq(4.29) between the slices 1 and slice 1 [9] :

$$\mathcal{G}_{11} = \mathcal{G}_{11}^0 + \mathcal{G}_{1x}^0 V (1 - V \mathcal{G}_{xx}^0)^{-1} \mathcal{G}_{x1}^0 \qquad (4.30)$$

The subindex in this formula refers to the slices between which the Green's function is taken. x refers here to the slice where is situated the tip(we omit the subindex in x_0 when there is no confusion.). The fact that the potential is a Dirac delta function, non-zero solely on one site makes the calculation easier. In fact, we can write the correction of the Green's function due to the tip, $\Delta \mathcal{G}_{11} = \mathcal{G}_{11} - \mathcal{G}_{11}^0$ as follows:

$$\Delta \mathcal{G}_{11} = \mathcal{G}_{1x}^0 v (1 - v \mathcal{G}_{xx}^0)^{-1} \mathcal{G}_{x1}^0 \qquad (4.31)$$

In this relation, every element is a scalar if we restrain ourselves to the axis $y = 0$: $\mathcal{G}_{11}^0$ is the Green's function from and to the connected site, $\mathcal{G}_{1x}^0$ is the Green's function element from the connected site $(1,0)$ to the site where is the tip $(x,0)$ and $\mathcal{G}_{11}^0$ is between the sites $(x,0)$ and $(x,0)$.

Now comes the second step where we use the method of images to express the Green's function $\mathcal{G}_{1,x}^0$ of the semi-infinite lead, from the knowledge of the Green's function G_{1x}^0 of the perfect infinite lead. This method claims:

$$\mathcal{G}_{1x}^0 = G_{1,x}^0 - G_{1,-x}^0 \qquad (4.32)$$

Now, one needs to take the book by Economou [58], and uses the asymptotic expansion of Hankel functions to obtain after careful calculations for $x \gg \lambda_F$:

$$G_{0,x}^0 \sim -\frac{1+i}{4\sqrt{\pi}} \frac{e^{ikx}}{\sqrt{kx}}. \qquad (4.33)$$

With this result, we obtain the expression of the change in the Green's function element $\Delta \mathcal{G}_{11}^0$:

$$\Delta \mathcal{G}_{11}^0 = \frac{-ikv}{2\pi(1 - v\mathcal{G}_{xx}^0)} \frac{e^{2ikx}}{x} + O(\frac{1}{x\sqrt{x}}) \qquad (4.34)$$

where

$$\mathcal{G}_{xx}^0 \sim -\frac{1}{2\pi}[\mathcal{K}(\frac{E}{4}) - i\mathcal{K}(1 - (\frac{E}{4})^2)] + \frac{1+i}{4\sqrt{\pi}} \frac{e^{i2kx}}{\sqrt{2kx}} \qquad (4.35)$$

We remind that self energy of the lead containing the tip is:

$$\Sigma = t_c^2 \mathcal{G}_{11}$$

Now, the position dependence of the Green's function or the self energy of the lead containing the tip is very clear and moreover, the dependence on the strength of the tip is also simple ad contained in the same formula. Now, we become ready to study the change in the conductance due to the tip.

---

9. $\mathcal{G}_{1x}^0$ is a submatrix of the whole Green's function matrix. it gives the Green's function between the slice number 1 and the slice number x

4.3 Decay law of the fringes in scanning gate microscopy.

The tip induces a direct change in the self energy of the lead containing this tip. This change in the self energy, induces a variation in the conductance of the whole system. To study the transmission of the resonant level model (RLM), we start by expressing the Green's function on the scattering site in the center of the system:

$$G = \frac{1}{E - v_g - \Sigma^L - \Sigma^R} \tag{4.36}$$

v_g is the potential on the central site and Σ^L, Σ^R are, respectively, the left and right self energies. Every thing is a scaler in this expression, and this is due to scattering system which is a unique site. The transmission is also simple to express:

$$T(E) = \Gamma^R G \Gamma^L G^\dagger \tag{4.37}$$

Γ^L and Γ^R are, respectively, the left and right broadening elements.
In the absence of the tip, it is obvious that $\Sigma^L = \Sigma^R = \Sigma$ and therefore $\Gamma^L = \Gamma^R = \Gamma$. However, in the presence of the tip, there is a small change in the right self energy which induces the following changes:

$$\delta\Sigma = \Sigma^R - \Sigma \tag{4.38}$$
$$\delta\Gamma = \Gamma^R - \Gamma \tag{4.39}$$

These changes in the self energy (real and imaginary parts) are small since they behave like $\frac{1}{x}$ as it can be directly seen in expression (4.34). This allows us to make a perturbation expansion of the transmission. We start by writing the transmission as follows, taking care to separate the change in the real part and in the imaginary part of the self energy:

$$T(E) = \frac{\Gamma(\Gamma + \delta\Gamma)}{(E - v_g - 2\Re\Sigma - \delta\Re\Sigma)^2 + (-2\Im\Sigma - \delta\Im\Sigma)^2} \tag{4.40}$$

We define the following variables [10]:

$$\epsilon = \frac{\delta\Re\Sigma}{\Gamma} \tag{4.41}$$
$$\eta = \frac{\delta\Im\Gamma}{\Gamma} \tag{4.42}$$

Doing the expansion, in the case $E - V_g - 2\Re\Sigma > 0$, in terms of the variable ϵ and η, gives the following result:

$$\begin{aligned}
\frac{\Delta T}{T^\circ} \quad &\sim \quad 2\sqrt{T^\circ(1 - T^\circ)}\epsilon + (1 - T^\circ)\eta \\
&+ \quad T^\circ(3 - 4T^\circ)\epsilon^2 + (-\frac{5}{4}T^\circ + T^{\circ 2})\eta^2 \\
&+ \quad 2\sqrt{T^\circ(1 - T^\circ)}(1 - 2T^\circ)\epsilon\eta
\end{aligned}$$

This formula gives the relative change in the conductance as function of the changes in the real and imaginary parts of the self energy. The first important information we directly extract from this formula is that the result depend solely on the transmission T° of the system.
If the system without the tip is not completely open($T^\circ < 1$), we do not need to go to the second order in the expansion. The first order expansion reads:

$$\frac{\Delta T}{T^\circ} \quad \sim \quad 2\sqrt{T^\circ(1 - T^\circ)}\epsilon + (1 - T^\circ)\eta \tag{4.43}$$

---

10. ϵ and η are very small since they decay like $1/x$

Now, we start to use the results we obtained concerning the position dependence of the Green's function(4.34) in order to simplify this expansion:

$$\Delta\Sigma = t_c^2 \frac{v}{1 - v\mathcal{G}_{xx}^0} \frac{k}{2\pi x} e^{i(2kx - \frac{\pi}{2})} \tag{4.44}$$

$$= t_c^2 \left| \frac{v}{1 - v\mathcal{G}_{xx}^0} \right| \frac{k}{2\pi x} e^{i(2kx - \frac{\pi}{2} + \phi)} \tag{4.45}$$

$$= t_c^2 \mathcal{A} \frac{k}{2\pi x} e^{i(2kx - \frac{\pi}{2} + \phi)} \tag{4.46}$$

Where $\mathcal{A} = \left| \frac{v}{1 - v\mathcal{G}_{xx}^0} \right|$ and $\phi = \arg(\frac{v}{1 - v\mathcal{G}_{xx}^0})$.
$\mathcal{A}$, ϕ are here x-independent. The dependence in x will be taken as a correction in the expansion of the original formula (For the expansion see (4.35)).
All the dependence of the effect strength, related to the tip potential is contained in the variable $\mathcal{A}$
We need to express Γ as a function of the wavenumber k in order to simplify the expressions of ϵ and η. We start with the expansion (4.24) made at the continuum limit:

$$\Im\Sigma \sim -(1 + m), \quad m = \frac{E}{4}$$

If we remind that $t_h = \frac{\hbar^2}{2m^*a^2} = 1$ and that the bottom of the conduction band is shifted to $E = -4$ the dispersion relation reads in the continuum:

$$k^2 = E + 4$$

Therefore the expression of $\Gamma = -2\Im\Sigma$ becomes:

$$\Gamma \sim \frac{k^2}{2} \tag{4.47}$$

We are now ready to express the variables ϵ and η:

$$\epsilon = \frac{\mathcal{A}}{\pi k x} \cos(2kx - \frac{\pi}{2} + \phi) \tag{4.48}$$

$$\eta = -\frac{2\mathcal{A}}{\pi k x} \sin(2kx - \frac{\pi}{2} + \phi) \tag{4.49}$$

Everything is expressed now with simple parameters. We use all these expressions to answer the important question of this thesis: what is the decay law of the fringes in the experiments of Scanning Gate Microscopy?

4.3.1   Decay law of the fringes when $T^\circ < 1$

We start with the case of pinched off system for which $T^\circ < 1$. In this limit, where only the first order of the expansion needed, the results becomes, after some straightforward trigonometric manipulations as follows:

$$\frac{\Delta T}{T^\circ} \sim 2\mathcal{A}\sqrt{1 - T^\circ} \frac{\sin(2kx + \phi + \phi_T)}{\pi k x} \tag{4.50}$$

where we introduced the new phase ϕ_T defined as follows:

$$\begin{cases} \cos(\phi_T) &= \sqrt{T^\circ} \\ \sin(\phi_T) &= \sqrt{1 - T^\circ} \end{cases}$$

We obtain fringes spaced with $\lambda_F/2$ with a $\frac{1}{x}$ decay law. The change in the transmission ΔT takes both signs (negative and positive). All this is with a good agreement with what is found by numerical simulation either for the RLM model Fig. (4.4) or the realistic model Fig(3.10). Moreover, we deduce how the effect depends on the strength of the tip v: For small values of the tip potential, the effect is linear in v whereas it becomes v-independent at very large values of v.

4.3.2 Decay law of the fringes when $T° = 1$

The reader can notice a factor $\sqrt{1 - T°}$ in the formula of the relative change of the transmission in Eq. (5.51). This factor becomes smaller and smaller when we approach the full transparency until it exactly vanishes at $(T° = 1)$. At this limit, the first order disappears, and we therefore need to go to second order in the expansion of ΔT Eq. (4.43). We obtain for $T° = 1$:

$$\frac{\Delta T}{T°} \sim -(\epsilon^2 + \frac{\eta^2}{4}) \tag{4.51}$$

If we replace now ϵ and η by their expressions Eq. (4.49), we obtain the very simple following result:

$$\frac{\Delta T}{T°} \sim -\left(\frac{\mathcal{A}}{\pi k x}\right)^2 \tag{4.52}$$

This result shows that the effect of the tip on the conductance of a QPC decays as $\frac{1}{x^2}$ with almost no oscillations at full transmission! Indeed, the fringes come from the higher orders which contain oscillating terms.The second remark concerns the sign of the conductance change [11]: It is always negative, which means that the tip always reduces the conductance of full open systems. This is exactly what we noticed with numerical simulations in a realistic QPC open for the first mode with both Delta Dirac tip Fig. (3.4) and a Lorentzian extended tip Fig(3.11). The dependence on the strength of the tip v is also different: For small values of v the change in the conductance is proportional to v^2 (and not linearly like in the case of pinched off QPC) and remains v-independent for larger values of v.

It seems now, that we obtained the answers to the questions we were asking, and every thing becomes accessible by analytical formulas. The dependence on energy, position or the tip potential value are expressed in an easy way and explains well either the numerical results or the experimental data. We just need now to review what someone absolutely needs to keep in mind after these long calculations:

– The decay law of the conductance change do not depend explicitly on the coupling to the lead t_c: Only the transmission $T°$ matters.
– The decay law of the fringes is $\frac{1}{x}$ for $T° < 1$ while there is almost no fringes (higher smaller orders) with an effect decaying like $\frac{1}{x^2}$ for fully open QPC $T^0 = 1$.
– The dependence of the conductance change on the small values v of the tip potential is linear for more or less closed QPC, whereas for fully open QPCs $(T° = 1)$ it is quadratic. In both cases, it becomes v-independent at large values of v.
– The fringes are spaced by half the Fermi wavelength: $\lambda_F/2$.

4.3.3 Change in the density of state

We focused on the change in the transmission due to the tip. Now, We try to look at another quantity: The change in the density of states on the central site biased at a potential v_g. We start by recalling the Green's function on the central site:

$$G = \frac{1}{E - v_g - \Sigma^L - \Sigma^R} \tag{4.53}$$

The density of state on the central site, is obtained by the imaginary part of this Green's function:

$$\rho = -\frac{1}{\pi}\Im G \tag{4.54}$$

It follows:

$$\rho = \frac{1}{\pi}(\Im\Sigma^L + \Im\Sigma^R)|G|^2 \tag{4.55}$$

$$= \frac{\Gamma^L + \Gamma^R}{2\pi}|G|^2 \tag{4.56}$$

$$= \frac{\Gamma^L + \Gamma^R}{\Gamma^L\Gamma^R}\frac{T}{2\pi} \tag{4.57}$$

---

11. We remind that $\Delta T = T - T°$, with $T°$ the transmission of the system without the tip.

We need now to make visible the quantities without the tip:

$$T = T^\circ(1 + \frac{\Delta T}{T^\circ}), \quad \Gamma^L = \Gamma, \quad \Gamma^R = \Gamma(1 + \frac{\delta\Gamma}{\Gamma}). \tag{4.58}$$

If we use these formulas, the expression of ρ reads:

$$\rho = \frac{T^\circ}{2\pi\Gamma}(1 + \frac{\Delta T}{T^\circ})(1 + \frac{1}{1 + \frac{\delta\Gamma}{\Gamma}}). \tag{4.59}$$

With the help of the expansion of $\frac{\Delta T}{T^\circ}$ in terms of the variable ϵ and η we obtain:

$$\frac{\Delta\rho}{\rho^\circ} = 4\sqrt{T^\circ(1 - T^\circ)}\epsilon - (1 - 2T^\circ)\eta \tag{4.60}$$

Where the density of state in the absence of th tip is $\rho^\circ = \frac{T^\circ}{2\pi\Gamma}$.
Since ϵ and η decay both with a law $\frac{1}{x}$ (see 4.49), it appears that the relative change in the density of state on the central site of the RLM, decays as $\frac{1}{x}$ whatever is the transmission of the system.

4.3.4 Semi-classical approach of the determination of ΔG

Our approach to study the change in the conductance due to the presence of the tip, is based on the Green's function formalism and the Dyson equation. At the same time, the group of Strasbourg (Jalabert et al) followed a different way to obtain the same results [59]. Their approach is based on exploring the wave function of the electrons scattered by the QPC and the tip. The perturbation induced by the tip is expressed using the Lippmann-Schwinger equation. The first order of the perturbation they get reads [12]:

$$G^{(1)} = -4\pi\Im\{\text{Tr}[r^\dagger t' \mathcal{V}^{2,1}]\} \tag{4.61}$$

r, t are respectively, the reflection and transmission matrices and $\mathcal{V}^{2,1}$ is a matrix containing the perturbation and the incoming wave functions. This first order is relevant only in the vicinity of the conductance steps and suppressed on the plateaus. It follows that, on the plateau, the second order is needed:

$$G^{(2)} = -8\pi^2 \sum_{a=0}^{N-1} |\mathcal{V}_{a,a}^{2,1}|^2 \tag{4.62}$$

The complicated form of the matrix $\mathcal{V}$ is simplified if a delta potential is assumed for the tip. they therefore find that in the vicinity of the steps, the perturbation is dominated by the first order which implies a $\frac{v}{x}$ decay for the fringes whereas on the plateau, this order being suppressed, the second order shows a $(\frac{v}{x})^2$ decay of the tip effect.

4.4 Thermal enhancement of the fringes in the interference pattern of a quantum point contact

In the previous sections, we were interested in the change of the zero-temperature conductance due to the presence of a tip in one of the leads. We now, include temperature in order to study its effect on the decay law of the fringes. In fact, the presence of two different decay law of the fringes, depending on the transmission of the system, and thus the energy of the electrons, made us more aware about the importance of temperature for this model: Indeed, for non vanishing temperatures, all the electrons in a range $k_b\mathcal{T}$ around the Fermi energy, participate in the quantum transport. Hence, the transmission of the system is different for different energies and therefore, puts in the balance two laws decay corresponding to fully open ($T^\circ \sim 1$, $\frac{1}{x^2}$ decaying effect) and pinched off ($T^\circ < 1$, $\frac{1}{x}$ decaying effect) system. In more clear words, if we start with a system fully open ($T^0 \sim 1$), we obtain by SGM technique an interference pattern, with almost now fringes at

---

12. $\Delta G \sim G^{(1)} + G^{(2)}$

zero temperature. Rising temperature involves electrons for which the system is less transparent and therefore induces fringes with $\frac{1}{x}$ law decay. This means that we induced interference fringes by increasing temperature!. This is the contrary of the idea we have generally in mind: We used to say that temperature makes the quantum effects vanish while here, we found an effect where the quantum effect (interferences) is enhanced by temperature.

This argumentation, done by hands, shows how things became more clear with the resonant level model RLM after we expressed everything as a function of the energy, position or the tip strength. In what follows, in the light of this, we start now to give an analytical base of temperature effects in the RLM.

4.4.1 Temperature dependence of the RLM conductance

The conductance of a system at a given temperature is given by the following well known formula:

$$G(\mathcal{T}) = \frac{2e^2}{h} \int -\left(\frac{\partial f}{\partial E}\right) T(E) dE, \qquad (4.63)$$

where $f(E)$ is the Fermi-Dirac distribution:

$$f(E) = \frac{1}{1 + e^{\frac{E-\mu}{k_b \mathcal{T}}}}. \qquad (4.64)$$

The transmission of the RLM, without the tip, is known at all energies:

$$T(E) = \frac{1}{1 + \left(\frac{E - V_g - 2\Re(\Sigma)}{\Gamma}\right)^2} \qquad (4.65)$$

where Σ is given by Eq. (4.16) and $\Gamma = -2\Im\Sigma$.

This means that we have all the necessary tools to obtain the conductance at different temperatures. The curves obtained by numerical integration are given in Fig. (4.7) show the profile of conductance at different temperatures for the resonant level model (RLM). The effect of temperature on the resonance is to reduce its height and widen its width. This effect is more visible for weakly coupled system $t_c \ll 1$ where the reduction of the height of the resonance becomes important as soon as $\Gamma \sim t_c^2 < k_b \mathcal{T}$: For instance, the case $k_b \mathcal{T} = (500)^{-1}$ in Fig. (4.7) shows a resonance reduced by almost 60%compared to zero temperature case!. We need to keep this in mind when we include temperature in this model.

Temperature and the energy scales of the RLM

This subsection is devoted to link the energy scales of the theoretical approach with those of the experimental study. Till now, all the energies are expressed in units of the hopping term t_h whereas the experimental data are related to the temperature energy scale. We want to link the temperature of the problem to the energies of the RLM. To accomplish this task, we shall start by recalling that the typical effective mass in the GaAs/AlGaAs heterostructures is $m^* = 0.067m_e$. We add to this the fact that the discretization in numerical simulations introduces the parameter a which represents the lattice spacing. This parameter is evaluated to $a = 2$nm [13]. This assumptions yield the following energy scale: $t_h = 147$mev [14]. All the energies of the problem are expressed in units of t_h which can be converted to Kelvins by mean of the following relation:

$$1\text{mev} = 11.6K$$

From the experimental side, it was reported by the group of Stanford(Goldhaber Gordon) [18] that the fringes of interference pattern obtained by SGM techniques in very clean samples, disappear at temperature $1.7K$. That is why we try to keep studying systems at very low temperatures, usually less that $1K$.

---

13. Bigger than the atomic scale but small to approach the continuum limit

14. We remind the following definition: $t_h = \frac{\hbar^2}{2m^* a^2}$
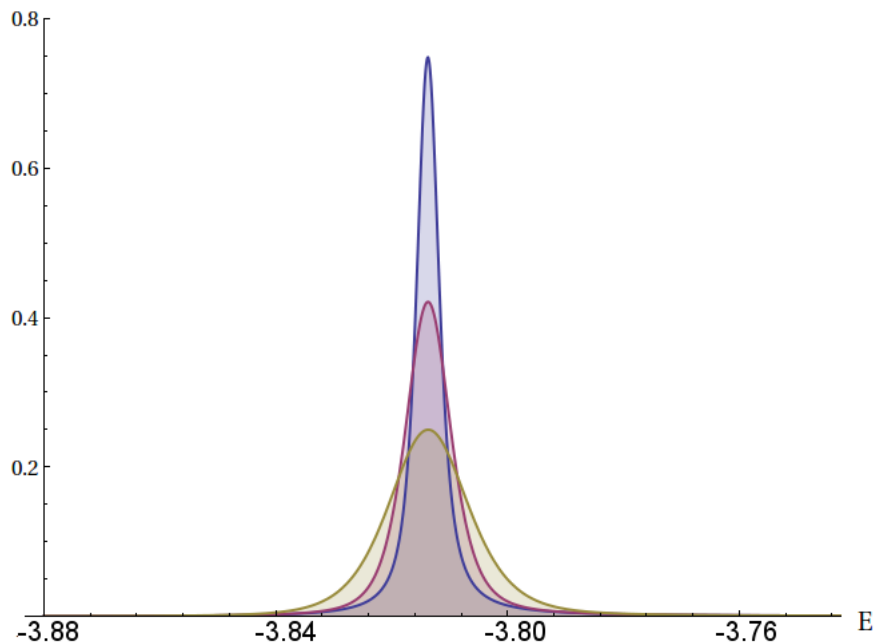
Figure 4.7: Conductance profile of RLM at different temperatures: Blue curve $k_b\mathcal{T} = (1500)^{-1}$, Purple curve $k_b\mathcal{T} = (500)^{-1}$ and Green curve $k_b\mathcal{T} = (250)^{-1}$.(these energies are expressed in units of the hopping term t_h). The effect of temperature is to lower the height of the profile and to widen the resonance. The resonance of all the curves in this figure are obtained at the same energy:$E_F = -3.8$. The coupling term is fixed to $t_c = 0.13$. G is expressed in units of $\frac{2e^2}{h}$.

Sommerfeld expansion and the temperature dependence of the conductance

Sommerfeld expansion is the classical tool we call when we introduce temperature in the system. It has the advantage of simplifying expressions and allows simple interpretation of the physical phenomena induced by temperature. To refresh memory, let us remind how does it work. We can write the following expansion for the energy dependent function H [61]:

$$\int_{-\infty}^{+\infty} H(\epsilon)f(\epsilon)d\epsilon = \int_{-\infty}^{\mu} H(\epsilon)d\epsilon + \sum_{n=1}^{\infty} a_n(k_b\mathcal{T})^{2n} H^{(2n-1)}(\mu) \qquad (4.66)$$

where $a_n = \int_{-\infty}^{+\infty} \frac{x^{2n}}{(2n)!}[-\frac{d}{dx}(\frac{1}{1+e^x})]dx$, which can be given by

$$a_n = [2 - \frac{1}{2^{2(n-1)}}]\zeta(2n)$$

and $\zeta(2n) = 2^{(2n-1)} \frac{\pi^{2n}}{(2n)!} B_n$, and B_n are Bernoulli numbers.
$H^{(m)}$ is the m-derivative of the function H. μ is the chemical potential.
If we define the function $K(\epsilon)$ as :

$$H(\epsilon) = \frac{dK}{d\epsilon}$$

we can write,after integrating by part :

$$\int_{-\infty}^{+\infty} K(\epsilon)(-\frac{\partial f}{\partial \epsilon})d\epsilon = K(\mu) + \sum_{n=1}^{\infty} a_n(k_b\mathcal{T})^{2n} K^{(2n)}(\mu) \qquad (4.67)$$

This kind of integral appears so often when we calculate transport coefficients. Let us apply this relation to express the conductance of the RLM. One finds:

$$G(\mathcal{T}) = T(\mu) + \sum_{n=1}^{\infty} a_n(k_b\mathcal{T})^{2n} T^{(2n)}(\mu) \qquad (4.68)$$

This relation gives the dependence on the temperature $\mathcal{T}$ at all orders. Of course, for very low temperatures, we do not need to go further, and the first order is enough.

Thermal enhancement of the interference effect in RLM

We would like now, to look at the effect of temperature on the results of scanning gate microscopy. If we restrain ourselves on very low temperatures, we can omit the higher orders in the Sommerfeld expansion and keep only the first one:

$$G(\mathcal{T}) \sim T(\mu) + \frac{\pi^2}{6}(k_b\mathcal{T})^2 T^{''}(\mu) \tag{4.69}$$

It follows straightforwardly, that the change in the conductance due to the presence of the tip, becomes:

$$\Delta G = \Delta T(\mu) + \frac{\pi^2}{6}(k_b\mathcal{T})^2 \Delta T^{''}(\mu) \tag{4.70}$$

Now, we use the results obtained in the previous section concerning the relative change in the transmission $\frac{\Delta T}{T^\circ}$, to include temperature in the RLM. We consider a Fermi energy at the resonance of the RLM, ie $E_F - V_g - 2\Re\Sigma = 0$ and the transmission $T^\circ = 1$, and apply the Sommerfeld expansion:

$$\Delta G \sim -\epsilon^2 - \frac{\eta^2}{4} + \frac{\pi^2}{6}(k_b\mathcal{T})^2[2\dot{a}^2\eta + 2\ddot{a}\epsilon] \tag{4.71}$$

The constants $\dot{a}$ and $\ddot{a}$ are given by the following relations which become simpler for weakly coupled leads:

$$\dot{a}^2 = (\frac{1 - 2\Re\dot{\Sigma}}{\Gamma})^2 \approx \frac{1}{\Gamma^2} \propto \frac{1}{t_c^4} \tag{4.72}$$

$$\ddot{a} = \frac{-2\Re\ddot{\Sigma}}{\Gamma} - 2\frac{(1 - 2\Re\dot{\Sigma})\dot{\Gamma}}{\Gamma^2} \propto \frac{1}{t_c^2} \tag{4.73}$$

We just mention that remembering $E_F - V_g - 2\Re\Sigma = 0$ is for great help in the simplification of these expressions.
So, we can say that for weak coupling , $\dot{a}^2 \gg \ddot{a}$ and therefore, one obtains [15]:

$$\Delta G = -(\frac{v}{\pi k x})^2 + \frac{\pi^2}{6}(\frac{k_b\mathcal{T}}{\Gamma})^2 \frac{4|v|}{\pi k x} \sin(2kx - \frac{\pi}{2}) \tag{4.74}$$

This is a very interesting result which shows explicitly the dependence on temperature and position. It shows that the first correction, due to temperature, scales like $(k_b\mathcal{T})^2$. Actually, what makes this result very important, is the enhancement of the fringes of the interference pattern: Indeed, the system (RLM) at zero-temperature shows almost no fringes. By increasing temperature, an oscillating term decaying like $\frac{1}{x}$ appears in the expression of the temperature-conductance change Eq(4.74). This term is the manifestation of an enhancement of the fringes due to temperature!. Unlike the general idea we have from quantum mechanics, which states that temperature kills quantum phenomena, here we induce the interference pattern with temperature. At higher temperatures, we expect the first order Sommerfeld expansion to deviate from the correct result and therefore, higher orders are needed. Instead of going further in the expansion, we will try here to do the following integral in the case of very sharp resonances($t_c \ll 1$):

$$\Delta G = \int_{-\infty}^{+\infty} \Delta T(E)(-\frac{\partial f}{\partial E})dE \tag{4.75}$$

To obtain this integral, we need to do the following approximation[62]:

$$-4k_b\mathcal{T}\frac{\partial f}{\partial E} \sim \exp^{-[(E-E_F)/4k_b\mathcal{T}\pi^{-1/2}]^2} \tag{4.76}$$

---

15. We give the result for small values of v where $\mathcal{A} \sim v$
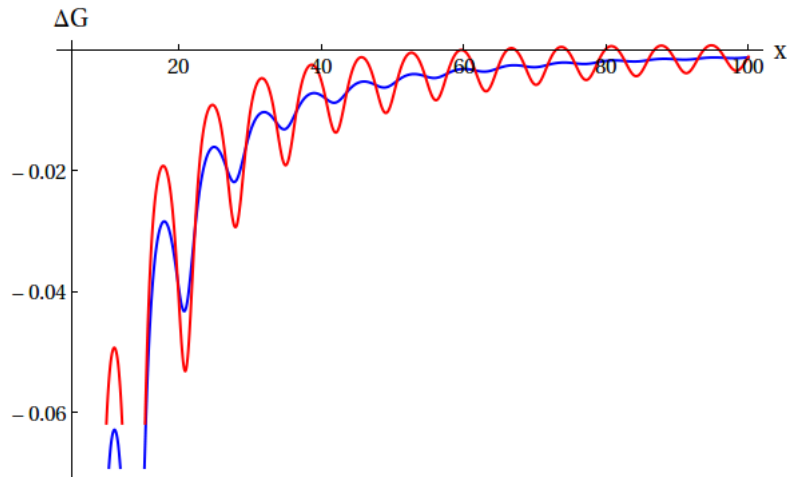
Figure 4.8: Thermal enhancement of interference fringes: The blue curve represents the conductance change ΔG as a function of the tip position x at zero temperature for the RLM. red curve represents ΔG at higher temperature $\mathcal{T} = 682mk$. The system is fully open ($T^\circ = 1$) and the Fermi energy is $E_F = -3.8$. The lattice step is $a = 2nm$ and $\mathcal{A} = -5$. The coupling to the leads is weak, $t_c = 0.2$
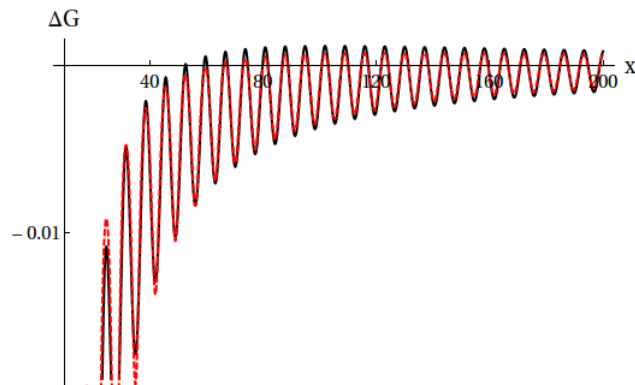
Figure 4.9: Temperature effect on the conductance change ΔG: Comparison between the Sommerfeld expansion (black curve) and the result of the numerical integration of the exact formula which gives ΔG. the comparison is good and becomes nicer far from the center of the system. The result is obtained for RLM with $t_c = 0.2$, $E_F = -3.8$ and $\mathcal{T} = 682mK$. The transmission of the system is $T^\circ = 1$.

The integration of the formula obtained so far for ΔT gives:

$$\frac{\Delta G(\mathcal{T})}{G^\circ(\mathcal{T})} \sim A\left(\frac{x}{l_\Gamma}, \frac{l_T}{l_\Gamma}\right) \frac{A\cos(2k_F x + \phi)}{2\pi k_F x} - \left(\frac{A}{\pi k_F x}\right)^2 \qquad (4.77)$$

The amplitude A is given by

$$A(\mu, \nu) = \frac{(1 + 2\mu + 4\nu^2)F_+ + F_- - G}{\mathrm{erfc}(\nu)} \qquad (4.78)$$

where $F_\pm = e^{\pm\mu}\mathrm{erfc}[\frac{2\nu^2 \pm \mu}{2\nu}]$ and $G = (4\nu/\sqrt{\pi})e^{-\nu^2 - (\mu^2/4\nu^2)}$.
In expression(4.77), we introduced the two lengths l_T and l_Γ. The first one is the thermal length which is defined as

$$l_T = \frac{k_F}{4k_b \mathcal{T}\pi^{-1/2}}$$

It corresponds to the length over which an electron propagates at a Fermi velocity during a time $\hbar/k\mathcal{T}$. The second length is related to the width of the resonance in the RLM. [16] It is defined as follows:

$$l_\Gamma = \frac{k_F}{\Gamma}$$

We can see that we recover the conclusions we obtained with the Sommerfeld expansion: When $T \to 0$, the oscillating term vanishes($A \to 0$) and the change in the conductance is given by the $-(A/\pi k_F x)^2$ which of course do not show fringes (actually there is a very tiny amplitude of an oscillating term coming from the correction of the higher orders of the expansion). At higher temperatures, the amplitude A is non-zero and leads to an enhancement of the fringes which become clearly visible Fig. (4.12). These conclusions show the existence of two regimes: The first one is when $l_T \gg l_\Gamma$ and corresponds to the case where $\mathcal{T} \to 0$. The second regime is achieved when $l_T \ll l_\Gamma$. In this case, for long distances $x \gg l_T$, the decay is characterized by the asymptotic behavior $\exp(-x/l_\Gamma)$ which means that the decay is controlled by l_Γ and not by l_T. This is why we can observe fringes beyond the thermal length as it can be noticed in Fig. (4.12).

4.4.2   Thermal enhancement of the fringes in a Realistic QPC.

The thermal enhancement of the fringes in the resonant level model (RLM) is now clear and verified either with analytical expressions or with numerical simulations. Now, since the same arguments apply to a realistic QPC model, we want to check this effect and try to understand it within the physics of QPCs. The first remark we point out is the absence of resonance in the transmission profile of QPCs which is replaced by the presence of plateaus of conductance quantification. This does not alter the argumentation presented for the RLM: Indeed, if we take a Fermi energy at the end of the step of the transmission profile (in other words the beginning of the plateau), the figure of interference pattern will show almost no fringes at zero temperature because $T^\circ \sim 1$ and therefore the effect of the tip decays like $\frac{1}{x^2}$. If one "switches on" temperature, the QPC becomes nearly open for electrons with energy in a range $K_b\mathcal{T}$ around the Fermi energy. This gives more weight to the contribution of the step region (See Fig 4.10) for which the effect of the tip on the conductance change ΔG decays like $\frac{1}{x}$ (ie slower than the law $\frac{1}{x^2}$) with an oscillating amplitude. To verify this numerically, we assume a realistic model for the QPC, presenting a sharp step in the conductance profile (See page 20 to understand how to obtain this condition) in order to use small temperatures to see this effect. We choose the following model for the QPC (model 1):

$$V(x, y) = \begin{cases} a\frac{1}{2}y^2(1 - 3(\frac{2x}{l})^2 - 2|\frac{2x}{l}|^3)^{1/4} & If \quad |2x| < l \\ 0 & If \quad |2x| > l \end{cases} \qquad (4.79)$$

a is a constant which controls the T° and $2l$ is the length of the QPC region.
First we set temperature to be zero and choose an opening and a Fermi energy for which the transmission of the system is around the first values of the plateau of conduction as explained in Fig. (4.10). The result of the SGM is the interference pattern shown in Fig. (4.12 a). We see almost

---

16. In the case of a realistic QPC model, it corresponds to the sharpness of the steps of the conductance profile
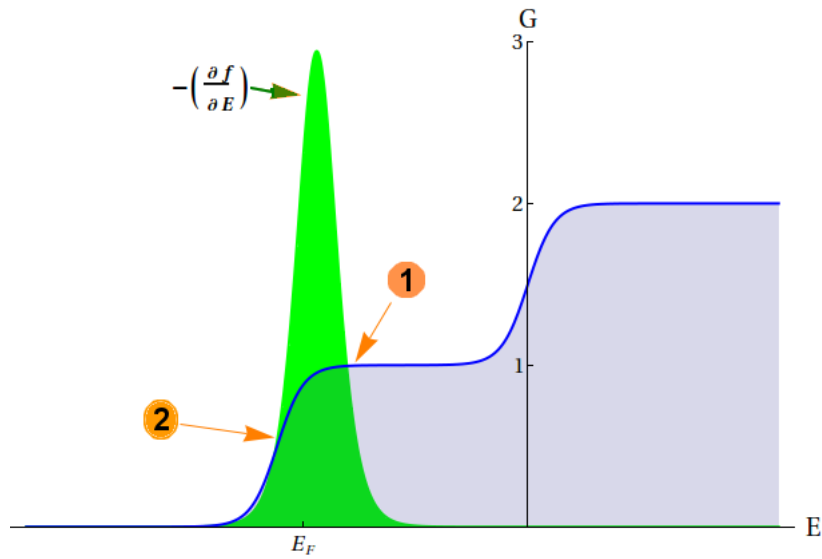
Figure 4.10: Thermal effect in a realistic QPC: Including temperature makes the QPC nearly open to electrons with energy in a range $k_b\mathcal{T}$ around the Fermi energy E_F. Here E_F is at the first points in the transmission profile having $T°$ almost equal to one. For transmissions in region 2, the tip effect decays like $1/x$ while in region 1 the effect decays like $\frac{1}{x^2}$. Temperature lets region 2 having more weight and therefore enhances the effect of the tip. The profile of the transmission (blue curve) is obtained for a realistic QPC, and shows quantized plateaus.
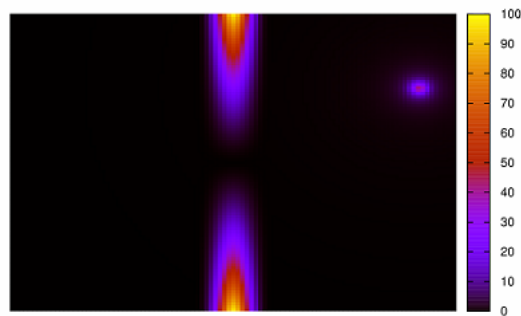
Figure 4.11: Realistic QPC model with adiabatic opening and smooth connection to the leads.

no fringes with a negative effect on the conductance change ($\Delta G < 0$). This agrees with the conclusion obtained from the RLM study: For an open QPC($T^\circ \sim 1$), the tip reduces the conductance and there is almost no fringes in the interference pattern. This can be easily understood: Since the QPC is fully open for the first mode of conduction, the Fabry-Perot interferences between the QPC and the tip have small amplitudes and we can say that the system acts like a bad electronic interferometer. Now, the temperature being switched on, the interference pattern becomes more visible and the fringes are well spaced as shown in Fig. (4.12 b). In fact, with temperature, electrons with different energies get involved. For these electrons, the system is not completely open and therefore the Fabry-Perot interferences have a bigger amplitude and therefore the fringes are more visible. The system acts here like a good electronic interferometer.

4.5   Thermal effect in SGM of highly opened QPCs

In the previous subsection, we pointed out the thermal enhancement of the fringes in a QPC fully open for the first mode of conduction. Actually, the arguments we invoked are not restrained to the first mode of conduction. Indeed, in the plateaus of conduction, the tip can not open a new mode of transmission. It can only reduce the conduction and has a small effect. On the contrary, in the steps, its effect on the conductance is either negative or positive and has a slower decay law. Therefore, if the Fermi energy is on the edge of the plateau of the higher modes of conduction, we expect temperature to enhance the fringes in the interference pattern like for the first mode. We test this assumption with the following QPC model(model 2) defined with a hard wall boundary conditions at the sites lying in the curve:

$$|y| = l_y + 3(x/l_x)^2 \tag{4.80}$$

$l_y = 6$ and $l_x = 20$. The total length of the QPC region is $2l_x$.

As it can be seen in Fig. (4.12 c and d), the interference pattern obtained at zero temperature has almost no fringes whereas, they are clearly visible after we turned on temperature. Moreover, we notice that the fringes persist beyond the thermal length l_T. The interference pattern of the SGM on the second mode of conduction shows two preferential directions $\pm 45^\circ$.

Summary: The RLM simplifies a lot the description of interference pattern in scanning gate microscopy and allows an analytical treatment of the change in the conductance due to an external AFM charged tip. The main result in this chapter is that the decay law of the tip effect on the conductance of a QPC fully open to the first mode of conduction is $(\frac{v}{x})^2$ with almost no fringes. For less opened QPCs, the fringes of the interference pattern decay slowly like $\frac{v}{x}$. The existence of these two different laws of the tip effect, suggests an enhancement of the fringes when we go from a QPC open, in the edge of the plateau of conduction and raise temperature. Moreover, we find that the fringes last beyond the thermal length. The verification of these results in a realistic QPC strengthen this study and makes the Resonant Level Model (RLM) a good candidate, at least for some problems,to model quantum point contacts.
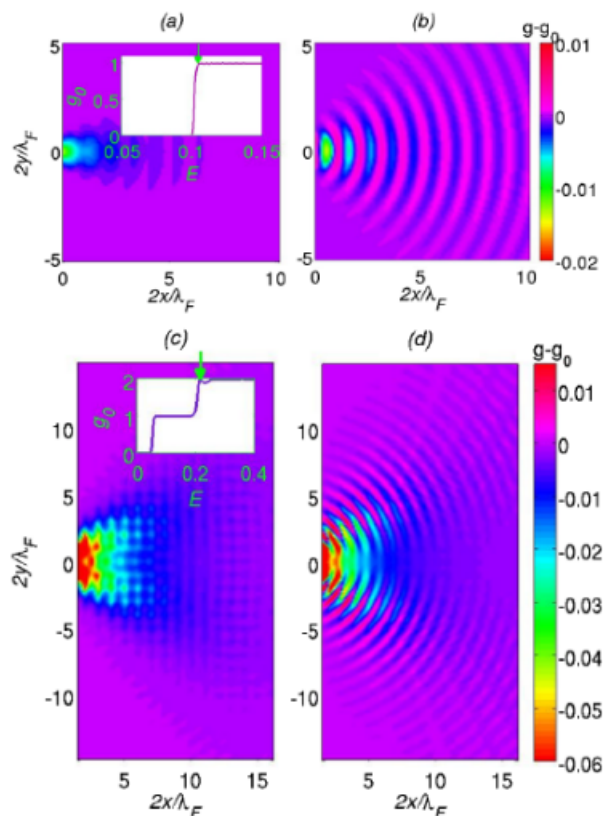
Figure 4.12: $\delta g(\mathcal{T}) = g(\mathcal{T}) - g_0(\mathcal{T})$ as a function of the tip position(in units of $\lambda_F/2$). The left figures correspond to $T = 0$, while $T \neq 0$ for the right figures. g_0 is biased as indicated by the arrow in the insets[giving $g_0(\mathcal{T} = 0)$ as a function of E_F]. (a), (b), QPC opened at beginning of the first plateau using model 1 with $v = 1$ and $\lambda_F/2 = 9.65$. $\frac{k_b\mathcal{T}}{E_F} = 0.01$ for (b) ($2l_T/\lambda_F = 14.6$.).(c) (d): QPC opened at the beginning of the second plateau using model 2 with $v = -2$ and $\lambda_F/2 = 6.7$. $\frac{k_b\mathcal{T}}{E_F} = 0.035$ for (c) $2_T/\lambda_F = 4$

Chapter 5

Scanning Gate Microscopy of Thermopower in Quantum Point Contacts

Contents

Summary of chapter 5

In this chapter, we are interested in the Seebeck coefficient of a quantum point contact(QPC). After a quick introduction to thermopower and the different formulas with which it can be expressed, we turn to the experimental setup of Scanning Gate Microscopy of Seebeck coefficient in quantum point contacts . A charged tip moving above the electron reservoir of a QPC, allows us to obtain the interference pattern of Seebeck change ΔS_k, due to the depletion region in the electronic charge density induced by the tip. The fringes are obtained by numerical simulation, first in the case of fully open QPC for the first mode ($T^\circ = 1$), and secondly for half closed QPC. We notice a focusing effect (the tip has a significant effect only in an angle between $\pm 45°$) that we explain by expressing the 2D change in the self energy the tip induces. As we did successfully in the previous chapter to study the change in the conductance, we propose a resonant level model (RLM) to study the change ΔS_k as a function of the tip position. At very low temperatures (Where the Cutler-Mott formula is valid), we find the following main results:

  – case $T^\circ = 1$: If the RLM is fully open (corresponds to a realistic QPC open in the edge of the first plateau), the fringes decay like $1/x$ to vanish at very long distance.
  – case $T^\circ = 0.5$: If the system is half closed, the fringes decay also like $1/x$ but oscillates with a constant amplitude at large distances before they vanish at infinity, where the Cutler-Mott formula do not work anymore. In other words, there is a range where the amplitude of ΔS_k do not decay.

These results are obtained by analytical calculations based on the Cutler-Mott formula. They are well verified, at low temperatures, by numerical simulations using the recursive Green's functions algorithms and the numerical integration of the exact Seebeck formula.
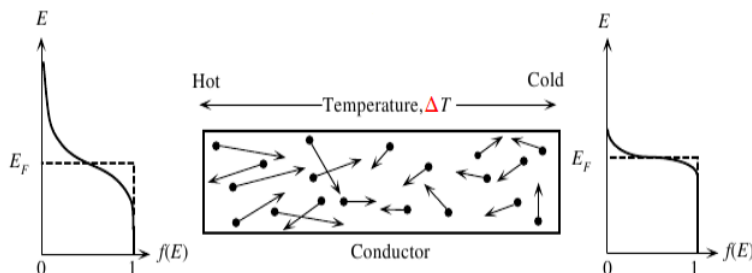
Figure 5.1: A conductor sketched between a hot and a cold electron reservoir. The Seebeck coefficient is given by the ratio between the difference of the two reservoirs temperatures and the voltage ΔV induced by the difference $\Delta \mathcal{T}$. Taken from [63]

5.1 Introduction

In the previous chapters, we were interested in the transmission of a quantum point contact (QPC) and the figures of interference pattern of the conductance change of such QPCs. We remind that the transmission is the transport coefficient within the linear response theory in a system connected to two reservoirs biased to slightly different voltages. If the two reservoirs are set to two slightly different temperatures rather than voltages, the linear response theory defines the thermoelectric coefficient: Seebeck coefficient S_k. This coefficient is obtained as follows:

$$S_k = -\frac{\Delta V}{\Delta \mathcal{T}}$$

where ΔV is the voltage difference induced by the difference in temperature ΔT.

Here, in this chapter, we will be interested in the quantum ballistic regime at very low temperature and look at the Seebeck coefficient of a quantum point contact. The purpose of the study is to look at the change in the Seebeck coefficient induced by a scanning gate microscope. We want to obtain figures of interference pattern of Seebeck coefficient change ΔS_k as we did it previously for the transmission coefficient. Of course, we are interested in the decay law of the fringes and the temperature dependence of the fringes.

5.2 Thermoelectric quantum transport and linear response theory

5.2.1 Onsager matrix

To express the transport coefficients, one needs to write using linear response theory the electrical and thermal currents:

$$J = L^{11}[-\frac{1}{\mathcal{T}}\nabla(\mu + eV)] + L^{12}\nabla(\frac{1}{\mathcal{T}}) \tag{5.1}$$

$$J_Q = L^{21}[-\frac{1}{\mathcal{T}}\nabla(\mu + eV)] + L^{22}\nabla(\frac{1}{\mathcal{T}}) \tag{5.2}$$

μ is the chemical potential and V is an electrostatic potential. The coefficients L^{ij} are obtained using Kubo formula [64].

These coefficients represent the elements of a matrix L known as the Onsager matrix. There exists a reciprocity relation between the off diagonal elements of this matrix. It claims that, in the presence of time reversal symmetry, the Onsager matrix is symmetric:

$$\text{Time reversal symmetry} \Rightarrow L = L^T \tag{5.3}$$

If the chemical potential is constant, one finds:

$$G = e^2 L^{11}/\mathcal{T} \tag{5.4}$$

$$S_k = -\frac{\Delta V}{\Delta \mathcal{T}} = \frac{1}{e\mathcal{T}}\frac{L^{12}}{L^{11}} \tag{5.5}$$

$$\mathcal{K} = \frac{1}{\mathcal{T}^2}\left(L^{22} - \frac{L^{12}L^{21}}{L^{11}}\right) \tag{5.6}$$

$\mathcal{K}$ is the electronic part of the thermal conductivity.

5.2.2 Wiedemann-Franz Law

With these coefficients, we define the following ratio known as the Lorentz number:

$$L = \frac{\mathcal{K}}{G\mathcal{T}} = \frac{1}{e^2\mathcal{T}^2}\frac{L^{11}L^{22} - L^{12}L^{21}}{(L^{11})^2} \tag{5.7}$$

This number, constant for a lot of metals, is indeed equal to the following constant

$$L = (\frac{k_b}{e})^2\frac{\pi^2}{3} \tag{5.8}$$

This is known as the Wiedemann-Franz law. It is an exact result for independent electrons interacting with static impurities [64].
From the calculation of the coefficient L^{ij} using the Kubo formula and simplified using the Green's function properties, we deduce the important following formula, on which we will focus all over this chapter:

$$S_k = \frac{1}{e\mathcal{T}}\frac{\int(-\frac{\partial f}{\partial E})(E - \mu)T(E)dE}{\int(-\frac{\partial f}{\partial E})T(E)dE} \tag{5.9}$$

Where μ is the chemical potential and T the transmission of the system we study.
This expression is the exact formula we should use to calculate the Seebeck coefficient. Nevertheless, the integral form hides a lot of information which can not be reached with this expression. As we can see, it can be more simplified if we use the Sommerfeld expansion.

5.2.3 Sommerfeld expansion and the Cutler-Mott formula

The Sommerfeld expansion introduced in the previous chapter (see also [61]) helps us to drop the integrals and get a more convenient form. We start by writing the following expression easily obtained from the Sommerfeld expansion of each integral of the form (5.9):

$$S_k = \frac{\sum_{n=0} 2na_n(k_b\mathcal{T})^{2n}T^{(2n-1)}(\mu)}{\sum_{n=0} a_n(k_b\mathcal{T})^{2n}T^{(2n)}(\mu)} \tag{5.10}$$

Here $T^{(m)}$ means the m derivative of the transmission function and $a_n = [2 - \frac{1}{2^{2(n-1)}}]\zeta(2n)$. This form can be useful for numerical calculations but it is more interesting since it is the starting point to the first orders in the temperature expansion of the Seebeck expression.

Cutler-Mott formula

The first order in the temperature expansion of the Seebeck coefficient is known as the Cutler-Mott formula. It reads:

$$S_k = \frac{\pi^2}{3}\left(\frac{k_b^2\mathcal{T}}{e}\right)\left(\frac{\partial \ln(T)}{\partial E}\right)_{E=\mu} \tag{5.11}$$

This expression, valid at low temperatures, shows clearly the dependence on the temperature and requires the energy dependence of the transmission solely around the Fermi energy. Of course, for

higher temperatures, this formula deviates from the exact result(See for example [65]). Another form referred as the Mott formula can be found in literature[66] [67]:

$$S_k^M = \frac{\pi^2}{3}\left(\frac{k_b^2 \mathcal{T}}{e}\right)\left(\frac{\partial \ln(G(\mathcal{T}))}{\partial E}\right)_{E=\mu} \tag{5.12}$$

This formula uses the conductance G at temperature $\mathcal{T}$ instead of the transmission (i.e the zero temperature conductance). It is easy to understand that this formula is more suitable for experimentalist since they access more easily to the conductance $G(\mathcal{T})$ than the zero-temperature conductance.

First correction to the Cutler-Mott formula

Sometimes, we need to go further in the expansion and seek for the correction to the Cutler-Mott formula. We can express this correction (second order in the expansion) as follows:

$$S_{\text{corr}} = \frac{\pi^4}{90e}k_b^4 \mathcal{T}^3 (2\frac{T^{(3)}}{T} + 5\partial_E \frac{T^{(2)}}{T}) \tag{5.13}$$

5.3 Scanning gate microscopy and thermopower of quantum point contacts

We want to study here a system similar to what we saw in the previous chapters(QPC) but we will focus on the change of thermopower ΔS_k (Seebeck coefficient) rather than the change in the conductance: Indeed, the two reservoirs sketching a quantum point contact are set to slightly different temperatures. This difference in temperature leads to the appearance of a voltage difference ΔV between the two reservoirs. The Seebeck coefficient is directly obtained by the ratio :$S_k = -\frac{\Delta V}{\Delta T}$. Now, with a charged AFM tip, situated above the 2DEG of the lead (electron reservoir), we create a depletion region in the charge density. This will lead to a change ΔS_k in the Seebeck coefficient of the system [1]. Acquiring these changes as a function of the tip position gives an interference pattern of fringes separated by half the Fermi wavelength $\lambda_F/2$. We want to study these figures, and obtain the decay law of the fringes for systems at very low temperatures.

Numerical simulation of the interference pattern of Thermopower

When we look at expression Eq. (5.9) of thermopower, we realize that all what we need is the transmission T of the system and to do numerically the integrals. All the previous chapters where dedicated to the calculation of the transmission of different QPC models using the Green's function formalism. It becomes easy now to obtain the figures of the interference pattern of the thermopower change ΔS_k. For this task, we consider the following realistic QPC model:

$$V(x,y) = \begin{cases} a_0 \frac{1}{2}y^2(1 - 3(\frac{2x}{l})^2 + 2|\frac{2x}{l}|^3)^2 & \text{if} \quad |2x| < l \\ 0 & \text{if} \quad |2x| > l \end{cases} \tag{5.14}$$

$2l$ is the length of the QPC.
This model has an adiabatic opening and a smooth connection to the lead. The numerical simulation based on the Green's function formalism and the numerical integration of the exact formula of the Seebeck coefficient give the figures of interference pattern presented in Fig. (5.2 (a) and (b)). Before analyzing these figures we need to make some remarks. It is not interesting to look at the Seebeck coefficient for a QPC open at the middle of a plateau of conduction for the following obvious reason: At the plateau of conduction, the profile of the conductance is symmetric on a range $k_b \mathcal{T}$ around the Fermi energy. It follows that the function to integrate in Eq (5.9) is odd and therefore the result vanishes. This can also easily be understood using the Mott formula: The derivative of the conductance vanishes at the plateau [2]. For this reason we choose a QPC opened outside or at the edge of the plateaus.

---

1. $\Delta S_k = S_k - S_k^\circ$. S_k° is the Seebeck coefficient in the absence of the tip
2. Of course this argument is valid at very low temperature

Figure (5.2(a)) is obtained with the realistic QPC model defined above, completely open to the first mode of conduction in the absence of the charged tip ($T° = 1$). Moreover, the transmission of the QPC is at the left edge of the first plateau of conduction. Figure (5.2(b)) is obtained with a QPC closed for half the first mode of conduction ($T° = 0.5$). For both simulations, the Fermi energy is taken close to what assumed in SGM experiments [1] ($E_F = 15.5$mev if the lattice spacing is $a = 2$nm). The temperature $\mathcal{T}$ is set to 852 mK which is higher than what is usually taken in the SGM on very clean samples [18].

Figures (a) and (b) show an interference pattern of fringes spaced by half the Fermi wavelength
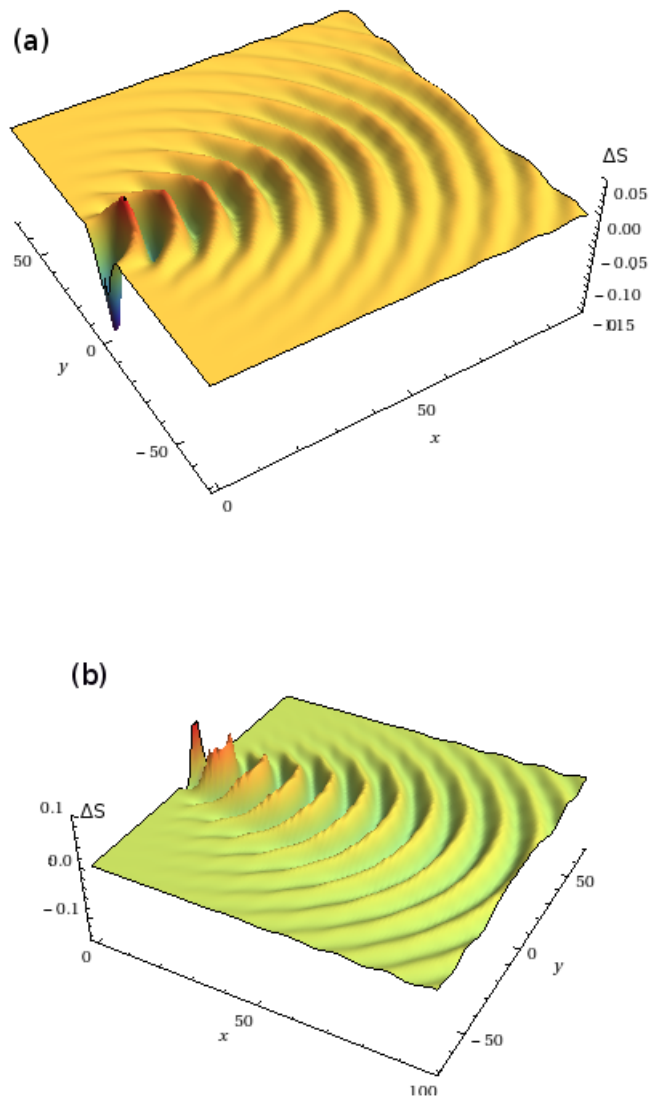
Figure 5.2: Seebeck change (ΔS_k), as a function of the tip position(x, y). Figure (a) is obtained when $T° = 1$, at the edge of the first plateau of conduction of the realistic QPC. Figure (b) is obtained for $T° = 0.5$. In both cases, we can see an interference pattern with decaying fringes spaced by $\lambda_F/2$. The parameters of the simulation are chosen to be close to what are used in SGM Experiments [1]: $E_F = 15.5$mev and $\lambda_F = 39$nm. x, y are expressed in units of the lattice parameter $a = 2$nm. The Seebeck is calculated by numerical integration using the exact formula for S_k. Temperature is set here to $\mathcal{T} = 852$mK.

($\lambda_F/2$). We can notice that the fringes decay with the distance from the QPC. We also clearly notice a focusing effect: The fringes are concentrated between $\pm 45°$ and outside this region, there is almost no fringes with a smooth appearance. To explain focusing effect, we proceed as follows.

First, we know that the presence of the charged tip induces a change in the self energy of the lead connected to the QPC. This change in the self energy is responsible for the change in the conductance of the system and therefore the change in the Seebeck coefficient. It comes out from this argument, that we need the 2D change in the self energy.

5.4   Focusing effect and the change in the self energy of a 2D lead
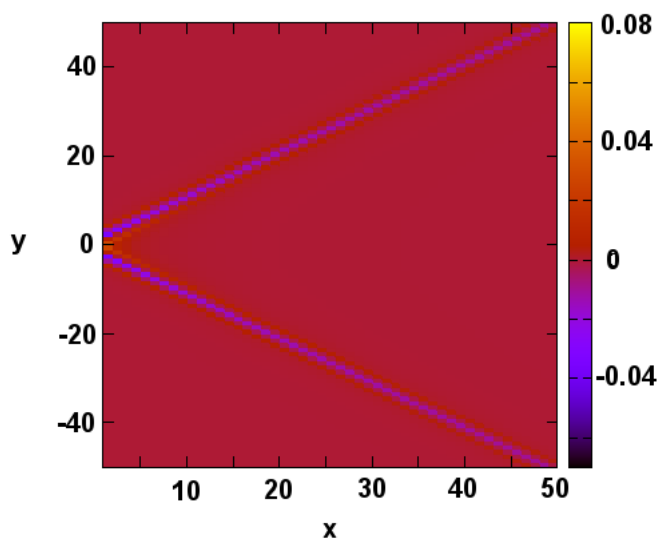
Figure 5.3: The change $\Delta\Re\Sigma(x,y)$ in the real part of the self energy of a 2D lead as a function of the tip position. This result is given at the half filling limit. The effect of the tip is significant only in two directions $\pm 45°$.

We have seen in the previous chapter, using the method of mirror images, how to express the change in the self energy of the lead due to the presence of the tip. The result was obtained for a tip situated in the central axis of the lead (y=0). Here, we want to give another different method, which allows us to generalize that result to all the positions (x,y) in the lead. This helps us to comment the 2D pictures of fringes interference pattern in the Scanning Gate Microscopy experiments and simulations. The starting point of our calculation is the Green's function element between the site of the lead connected to the central region (See Fig 4.5) and the tip[27]. This element reads [3]:

$$G_{1x}(p,q) = \frac{2}{N+1} \sum_{m=0}^{N} \sin(\frac{m\pi}{N+1}p) \sin(\frac{m\pi}{N+1}q) e^{-ix\theta_m} \qquad (5.15)$$

Where we noted the position of the tip (x,q) and the site connected to the central system $(1,p)$.

---

3. $\sqrt{\frac{2}{N+1}} \sin(\frac{m\pi}{N+1}p)$ is the transverse wave function in a perfect lead. N is the number of sites in the transverse direction.

The angle θ_m is defined as follows:

$$\cos(\theta_m) = \frac{E}{2} + \cos(\frac{m\pi}{N+1}) \tag{5.16}$$

5.4.1 Half filling limit: $E = 0$

We start with the simple case of the half-filling limit ($E = 0$), where the expression of θ_m becomes $\theta_m = \frac{m\pi}{N+1}$. It follows, for large value of N, the sum becomes the following Riemann integral:

$$\begin{aligned} G_{1x}(p,q) &= \frac{2}{\pi} \int_0^\pi \sin(p\theta)\sin(q\theta)e^{-ix\theta}d\theta \tag{5.17} \\ &= \frac{2}{\pi} \int_0^\pi \frac{\cos[(p-q)\theta] - \cos[(p+q)\theta]}{2} e^{-ix\theta}d\theta \tag{5.18} \\ &= \frac{1}{\pi} \int_0^\pi \cos(y\theta)e^{-ix\theta}d\theta \tag{5.19} \end{aligned}$$

We defined the variable $y = p - q$. The term containing $\cos[(p+q)\theta]$ is much oscillating [4] and leads to a vanishing contribution in the integral.
This last integral is easily done to finally obtain:

$$G_{1x}(y) = \begin{cases} 0 & \text{if} \quad x - y = 0[2] \\ \frac{1}{2} & \text{if} \quad x = |y| \\ -i\frac{2}{\pi}\frac{x}{x^2-y^2} & , \quad \text{elsewhere} \end{cases} \tag{5.20}$$

If we remind that the change in the self energy verifies:

$$\Delta\Sigma \propto (G_{1x}(y))^2$$

we find that $\Delta\Sigma$ has significant values only near the lines $x = |y|$, that is to say in the two directions $\pm 45°$. This result, obtained at the half-filling limit ($E = 0$), can be understood as an effect due to the discretization of the lattice.

5.4.2 Continuum limit: $E \sim -4$

To approach what happens in experiments, we need to look at the continuum limit, for energies near the bottom of the conduction band. At this limit, only the lowest modes are conducting and therefore in the sum (5.15), we only consider [5] the terms which verify $\frac{m\pi}{N+1} \ll 1$. The relation(5.16) becomes:

$$\cos(\theta_m) \sim \frac{E+2}{2} - \frac{1}{2}(\frac{m\pi}{N+1})^2 \tag{5.21}$$

The expansion of the function arccos leads to the following expression of θ:

$$\theta_m \sim \arccos(\frac{E+2}{2}) + \frac{1}{2\gamma}(\frac{m\pi}{N+1})^2 \tag{5.22}$$

and γ reads:

$$\gamma = \sqrt{1 - (\frac{E+2}{2})^2}$$

Passing to Riemann integral for large N, the sum. (5.15) becomes:

$$G_{1x}(p,q) = \frac{2}{\pi} \int_0^{\frac{M\pi}{N+1}} \sin(pt)\sin(qt)e^{-ix[\arccos(\frac{E+2}{2}) + \frac{t^2}{2\gamma}]}dt \tag{5.23}$$

$$\tag{5.24}$$

---

4. p scales like $\frac{N}{2}$ (the middle of the lead)
5. For the higher modes, θ_m becomes complex and therefore the corresponding terms in the sum decay exponentially.

M is the index of the higher conducting mode.

To carry on the next calculation, we need to make the following important remark: The wave number k can be expressed in different ways:

$$k \sim \begin{cases} \frac{M\pi}{N+1} \\ \sqrt{E+4} \\ \sqrt{1-(\frac{E+2}{2})^2} \\ \pi - \arccos(\frac{E+2}{2}) \end{cases} \tag{5.25}$$

We give a demonstration of this result in the appendix E.

Using these expressions of the wave number we obtain:

$$G_{1x}(p,q) \sim \frac{(-1)^x}{\pi} e^{ikx} \int_0^k \left(\cos[(p-q)t] - \cos[(p+q)t] \right) e^{-ix\frac{t^2}{2k}} dt \tag{5.26}$$

Again, we put $y = p - q$ and omit the term which contains $p + q$ (too much oscillating) to obtain:

$$G_{1x}(y) \sim \frac{(-1)^x}{\pi} e^{ikx} \int_0^k \cos(yt) e^{-ix\frac{t^2}{2k}} dt \tag{5.27}$$

We can write this last integral as follows:

$$G_{1x}(y) \sim (-1)^x \frac{F_x(y) + F_x(-y)}{2\pi} e^{ikx} \tag{5.28}$$

Where we defined the function $F_x(y)$ as follows:

$$F_x(y) = \int_0^k e^{-i(x\frac{t^2}{2k} - yt)} dt \tag{5.29}$$

After standard straightforward change of variables we can rewrite $F_x(y)$ using the Fresnel integrals:

$$F_x(y) \sim \left(\frac{\pi k}{x} \right)^{\frac{1}{2}} e^{ik\frac{y^2}{2x}} \int_a^b e^{-i\frac{\pi}{2}z^2} dz \tag{5.30}$$

$a = -\left(\frac{k}{\pi x} \right)^{\frac{1}{2}} y$ and $b = \left(1 - \frac{y}{x}\right)\left(\frac{kx}{\pi}\right)^{\frac{1}{2}}$ From the study of the sign of a and b, the Fresnel integral gives:

$$G_{1x}(y) \sim \begin{cases} \left(\frac{2\pi k}{x}\right)^{\frac{1}{2}} e^{i(k\frac{y^2}{2x} - \frac{\pi}{4})} & 0 < y < x \\ 0 + \text{correction} & \text{elsewhere} \end{cases} \tag{5.31}$$

We come back to the relation(5.28) and get:

$$G_{1x}(y) \sim \begin{cases} (-1)^x \left(\frac{k}{2\pi x}\right)^{\frac{1}{2}} e^{i(kx + k\frac{y^2}{2x} - \frac{\pi}{4})} & |y| < x \\ 0 + \text{correction} & \text{elsewhere} \end{cases} \tag{5.32}$$

We finally arrive to the formula giving the change in the self energy due to the presence of the tip situated at the position (x, y):

$$\Delta\Sigma = t_c^2 \frac{v}{1 - v\mathcal{G}_{xx}^0} G_{1x}^2$$

and therefore we can write:

$$\Delta\Sigma \sim \begin{cases} t_c^2 \mathcal{A} \frac{k}{2\pi x} e^{i(2kx + k\frac{y^2}{x} - \frac{\pi}{2} + \phi)} & |y| < x \\ 0 + \text{correction} & \text{elsewhere} \end{cases} \tag{5.33}$$

$\mathcal{A} = \left| \frac{v}{1 - v\mathcal{G}_x^0} \right|$ and $\phi = \arg(\frac{v}{1 - v\mathcal{G}_x^0})$. t_c is the coupling element.

This formula has to be compared to the result obtained in the case $y = 0$ using the method of mirror images Eq. (4.46). We find the same result. The interesting remark we do using this result is to
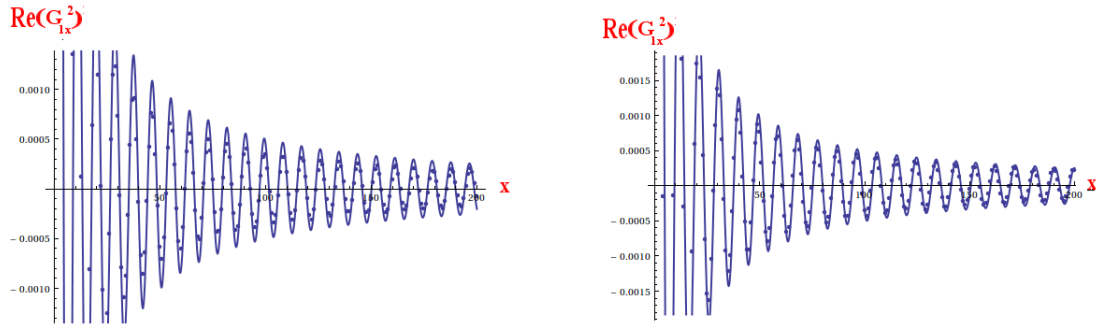
Figure 5.4: Comparison between numerical calculation(blue dots) obtained with the exact formula and the formula (5.32) (Blue curve) for the 2D change in the $\Re(G_{1x(y)})^2$. The figure in the right is obtained for an angle $\alpha = 18.43$ (i.e $x = 3y$) and the figure in left is obtained for $\alpha = 26.56$ (i.e. $x = 2y$)
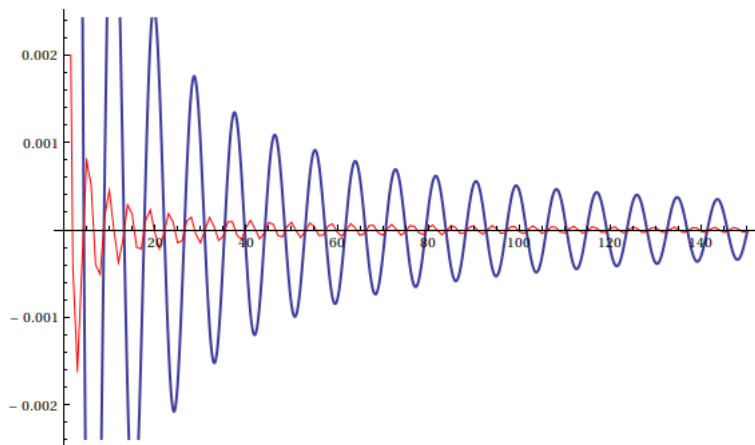
Figure 5.5: Comparison of between two angles of the quantity $\Re(G_{1x(y)})^2$: $45 + \beta$ (red curve) and $45 - \beta$ (blue curve). $\beta = 18.44$. This justifies the focusing effect.

explain why there is a focusing effect in the SGM experiments and numerical simulations. We see that $\delta\Sigma$ has significant values only between the two directions $\pm 45°$ and therefore the change in the conductance due to the tip is significant only between theses directions which leads to a focusing effect in the pictures of the interference pattern.For the same arguments, this focusing effect exists even for the SGM of conductance change (see for example Fig. (4.12)). Moreover, in the presence of disorder in the leads, this effect is more visible and the branches of electronic flow lasts for long distances [1]. This formula helps us to reach more the understanding of the 2D pictures of Scanning Gate Microscopy.

5.5 Decay law of the fringes of thermopower change

5.5.1 Thermopower change and the resonant level model RLM

As we did it for the change in the conductance (previous chapter), we will assume a resonant level model for the QPC. The advantage of this, is the simplicity of equations. Moreover, this model reproduces well the figures we obtain with a realistic model. We will assume in this work very low temperatures in order to get rid of the integrals in the Seebeck formula Eq. (5.9) and just use the Cutler-Mott formula, more convenient for calculations. The starting point is therefore:

$$S_k = \frac{\pi^2}{3}\left(\frac{k_b^2 \mathcal{T}}{e}\right)\left(\frac{\partial \ln(T)}{\partial E}\right)_{E=\mu} \tag{5.34}$$

We want to express the change $\Delta S_k = S_k - S_k^\circ$:

$$\Delta S_k = \frac{\pi^2}{3}\left(\frac{k_b^2 \mathcal{T}}{e}\right)\left(\partial_E \ln(\frac{T}{T^\circ})\right)_{E=\mu} \tag{5.35}$$

$$= \frac{\pi^2}{3}\left(\frac{k_b^2 \mathcal{T}}{e}\right)\left(\partial_E \ln(1+\frac{\Delta T}{T^\circ})\right)_{E=\mu} \tag{5.36}$$

$$\sim \frac{\pi^2}{3}\left(\frac{k_b^2 \mathcal{T}}{e}\right)\left(\partial_E(\frac{\Delta T}{T^\circ})\right)_{E=\mu} \tag{5.37}$$

From now on, we will work with the formula

$$\Delta S_k = \partial_E\left(\frac{\Delta T}{T^\circ}\right)|_\mu \tag{5.38}$$

Where the Seebeck coefficient is expressed in units of $\frac{\pi^2}{3}\left(\frac{k_b^2 \mathcal{T}}{e}\right)$. This relation is very interesting, because we already expressed, in the previous chapter, the change in the conductance $\frac{\Delta T}{T^\circ}$ as a function of the tip position:

$$\frac{\Delta T}{T^\circ} = 2\sqrt{T^\circ(1-T^\circ)}\epsilon + (1-T^\circ)\eta \tag{5.39}$$

$$+ T^\circ(3-4T^\circ)\epsilon^2 + (-\frac{5}{4}T^\circ + T^{\circ 2})\eta^2$$

$$+ 2\sqrt{T^\circ(1-T^\circ)}(1-2T^\circ)\epsilon\eta$$

Taking the derivative of this formula needs a lot of care. To accomplish this task, we need, the derivative of the elliptic functions of the first and second order, which enters in the expression of the self energy Eqs. (4.19).

Self energy derivative

The derivative of the self energy uses the derivatives of the complete elliptic integrals of the first and the second kind $\mathcal{K}$ and $\mathcal{E}$. We need for this to use the Picard-Fuchs equations[57]:

Lemma 1 *The functions $\mathcal{K}(m)$ and $\mathcal{E}(m)$ satisfy the following Picard-Fuchs equations:*

$$\begin{aligned}
\frac{d\mathcal{K}}{dm} &= \frac{1}{mm'^2}(\mathcal{E} - m'^2\mathcal{K}) \\
\frac{d\mathcal{E}}{dm} &= \frac{\mathcal{E} - \mathcal{K}}{m}
\end{aligned}$$

where $m^2 + m'^2 = 1$.

Now, we use these equations to obtain the derivative of the real and imaginary part of the self energy. We know from the previous chapter that:

$$\Re\Sigma(m) = m - \frac{2}{\pi}[s(\mathcal{E}(m) - m'^2\mathcal{K}(m))] \tag{5.40}$$

$$\Im\Sigma(m) = -\frac{2}{\pi}[\mathcal{E}(m') - m^2\mathcal{K}(m')] \tag{5.41}$$

We can therefore obtain the following derivatives:

$$\frac{d\Re\Sigma}{dm} = 1 - \frac{2}{\pi}|m|\mathcal{K}(m) \tag{5.42}$$

$$\frac{d\Im\Sigma}{dm} = \frac{2}{\pi}m\mathcal{K}(m') \tag{5.43}$$

5.5.2   Case of fully open QPC: $T^\circ = 1$.

If the resonant level model (RLM) is fully open, we use the expansion of $\frac{\Delta T}{T^\circ}$ near $T^\circ = 1$ before doing the energy derivative to obtain the Seebeck coefficient change. The expansion reads Eq. (5.40):

$$\frac{\Delta T}{T^\circ} \sim -(\epsilon^2 + \frac{\eta^2}{4}) + 2\sqrt{1 - T^\circ}\epsilon \tag{5.44}$$

The higher orders are neglected. In what follows, we will restrain the study to the central axis $y = 0$
We know from the previous chapter that $-(\epsilon^2 + \frac{\eta^2}{4}) = -\left(\frac{A}{\pi kx}\right)^2$, and therefore, even after the energy-derivation this term will decay faster like $\frac{1}{x^2}$. This term is useless and can be omitted.
The coefficient $\sqrt{1 - T^\circ}$ can be treated as follows:

$$T^\circ = \frac{1}{1 + \Lambda^2}, \qquad \Lambda = \frac{E - V_g - 2\Re\Sigma}{\Gamma} \tag{5.45}$$

It comes from this relation that near $T^\circ = 1$ we have :

$$\sqrt{1 - T^\circ} \sim \Lambda \tag{5.46}$$

We are now ready to obtain the change in the Seebeck coefficient ΔS_K in units of $\frac{\pi^2}{3}\left(\frac{k_b^2 \mathcal{T}}{e}\right)$:

$$\Delta S_k = \partial_E\left(\frac{\Delta T}{T^\circ}\right) \sim 2\dot{\Lambda}\epsilon \tag{5.47}$$

To obtain this result, we used the fact that when $T\circ = 1$ we have $\Lambda = 0$. We use again this property to make the derivative $\dot{\Lambda}$:

$$\dot{\Lambda} = \frac{1 - 2\Re\dot{\Sigma}}{\Gamma} \tag{5.48}$$

The derivative of the real part of the self energy is given by Eq. (5.41) and the expansion of the elliptic function in the continuum limit is given by Eq. (4.23). In the case of weakly coupled lead, $t_c \ll 1$, $\dot{\Lambda}$ becomes:

$$\dot{\Lambda} \sim \frac{1}{\Gamma} \propto \frac{1}{t_c^2} \tag{5.49}$$

The expression of ϵ is given in the previous chapter Eq. (4.49). With all this, the change in the Seebeck coefficient, when $T^\circ = 1$, reads:

$$\Delta S_K = 2\dot{\Lambda}\mathcal{A}\frac{\cos(2k_F x - \frac{\pi}{2} + \phi)}{\pi k_F x} \tag{5.50}$$

$\mathcal{A}$ and ϕ are, respectively, the modulus and the argument of $\frac{v}{1-v\mathcal{G}_{xx}^0}$ previously defined.

This expression shows that the fringes decay like $1/x$ if the system is completely open to the first mode of conduction. The spacing between the fringes is $\lambda_F/2$. We notice that the change $\Delta S_k \propto \frac{1}{t_c^2}$ and therefore more significant for weakly coupled leads.

5.5.3   Case of half-opened QPC: $T^\circ = 0.5$

For less opened QPC, we know from the previous chapter that the relative change in the transmission is:

$$\frac{\Delta T}{T^\circ} \sim 2\mathcal{A}\sqrt{1-T^\circ}\frac{\sin(2kx + \phi + \phi_T)}{\pi kx} \tag{5.51}$$

with $\cos(\phi_T) = \sqrt{T^\circ}$.

First we consider small tip voltage. This makes $\mathcal{A}$ and ϕ energy-independent. We need also to make the following remark:

$$\partial_E = \frac{1}{2k}\partial_k$$

We need also the derivative $\partial_k\phi_T$:

$$\cos\phi_T = \sqrt{T^\circ} \quad \Rightarrow \quad -\partial_k\phi_T\sin(\phi_T) = \frac{\partial_k T^\circ}{2\sqrt{T^\circ}} \tag{5.52}$$

$$\Rightarrow \quad \partial_k\phi_T = -\frac{\partial_k T^\circ}{2\sqrt{T^\circ(1-T^\circ)}} \tag{5.53}$$

The derivative $\partial_k T^\circ$ is big for a realistic QPC as well as for the RLM. Taking all these consideration into account we can find the change ΔS_k as follows:

$$\Delta S_k \sim \frac{\mathcal{A}\dot{T}^\circ}{\sqrt{1-T^\circ}}\frac{\sin(2k_F x + 2\phi_T)}{\pi k_F x} + 2\frac{\mathcal{A}}{\pi k_F^2}\cos(2k_F x + \phi_T) \tag{5.54}$$

This is an interesting result since the fringes decay like $1/x$ but not to zero! At large distances, ΔS_k oscillates without decaying, with a constant amplitude. This an unusual effect if we remind that for 2D systems the effect of the tip decays when one moves away from the QPC. Of course, we do not expect this effect to last for very long distances because the Cutler-Mott formula will not work any more because of very oscillating functions of the type $\sin(2k_f x + \phi)$. What we say here, is that there is a region where fringes do not decay.

To confirm that the thermopower change indeed decays as stated above, we need to compare the analytical results obtained by means of the Cutler-Mott formula with the numerical integration using the exact formula of the Seebeck coefficient(Eq 5.9). In figure (5.6) (a) and (b) , we give the result of numerical simulations using the exact formula of the Seebeck compared with the analytical result. We find the matching excellent and the analytical prediction well confirmed by simulation.

Summary: In this chapter we were interested in the Seebeck coefficient of a quantum point contact. As done in the experiments of scanning gate microscopy of the conductance in a quantum point contact, we wanted to do the same thing for this coefficient. First, we obtained the figures of the interference pattern due to a charged AFM tip moving above the QPC. We clearly noticed a focusing effect of the acquired change when the tip is in an angle $\pm 45^\circ$ seen from the QPC center. We explained this by expressing the change in the self energy for all the tip positions. After that, we were interested in the decay law of the fringes in the central axis. We found a $1/x$ decaying fringes for all the QPC opening but the decay is to zero when fully opened whereas the decay at large distances in a half opened QPC goes to an oscillating function with a constant amplitude. This interesting law is valid in a region where the Cutler-Mott formula is expected to be valid.
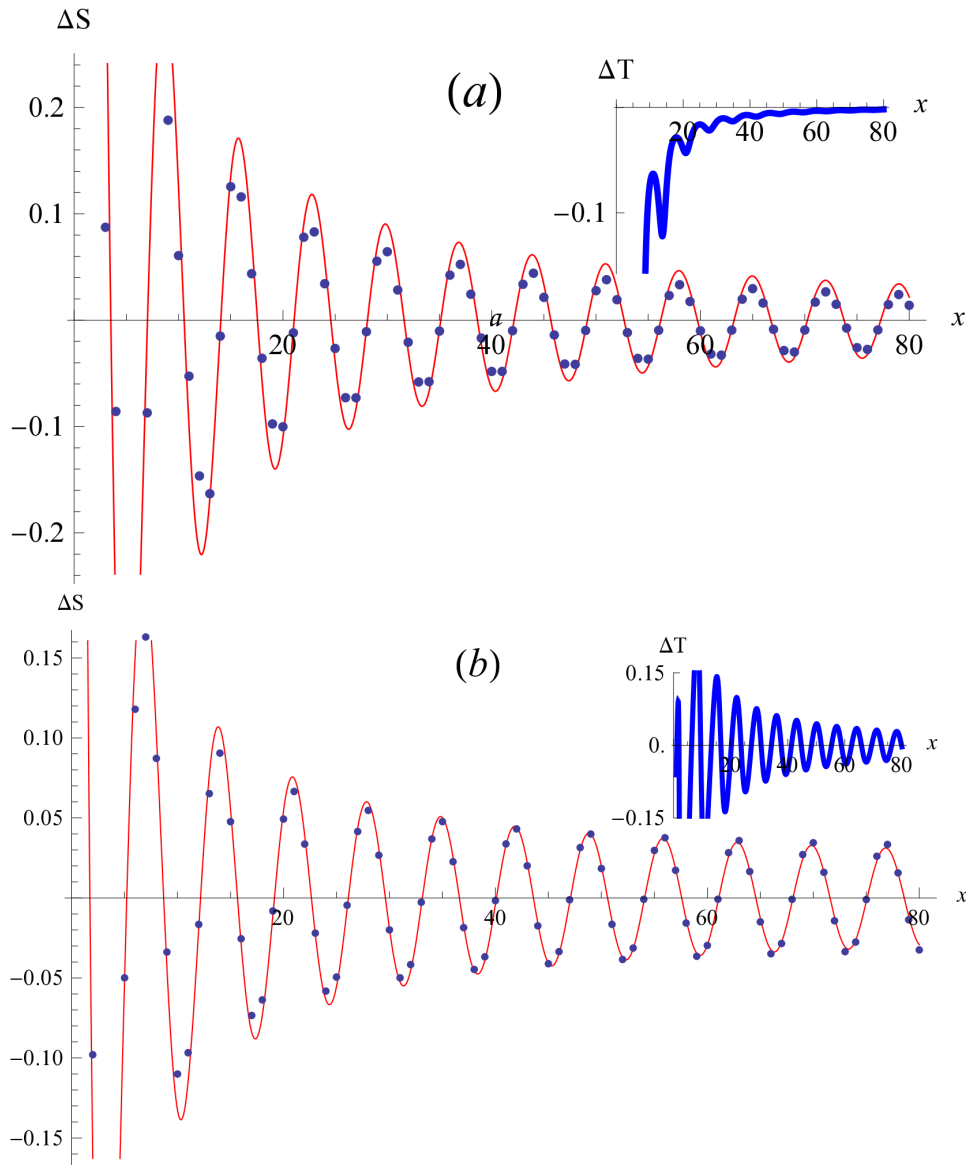
Figure 5.6: ΔS_k for the resonant level model (RLM). We notice a very good matching between the simulation using the exact integral form for Seebeck (blue dots) and the analytical formula (red line) in both cases: $T° = 1$ Fig(a) and $T° = 0.5$ Fig(b). Blue curves present the profile of the change in transmission ΔT due to the tip. Here, temperature $\mathcal{T} = 426$mk and the coupling $t_c = 0.2$. The results are given in the lead axis $(y = 0)$. In Fig (a), The fringes decay like $1/x$ and in Fig (b), they do not decay at large distances.

Chapter 6

Thermoelectric transport and random matrix theory

Contents

.

"Do you know," the Devil confided, "not even the best mathematicians on other planets – all far ahead of yours – have solved it? Why, there is a chap on Saturn – he looks something like a mushroom on stilts – who solves partial differential equations mentally; and even he's given up."

- Arthur Porges, "The Devil and Simon Flagg"

Summary of chapter 6

The purpose of this chapter is to determine the probability density function of the Seebeck coefficient S_k of a chaotic cavity connected to 1D leads. First we introduce the usual tools of the random matrix theory and the different family ensembles. After explaining the difference between a Hamiltonian approach and a scattering matrix approach, we start by assuming a Gaussian distribution for the cavity Hamiltonian. Then, we claim that, for big number of degrees of freedom in the cavity, this distribution is equivalent to a Lorentzian distribution. The Lorentzian family ensemble allows us to do two main things: For an appropriate choice of the center and the width of the Lorentzian distribution, we obtain uniformly distributed scattering matrices belonging to circular ensembles. The second simplification, is to reduce the degrees of freedom in the cavity by means of the decimation-renormalization procedure. The final system we obtain, is a 2×2 Lorentzian matrix and the corresponding scattering matrix is 2×2 matrix sampled from the circular ensemble. No approximation is done so far. The probability density function of the Seebeck coefficient of this simple model is obtained at all the Fermi energies. This distribution reads:

$$
p(S_k) = \left\{
\begin{array}{ll}
-\frac{a}{\pi} \log\left(\frac{|a S_k|}{1 + \sqrt{1 - a^2 S_k^2}}\right) & \text{if} \quad |S_k| < 1/a \\
0 & \text{if} \quad |S_k| > 1/a
\end{array}
\right.
$$

a is a parameter depending on the coupling to the leads.
The important conclusions of this form are:

  – The distribution is singular at the origin
  – The Seebeck coefficient is bounded and can not take any value.
  – The energy dependence of the distribution is contained in the coupling coefficient of the lead.

Both, the analytical and numerical methods to obtain this result are clearly explained.
In the last sections, we give a different approach based on the scattering matrix and link this result to the time delay matrix. We insist also on the concept of the decimation-renormalization procedure and give some interesting applications such as the distribution of two cavities in series.
Each time we give a new method or a different example, we verify the well known results concerning the probability density function of the transmission of a chaotic cavity. For instance, the distribution $P(T) = \frac{1}{2\sqrt{T}}$, giving the distribution of the transmission in a cavity in the presence of time reversal symmetry, is taken as a reference to test the numerical algorithms.
We put the attention on the fact that the self energy of the leads is taken exactly all over this work and no approximation is done. We show the consequences of doing approximations on the self energy such as neglecting its real part as considered in a lot of works: in fact the parameter a is proportional to $1/\Gamma^2$ in the exact result whereas it is only proportional to $1/\Gamma$ if the real part of the self energy is neglected. ($-\Gamma$ is twice the imaginary part of the self energy).

6.1 Introduction

In this chapter we will continue to look at quantum transport of electrons through nano-constrictions but with a new point of view: The tool we will use here is based on the theory of random matrices(RMT).

This theory was initiated by Wigner and Dyson more than 60 years ago. The early successful use of this theory was the explanation of the complex properties of the many body spectrum and nucleus compounds. The original idea introduced to study the properties of the energy levels of highly excited states of heavy nuclei is to describe the system with a random Hamiltonian whose eigenvalues statistics will give the same behaviour as the nuclei levels spectrum. For instance, this way of considering the problem is the basic statement of the random matrix theory. To understand the difference from the usual way we follow in quantum mechanics, we can remind that usually one fixes the Hamiltonian and averages over possible states of the system. The complexity with this method is that we need to solve the Schrödinger equation which is obviously a very complicated task and sometimes seems impossible for systems with very high degrees of freedom. In the random matrix theory approach, the Hamiltonian is taken random and only the symmetries of the system are relevant. This assumption seems to be fundamental and with universal consequences. In fact, the level spacing distribution in nuclei compound is well described by the Wigner-Dyson distribution obtained using RMT. Moreover, this theory describes also the classical chaos of systems where the classical dynamics is chaotic as in the Sinai billiard [68]. The universality of the RMT results makes this theory widely applicable and becomes a major tool in many fields such as nuclear reaction, finance[69], number theory, combinatorics and wireless communications[70]. The universality conjecture [1] interested many scientists since it states that for large dimension matrices, the local behaviour of the eigenvalues is independent of the matrix probability distribution. The Wigner semicircle law is a good example: The eigenvalues density of a real symmetric or complex Hermitian matrix, with independent, identically distributed random entries in the upper or lower triangle, with a variance $\frac{\sigma^2}{N}$, N being the dimension of the matrix is ($N \to \infty$), reads:

$$\rho(X) = \frac{1}{2\pi\sigma^2} \sqrt{4\sigma^2 - X^2} \qquad X \in [-2\sigma, 2\sigma]$$

It can be shown that this result holds for much broader class of matrices whose entries verify Pastur-Lindeberg's condition[71]

Quantum transport through chaotic cavities

We still continue to be interested in nano-devices where electrons are confined in a region smaller than the coherence length. The resulting quantum effects can be studied within the random matrix theory. In fact, systems like quantum dots scatter electrons randomly because of their irregular boundaries shape. This chaotic behaviour can be treated by considering random Hamiltonians to describe the chaotic quantum dots. This quantum dot will be seen as a chaotic cavity which is connected to two leads acting like electrons reservoirs and therefore treated with the tools of open systems. The treatment of this situation is different from the one of closed systems where the RMT is based on the level statistics. In fact, closed systems assume infinite size for the Hamiltonian in order to ensure the irrelevance of the choice of the Hamiltonian distribution and thus we can claim universal results. The approach for open systems is quite different: The scattering of electrons can be well described if we can link the incoming waves to the outgoing waves.This can be done using the scattering matrix S

$$\begin{pmatrix} O \\ O' \end{pmatrix} = S \begin{pmatrix} I \\ I' \end{pmatrix} \tag{6.1}$$

where O and O' are outgoing waves and I, I' are the incoming waves. The size of the scattering matrix S depends only on the total number of modes in the two leads and therefore has nothing to do with the size of the chaotic cavity Hamiltonian. This size is finite and we can even expect a 2×2 S-matrix (one mode in each lead) so that the universality can not be interpreted using the fact that for matrices with high dimension the fluctuation properties are independent from the choice

---

1. This conjecture is not true in general but expected to be valid within some families distributions
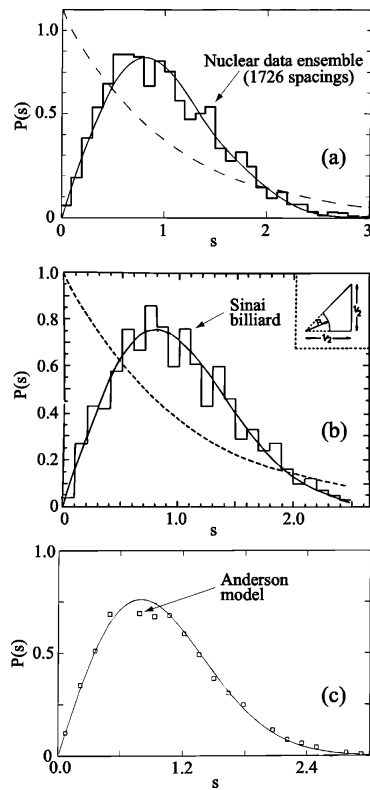
Figure 6.1: Verification of the RMT prediction on the nearest neighbor level spacing.(a)a nucleus compound [68].(b)a 2D chaotic system [68].(c) a disordered system[72]
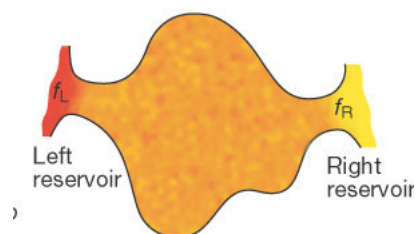
Figure 6.2: A quantum cavity connected to two electronic reservoirs (leads) to mimic the quantum dot.

of the distribution. Fortunately, we can always link the scattering approach with the Hamiltonian approach using the reaction matrix K [74][2]:

$$S(E) = \frac{1 - iK}{1 + iK}, \quad K = W \frac{1}{E - H} W^\dagger \tag{6.2}$$

The matrix W contains the information on how the quantum dot is coupled to the leads and its elements are usually non-random. We understand from this relation why we can still expect universality with a finite size scattering matrix: Indeed, the distribution of the Hamiltonian fixes which family of scattering matrix we need to handle. In general, we can expect universality when the injected carriers spend much more time in the cavity than the necessary time to explore the whole phase space of the cavity. We remind that the necessary time to cross a disordered system of length L is given by $\tau_D = \frac{L^2}{D}$, D is the diffusion constant[76][3]. So, we need larger time to expect the electrons to reach the irregular boundaries of the cavity. That is the case of quantum dots with high internal degrees of freedom.

The big number of levels in the dots allows us to neglect electronic interactions whereas for less populated dots, weakly coupled to the leads , the levels are quantized and the interaction can not be omitted.

In this part of the thesis, we will be interested in the fluctuation properties of chaotic cavities and the statistics of the physical observables related to quantum transport such as the conductance and the Seebeck coefficient. To fulfill this task, we need to use some families of random matrices, defined by the symmetry invariance of the systems in study.

6.2   Gaussian ensembles and symmetries

6.2.1   Gaussian distribution

To describe the behaviour of a cavity, completely chaotic, we seek a distribution which ensures a most random possible Hamiltonian. This can be translated in different ways and one of the most interesting approaches may be in terms of the maximum of the entropy $\mathcal{S}$. We define the entropy of the joint probability distribution function P of the independent elements of H by [77]:

$$\mathcal{S}[P] = - \int P \log(P) \mu(dH) \tag{6.3}$$

Where the measure is defined as the product of the independent elements dH_{ij}:

$$\mu(dH) = \prod_{1 \le i < j \le N} dH_{ij}$$

It can be proved [78]that the distribution P which maximizes the entropy $\mathcal{S}$ and subject to the constraint $\langle \mathrm{Tr}(H^2) \rangle_P = N^2$ is the Gaussian distribution:

$$P(H) = A e^{-\lambda \mathrm{Tr}(H^2)} \tag{6.4}$$

---

2. Sometimes in literature, this matrix is noted R

3. This time is associated to Thouless energy $\tau_D = \frac{\hbar}{E_{Th}}$

Proof:
We have a two constraints: one on the second moment and the second concerns the normalization of the distribution.

$$\langle \text{Tr}(H^2) \rangle_P = N^2$$
$$\langle 1 \rangle_P = 1$$

thus we can write:

$$\mathcal{S}[P] = -\langle \log(P) \rangle_P - \lambda(\langle \text{Tr}(H^2) \rangle_P - N^2) + (\log(A) + 1)(\langle 1 \rangle_P - 1)$$

where λ and$(\log(A) + 1)$ are Lagrange multiplier.
The maximum is obtained for a distribution verifying $\delta\mathcal{S} = 0$,
where the variation is made with respect to P. We get:

$$-\log P - \lambda \text{Tr}(H^2) + \log(A) = 0$$

Straightforward manipulation gives: $P(H) = Ae^{-\lambda \text{Tr}(H^2)}$.
The constraint fixes the value of λ to be $\frac{1}{2}$.

Now, we can understand what makes the Gaussian distribution so special and why it is widely used in literature to study the fluctuations of physical quantities.

The Gaussian distribution has also another interesting property from which it can be defined as the unique distribution which has its elements distributed independently(up to the symmetry constraints of the ensemble it belongs to). Indeed, it can be proven [79], that the joint probability density function which has its free elements completely independent is the Gaussian distribution and its form is restricted to [80]:

$$P(H) = \exp(-a\text{Tr}(H^2) + b\text{Tr}(H) + c) \tag{6.5}$$

Moreover, because $P(H)$ must be real and normalizable, the constants a, b, c, have to be real and the constant a must also be positive.

It is very important to know that the only distribution whose components are statistically independent with a symmetry invariance is the Gaussian distribution. Later, when we will introduce the Lorentzian and Circular ensembles, we quickly realize, using this theorem, that their component are not statistically independent and therefore, generating numerically these ensembles becomes a not simple task and a lot of care is required to obtain them [81]. On the other hand, the Gaussian ensembles, because of the independence of their component, are easily obtained and most of the mathematical packages offer this distribution.

The universality of random matrix theory results is based on the fact that a lot of different systems share some common fundamental proprieties : Symmetries. The symmetry of a system, such us time reversal symmetry, invariance under spin rotation adds a constraint on the joint probability distribution function and restrains the number of independent elements in the matrix representation. Therefore, It seems important to introduce these symmetries and the ensembles they define.

Symmetries in random matrix theory

It is important to know all the symmetries of a quantum system in order to take into account, when we define the best Hamiltonian matrix to describe the system, all the constraints existing between its elements. We remind that a system is said to be under the symmetry $\mathcal{C}$ if:

$$[H, \mathcal{C}] = 0 \tag{6.6}$$

Where $[\dots]$ denote the commutator.

One of the most important symmetries quantum systems obey is time reversal. We say that a Hamiltonian has a time reversal symmetry if it commutes with any antiunitary operator T. Moreover; if the system describes an even number of particles with no spin or spin $\frac{1}{2}$, then the operator T verifies [4]:

$$T^2 = 1 \tag{6.7}$$

---

4. If the systems describes an odd number of $\frac{1}{2}$ spin particles then: $T^2 = -1$

The implication of time reversal symmetry on the Hamiltonian describing the quantum system, with the additional property $T^2 = 1$, is that the matrix representation of H must be real symmetric.

Gaussian ensembles

The Gaussian ensembles are classified according to the transformation under which the distribution of the ensemble remains invariant. We list three different ensembles:

1)Gaussian Orthogonal Ensemble GOE: This class of matrices is defined as the ensemble of real symmetric matrices H verifying:
  – The ensemble is invariant under the transformation: $H \to W^T H W$.
    Where W is any real orthogonal matrix.
  – The various elements H_{ij}, $i \leq j$, are statistically independent.
  These matrices are real symmetric with $\frac{N(N+1)}{2}$ statistically independent Gaussian variables. The probability distribution is therefore:

$$P(H)dH = e^{-\frac{\mathrm{Tr}_{(H^2)}}{2}} \prod_{i \leq j} dH_{ij}$$

2)Gaussian Unitary Ensemble GUE: This ensemble describes systems without time reversal invariance, with a general Hermitian Hamiltonian not restricted to be real or self-dual. It has the following properties:
  – The probability P(H)dH that the system will belong to the volume element

$$dH = \prod_{i \leq j} dH_{ij}^a \prod_{i < j} dH_{ij}^b$$

  Where H_{ij}^a and H_{ij}^b are the real and imaginary parts of H_{ij}, is invariant under the transformation

$$H \to U^{-1} H U$$

3)Gaussian Symplectic Ensemble GSE: This ensemble is defined by self-dual Hermitian matrices with the following properties:
  – The ensemble is invariant under the the transformation:

$$H \leftarrow W^R H W$$

  W is any symplectic matrix.
  – The components of the matrix H are statistically independent.

These ensembles give the joint probability distribution for a system under some physical consideration and symmetry invariance. Nevertheless, given using the Hamiltonian matrix components, they are more convenient to numerical simulation than to direct interpretation of the physical observables. In fact, to do a direct comparison with experiments we need to access to the system eigenenergies and express the joint probability distribution in terms of these eigenvalues.

Joint probability distribution function and correlated eigenenergies:

The expression of the joint probability distribution function j.p.d.f in terms of the eigenenergies is for practical interest since it allows to study the correlations between them and gives direct interpretation of the physical quantities. Using the invariance relations listed above for the different Gaussian ensembles, we can express the probability density function in terms of the eigenvalues and eigenvectors of the Hamiltonian matrix. Indeed, the orthogonal, unitary and symplectic canonical transformations lead, after integration over the eigenvectors degrees of freedom, to the following distribution [78]:

$$P(E_1, E_2, \ldots, E_N) = C_\beta \exp\left(-\frac{1}{2}\beta \sum_{k=1}^{N} E_k^2\right) \prod_{j<k} |E_j - E_k|^\beta \tag{6.8}$$

$\beta = 1$ for Gaussian orthogonal ensemble (GOE).

$\beta = 2$ for Gaussian unitary ensemble (GUE).

$\beta = 4$ for Gaussian symplectic ensemble (GSE).

N is the dimension of the matrix and C_β is a normalization constant [5] which is given by [80]:

$$C_\beta^{-1} = (2\pi)^{N/2} \beta^{-N/2-\beta N(N-1)/4} [\Gamma(1+\beta/2)]^{-N} \prod_{j=1}^{N} \Gamma(1+j\beta/2) \tag{6.9}$$

The term $\prod_{j<k} |E_j - E_k|^\beta$ is the Jacobian of the transformation from the elements of the Hamiltonian to the eigenvalues variables. It shows a repulsion property of the levels which corresponds to a resistance to crossing. This term is generic to the different symmetries of the Hamiltonian and plays an important role in the universality of the spectral fluctuations.

> Remark:
> *The term 'repulsion' comes from the comparison with the problem of N point charges at positions $x_1, x_2, \ldots x_n$, free to move on a 1D line. Indeed, if we assume that the particles are in a harmonic potential and the space is two dimensional, then, the energy potential of the interacting system reads:*
>
> $$W = \tfrac{1}{2} \sum_i x_i^2 - \sum_{i<j} \ln |x_i - x_j|$$
>
> *The harmonic potential attracts the charges whereas the Coulombian interaction drives them apart. The probability density of the charges positions at thermodynamic equilibrium reads:*
>
> $$P(x_1, x_2 \ldots, x_n) = C \exp\left(-\tfrac{W}{kT}\right).$$
>
> *If we put $\beta = 1/kT$, the comparison with* (eq 6.8) *becomes straightforward.*

Eigenvectors distributions:

Sometimes, the only knowledge of the level density function distribution is not enough to express some physical quantities [82], and the distribution of the eigenvectors components seems to be necessary. In the case of *GOE* which is the ensemble we mostly deal with in this thesis, every eigenvector can be transformed with a real orthogonal transformation and still remains an eigenvector of a matrix in the GOE. This means that the only invariant of the eigenvectors is the norm. We conclude that the joint distribution of the vectors components $(u_1, u_2, \ldots u_N)$ is [83]:

$$P_{GOE}(u_1, u_2, \ldots u_N) = \frac{1}{C} \, \delta\left(1 - \sum_{p=1}^{N} u_p^2\right) \tag{6.10}$$

Where $C = 2\pi^{N/2} \Gamma(N/2)$.

We put attention to the fact that the components of the Gaussian orthogonal ensemble eigenvectors can be assumed real without loss of generality.

So often, the marginal distribution $P_{GOE}(u_1, u_2, \ldots u_n)$ with $n < N$, obtained after integrating over the remaining $N - n$ components is more useful. This distribution reads [78] [84]:

$$P_{GOE}(u_1, u_2, \ldots u_n) = \pi^{-n/2} \frac{\Gamma(N/2)}{\Gamma((N-n)/2)} \left(1 - \sum_{p=1}^{n} u_p^2\right)^{(N-n-2)/2} \tag{6.11}$$

And of course, the result becomes more interesting when the dimension N of the matrix becomes larger:

$$\frac{1}{N^{n/2}} P_{GOE}\left(\frac{u_1}{\sqrt{N}}, \frac{u_2}{\sqrt{N}}, \ldots \frac{u_n}{\sqrt{N}}\right) \sim \left(\frac{2}{\pi}\right)^{n/2} e^{-\frac{1}{2}\sum_{p=1}^{n} u_p^2} \tag{6.12}$$

---

5. $\beta = 0$ corresponds to the Poissonian ensemble which shows no level correlations.

In the case of the unitary ensemble, the vectors can be transformed to vectors of unit norm with a unitary transformation. The conclusions are the same as those of the orthogonal ensemble except that the eigenvectors components are complex and therefore we need only to change in the previous formula the components as follows:

$$u_p^2 \rightarrow |u_p|^2$$

Of course we need to take care to the normalization constant since the number of independent elements is different.

Now, with both of the distribution density of the eigenenergies and the eigenvectors components, we have all the necessary tools to put the equations expressing the fluctuations of the different physical quantities.

6.3 Random matrix theory of quantum transport in open systems:

In the previous chapters, we studied the quantum transport of electrons through nanoconstrictions and focused on the transport coefficients (Transmission and Seebeck coefficient) where the system, sketched between two reservoirs of electrons, is studied within the theory of open systems and the different approaches commonly used in. We want in this chapter to study the fluctuations of the transmission and the Seebeck coefficient of such systems. Of course, this kind of topic was closely studied in literature [76] [85] [89] but we want to give here an approach more based on the Green's function and the renormalization methods it allows to do. Moreover, we will show which is the most suitable ensemble which simplifies the operation of expressing analytically the different density functions of quantum transport coefficients. This study has the aim of proposing a minimum model which describes the quantum transport through nanoconstrictions and to give the analytical results we succeeded to calculate. First, we need to recall some important results obtained in literature concerning the transmission coefficients. We need also to introduce an important family ensembles: The circular ensembles.

6.3.1 Circular ensemble:

The circular ensembles were introduced by Dyson [90] [94] as a new way of describing the levels statistic of a quantum system. Indeed, an open system is better described with its scattering matrix rather than its Hamiltonian(Hermitian matrices). A scattering problem involving two leads, each with N channels, is described with its scattering matrix S:

$$S = \begin{pmatrix} r & t' \\ t & r' \end{pmatrix} \tag{6.13}$$

Where r, t are the $N \times N$ reflection and transmission matrices for carriers from left and r', t' for those from the right.
Dyson suggested to take uniformly distributed unitary scattering matrices S to describe the chaotic behaviour of a quantum system. As in the case of the Hermitian Hamiltonian, there is three families of circular ensemble depending on the different symmetries of the system: Circular orthogonal ensemble (COE), Circular unitary ensemble, Circular symplectic ensemble (CSE). The direct definition of the probability density of the circular ensembles is that the matrices are uniformly distributed and the probabilities to choose two different scattering matrices are equal. This uniform distribution is translated as follows:

$$P(S)dS = \frac{1}{V}d\mu(S) \tag{6.14}$$

Where $d\mu(S)$ is the Haar measure and V is a volume (Normalization) constant. The ensemble of unitary matrices admits a unique measure which is the Haar measure. We can prove that its form is given by the following relation:

$$d\mu(S) \propto S^{\dagger}dS \tag{6.15}$$

The invariance of the Haar measure on the orthogonal (uniform, symplectic) ensembles under the group transformation $S \to VSV'$, where V is an arbitrary orthogonal (uniform, symplectic) matrix seems to be very important to do integration over unitary ensembles and will help us to obtain some results solely by invariance considerations. The eigenvalues of an $N \times N$ matrix S, taken from the circular ensembles, are $e^{i\phi_j}$, with $0 \leq \phi_j < 2\pi$ and $j = 1, \ldots N$. The eigenvalues probability density function is thus given by the following form:

$$P\{\phi_j\} \propto \prod_{i<j} |e^{i\phi_i} - e^{i\phi_j}|^{\beta} \tag{6.16}$$

$\beta = 1$, 2 and 4 for respectively orthogonal, unitary or symplectic ensembles. We recognize in this formula the repulsion term which forbids to an eigenphase ϕ_i to be degenerate.
Considering this distribution for the scattering matrix S of a quantum system, Jalabert, Pichard

and Beenakker [96] and Baranger and Mello [95], showed that the distribution of the conductance of spinless electrons given by the formula:

$$G = \frac{e^2}{h} \mathrm{Tr}(tt^\dagger) \tag{6.17}$$

is easily expressed if someone assumes the following decomposition of the S matrix:

$$S = \begin{bmatrix} v^1 & 0 \\ 0 & v^2 \end{bmatrix} \begin{bmatrix} -\sqrt{1-\tau} & \sqrt{\tau} \\ \sqrt{\tau} & \sqrt{1-\tau} \end{bmatrix} \begin{bmatrix} v^3 & 0 \\ 0 & v^4 \end{bmatrix} \tag{6.18}$$

Where τ represents here an $N \times N$ diagonal matrix which contains the eigenvalues of the matrix $tt^\dagger$. v^i are arbitrary unitary matrices except that we have $v^3 = (v^1)^T$ and $v^4 = (v^2)^T$ in the presence of time reversal symmetry. Using this decomposition, the probability distribution(which is proportional to the Haar measure) reads [95]:

$$d\mu(S) = P_\beta(\tau) \prod_a d\tau_a \prod_i d\mu(v^i) \tag{6.19}$$

$d\mu(v^i)$ are the Haar measure.
In the case of the the orthogonal ensemble $\beta = 1$ and unitary ensemble $\beta = 2$ we can write:

$$P_1(\{\tau\} \propto \prod_{a<b} |\tau_a - \tau_b|^2 \tag{6.20}$$

$$P_2(\{\tau\} \propto \prod_{a<b} |\tau_a - \tau_b| \prod_c \frac{1}{\sqrt{\tau_c}} \tag{6.21}$$

As we can notice, we recover again the repulsion property which appears here in the $tt^\dagger$ matrix eigenvalues.
We can see in Fig(6.3) the distribution probability of the zero-temperature quantum conductance for some cases of systems having scattering matrices distributed according to the circular ensembles distributions. We can give for example the results for $N = 1$ (one mode in each lead), in the absence of magnetic field ($\beta = 1$) :

$$P_1(T) = \frac{1}{2\sqrt{T}} \tag{6.22}$$

and in the presence of a magnetic field (no time reversal symmetry $\beta = 2$):

$$P_2(T) = 1, \qquad \text{(uniform)} \tag{6.23}$$

These two formulas will be the references to which we should compare our results in the following sections to check whether our model is chaotic or not. Of course the notion of 'chaotic' is vague and we did not specify the exact conditions (if they exist) to say that the system is chaotic. We will put more clarity on this when we will discuss the relation between the scattering and the Hamiltonian approaches for the different random ensembles.

6.4   Quantum transport fluctuations in mesoscopic systems

Now that we introduced the different random ensembles, we start to use these tools to describe the fluctuations of quantum transport coefficients. We will be interested in the conductance of a chaotic cavity but mostly, it will be the Seebeck coefficient which will take the major part of this study. We will try to give to readers the minimal picture of a chaotic cavity model with the minimal necessary degrees of freedom which allows recovering the experimental results without loss of generality. The realistic system we want to study is a quantum cavity related to two semi-infinite leads as described in Fig. (6.4) (left picture). To be able to do numerical simulations using discrete Hamiltonians with a matrix representation, we propose the general lattice model of Fig. (6.4 right) where N randomly connected sites are sketched between two semi-infinite uniform 1D leads. This
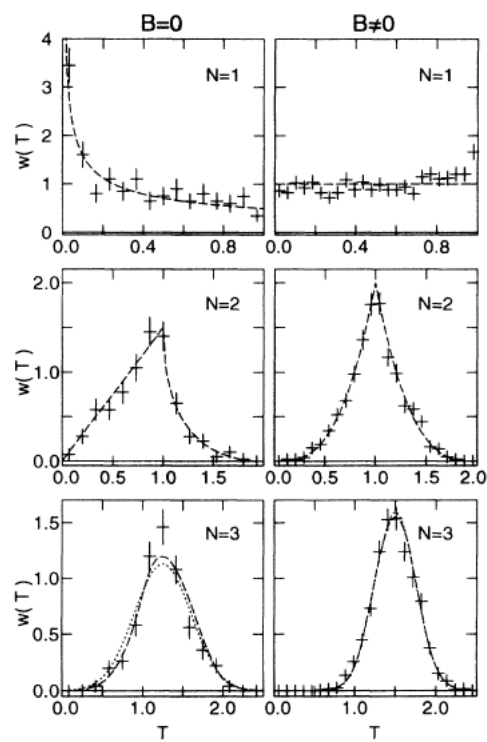
Figure 6.3: The distribution of the transmission of a chaotic cavity at fixed N=1,2 and 3 in the absence (first column) and presence (second column) of magnetic field. From [95].
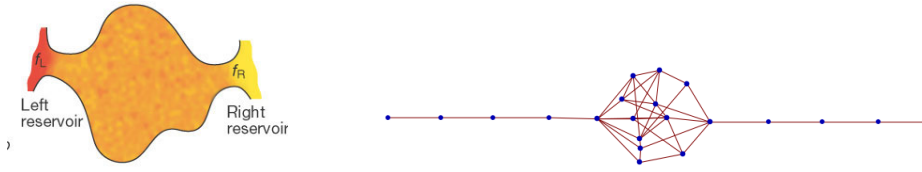
Figure 6.4: Quantum chaotic cavity: Realistic model(left figure) and a Tight Binding picture of a chaotic cavity based on lattice model(right figure).

model is suitable for the Green's function formalism discussed in this thesis and will be adopted in order to connect the formalism of Green's function to the scattering matrix approach.

We start by assuming a Gaussian distribution for the Hamiltonian of the scattering region. We discuss here the quantum transport through a chaotic cavity in the absence of magnetic field. Then, The Hamiltonian H of the cavity belongs to GOE ($\beta = 1$).

$$P(H) \propto \exp\left[-\frac{\text{Tr}(H^2)}{2a^2}\right] \tag{6.24}$$
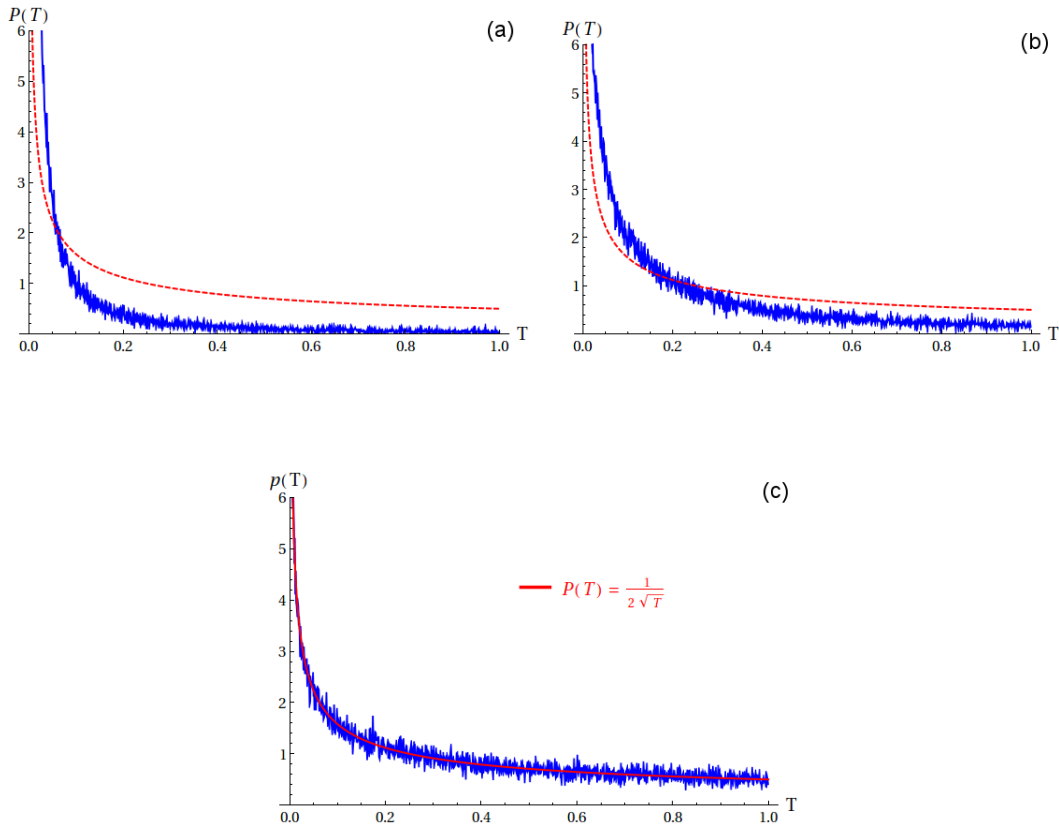
Figure 6.5: Probability density function of a chaotic cavity Fig. (6.4 right). The cavity is modeled with $N = 21$ sites and the Fermi energy is taken in the middle of the conduction band. The red curve represents the results of circular ensembles $P(T) = \frac{1}{2\sqrt{T}}$. Fig (a) and (b) show the results for a standard deviation a=0.1 and a=6 respectively. the deviation from the result of circular ensemble is clear. Fig (c) shows the results for a=1.5 . In this case we recover the results of circular ensembles COE (Red line).

The transmission of the system is obtained by the following formula based on the Fisher-Lee relation (1D Leads):

$$T = \Gamma G_{1n} \Gamma G_{n1}^{\dagger} \tag{6.25}$$

This is a scalar formula since the leads are 1D. The self energy of the leads is given by(the coupling coefficient is taken $t_c = 1$) [6]:

$$\Sigma = \frac{E}{2} - i \sqrt{1 - \left(\frac{E}{2}\right)^2} \tag{6.26}$$

and the broadening element reads:

$$\Gamma = -2\Im(\Sigma) \tag{6.27}$$

The results of numerical simulations, sampling Hamiltonians from GOE and giving the transmission probability function $P_a(T)$ for different values of the standard deviation a are shown in Fig. (6.5). Fig (c) shows how do we recover the result $p(T) = \frac{1}{2\sqrt{T}}$ obtained assuming a scattering matrix belonging to COE [95]. In this case the Hamiltonian distribution has a standard deviation $a = 1.5$. For smaller a (Fig (a), a=0.1) or larger a (Fig (b), a=6) we see a clear deviation from the result of a completely chaotic cavity (Scattering matrix uniformly distributed. COE).

More generally, we can define a parameter Δ which reflects the deviation from the orthogonal circular ensemble COE results when we sample the Hamiltonian from the Gaussian orthogonal ensemble GOE :

$$\Delta(a) = \int_0^1 [P_a(T) - \frac{1}{2\sqrt{T}}]^2 dT \tag{6.28}$$

Plotting this parameter as a function of the standard deviation of Hamiltonians sampled from
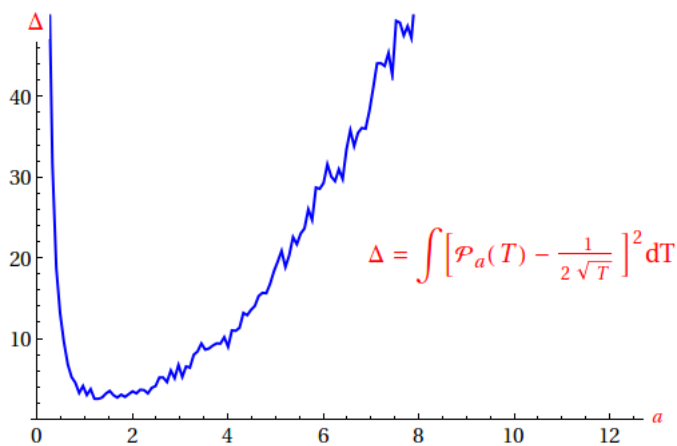
Figure 6.6: Deviation from the result of COE as a function of the standard deviation of the Hamiltonian distribution (From GOE). For standard deviation around the value $a = 1.5$ the deviation is minimal and we recover curves like in Fig (6.5 (c))

the GOE, we obtain the Fig. (6.6). The likely flat region around the minimum of the curve is a region where the probability density function of the transmission $P_a(T)$ is well fitted with the formula $\frac{1}{2\sqrt{T}}$ obtained assuming the scattering matrix S of the chaotic cavity uniformly distributed according to COE. For larger or smaller values of a, the deviation from the result $\frac{1}{2\sqrt{T}}$ becomes significant and the curve $P_a(T)$ can not be fitted by $\frac{1}{2\sqrt{T}}$ anymore as shown in Fig. (6.5 (a) and

---

6. For arbitrary coupling we need just to multiply Σ and Γ defined for an ideal coupling by the factor t_c^2

(b)).

We were hoping that taking an Hamiltonian from GOE could be equivalent to having a scattering matrix S belonging to COE, at least for large number of cavity sites. Now, we know that this can not be true for all deviation parameters a. For more clarity, we need to link the Hamiltonian approach to the scattering approach.

6.5   Hamiltonian vs Scattering approach

The scattering matrix is defined as the matrix relating the incoming wave amplitudes to the outgoing amplitudes as follows:

$$\begin{pmatrix} O \\ O' \end{pmatrix} = S \begin{pmatrix} I \\ I' \end{pmatrix} \tag{6.29}$$

where the scattering matrix reads:

$$S = \begin{pmatrix} r & t' \\ t & r' \end{pmatrix} \tag{6.30}$$

To study the scattering of electrons by a chaotic cavity, we need first to write down the whole Hamiltonian of the system which describes both of the cavity and the leads. This Hamiltonian reads:

$$\mathcal{H} = \sum_{\mu\nu} |\mu\rangle H_{\mu\nu} \langle\nu| + \int |\chi_a\rangle E \langle\chi_a| dE + \sum_{\mu} \{|\mu\rangle \int W_{\mu a} \langle\chi_a| dE + h.c\} \tag{6.31}$$

$|\chi_a\rangle$ is a lead channel wave function which is energy dependent [7]. $|\mu\rangle$, $\mu = 1 \ldots N$ are the bound states (levels) of the chaotic cavity (scattering region). The whole Hamiltonian of the system has three parts: The first one is the cavity Hamiltonian, the second is the leads Hamiltonian, written in the mode space and the third one is the coupling part(interaction of configuration between levels and channels). It may be interesting to know how to obtain this form of Hamiltonian from the lattice Hamiltonian picture (See Appendix F).

With this partition of the Hamiltonian, the Scattering matrix is straightforward [74] [8]:

$$S = 1 - 2\pi i W^\dagger \frac{1}{E - H - \Delta(E) + i\pi WW^\dagger} W \tag{6.32}$$

W is a matrix (not square in general) which contains the coupling elements $W_{\nu a}$. $\Delta(E)$ is the real part of the whole self energy matrix (takes into account all the connected leads) and $-\pi WW^\dagger$ is its imaginary part. The self energy is generally a sparse matrix where only the elements of the sites connected to leads are non-zero. The imaginary part is simply deduced from the Hamiltonian expression, whereas the real part should be obtained by others direct means [28] or by its relation to the imaginary part [52] [74] [97]:

$$\Delta(E) = P \int \frac{WW^\dagger}{E - E'} dE' \tag{6.33}$$

Where the letter P refers to the Cauchy principal value.

I will insist here to the fact that the self energy is an E-dependent function. Indeed, most of publications assume a wide band limit which consists to do an approximation in which the self energy is E-independent. The consequence of this assumption, as it can be simply deduced from Eq. (6.33) is that the real part $\Delta(E)$ becomes zero. Some other works, keep the energy dependence but neglect the real part of the self energy arguing that it represents no more than a shift in the energy levels. Here, in this work, we will keep this dependence on energy and do not do any

---

7. To include more channels, we need to sum over the channels index a

8. This definition is correct up to a phase factor which is irrelevant. Because of this factor, some references gives this relation with an opposite sign(compare our formula to the book of S. Datta [98]

approximation. We will show how the exact results are different from the situation where these assumptions are considered.

After these clarifications, we can write the self energy of the leads [9]:

$$\Sigma = \Delta(E) - i\pi WW^\dagger \tag{6.34}$$

It is more suitable, for the upcoming calculations, to write the relation between the scattering matrix and the Hamiltonian in the following form:

$$S = \frac{1 - i\pi W^\dagger \frac{1}{E-\Delta(E)-H} W}{1 + i\pi W^\dagger \frac{1}{E-\Delta(E)-H} W} \tag{6.35}$$

If we define the matrix $\tilde{H} = -\pi W^\dagger \frac{1}{E-\Delta(E)-H} W$ then the relation above becomes:

$$S = \frac{1 + i\tilde{H}}{1 - i\tilde{H}} \tag{6.36}$$

Starting from this, we can seek to express the Haar measure which defines the uniform distribution for circular ensembles. We can write [10]:

$$dS = \frac{1}{1 - i\tilde{H}} 2id\tilde{H} \frac{1}{1 - i\tilde{H}} \tag{6.37}$$

Reminding that the Haar measure is $d\mu(S) = \frac{1}{V} S^\dagger dS$, we continue and write:

$$d\mu(S) = \frac{1}{V} \frac{1}{1 + i\tilde{H}} 2id\tilde{H} \frac{1}{1 - i\tilde{H}} \tag{6.38}$$

We need for the next step to state a very important mathematical result [99] [78]:

If A and M belong respectively to $N \times N$ complex and Hermitian matrices, we can write the following useful relation:

$$A^\dagger dMA = \det(AA^\dagger)^{\beta(N-1)/2+1} dM \tag{6.39}$$

$\beta = 1$, 2 and 4 *refer respectively to orthogonal, unitary and symplectic ensembles.*

Using this formula to simplify the Haar measure, we obtain:

$$d\mu(S) = \frac{1}{V} \frac{d\tilde{H}}{\det(1 + \tilde{H}^2)^{\beta(N-1)/2+1}} \tag{6.40}$$

This means that if the scattering matrix S is distributed uniformly according to the circular ensembles, then the matrix $\tilde{H}$ is distributed according to Lorentzian ensembles. We need to remind that the matrix $\tilde{H}$ is different from the Hamiltonian matrix H of the chaotic cavity. Nevertheless, because of the amazing proprieties we will state soon of the Lorentzian ensembles, it seems that taking Hamiltonians from the Lorentzian ensembles has an interesting implications.

6.5.1 Eigenvalues distribution of Lorentzian ensembles

It is important to know the distribution of the eigenvalues of a matrix distributed according to one of the different Lorentzian ensembles: $\beta = 1$ Lorentzian orthogonal ensemble $\mathcal{L}$OE, $\beta = 2$ Lorentzian unitary ensemble $\mathcal{L}$UE, $\beta = 4$ Lorentzian symplectic ensemble $\mathcal{L}$SE. If we take a matrix

---

9. The reader should be careful to the meaning of the symbol Σ and to which part of the system does it correspond: Does it refer to the self energy of one lead or to the whole leads? Sometimes we use the same symbol for the self energy matrix and the only non-zero elements of this matrix.

10. To do this step, we used the following useful formula:

$$dA^{-1} = -\frac{1}{A} dA \frac{1}{A}$$

H distributed according to one of the Lorentzian ensembles with a mean ϵ and a width λ then we can write:

$$P(H)dH = \frac{1}{V}\frac{dH}{\det(\lambda^2 + (H - \epsilon)^2)^{\beta(N-1)/2+1}} \tag{6.41}$$

The distribution of the levels is therefore [86, 89]:

$$P(E_1, E_2 \ldots E_N) \propto \prod_{i<j} |E_i - E_j|^\beta \prod_{i=1}^{N} \frac{1}{[\lambda^2 + (E_i - \epsilon)^2]^{\beta(N-1)/2+1}} \tag{6.42}$$

We obtain again the repulsion term $\prod_{i<j} |E_i - E_j|^\beta$ as for the Gaussian ensembles and recover the picture of interacting particles in a potential which is logarithmic in this case($V(x) \propto \ln(\lambda^2 + x^2)$.) instead of the Harmonic potential ($V(x) = x^2$)of the Gaussian ensembles (See the remark (6.8)).

6.5.2 Lorentzian distribution characteristics

The Lorentzian distribution has two interesting properties which make it special and very useful for our study [100, 86, 89]:

– **Property 1:** If H is distributed according to Lorentzian ensembles with width λ and center ϵ, then $\frac{1}{H}$ again is distributed according to Lorentzian ensembles, with width $\tilde{\lambda} = \frac{\lambda}{\epsilon^2+\lambda^2}$ and center $\tilde{\epsilon} = \frac{\epsilon}{\epsilon^2+\lambda^2}$.
– **Property 2:** Any submatrix[11] of a Lorentzian matrix is Lorentzian with the same width and the same center.

These two properties are very interesting and simplify too much the calculations. Moreover, they allow to lower the degrees of freedom of the system thanks to decimation procedure.

6.5.3 Decimation-renormalization procedure

We already introduced a kind of decimation procedure: Indeed, when we reduce the infinite size of the whole Hamiltonian (Scattering region+ Leads) to the size of the scattering region by introducing the self energy of the leads we are renormalizing the scattering region to an effective Hamiltonian $H_{eff} = H^0 + \Sigma$. This trick works not only on the leads but on any part of the system: *We can remove any part of the system and renormalize the parts to which it is attached.*
It is important to understand that by decimation procedure, we mean that both of the original and new system(obtained after decimation and renormalization) are equivalent to compute transport coefficients(Conductance, Seebeck coefficient). This means that if we want to remove one part from the whole Hamiltonian, we can do the decimation procedure explained in Fig. (6.7) If we remove a part described by a Hamiltonian H from the whole system we need to renormalize the remaining system as follows [101] [104]:

$$H_a = H_a^0 + \tau_a \frac{1}{E - H}\tau_a^\dagger \tag{6.43}$$

$$H_b = H_b^0 + \tau_b^\dagger \frac{1}{E - H}\tau_b \tag{6.44}$$

$$\tau_{ab} = \tau_a \frac{1}{E - H}\tau_b \tag{6.45}$$

H_a^0, H_b^0 are the original left and right neighboring slice Hamiltonians. H_a, H_b and τ_{ab} are the new renormalized corresponding quantities after decimation procedure. τ_a and τ_b are respectively, the coupling matrix of the left and right parts to the removed Hamiltonian. This procedure is interesting when we consider Lorentzian distribution thanks to the property stating that if a matrix is Lorentzian its inverse is also Lorentzian.

---

11. A submatrix is obtained by removing some columns and the corresponding lines from the original matrix.
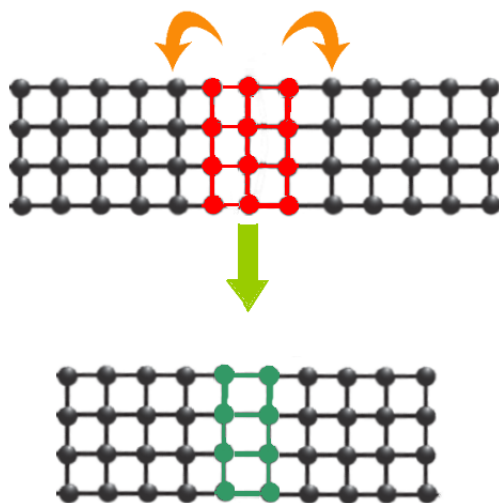
Figure 6.7: Decimation and renormalization procedure: We can remove one part(Red color) from a system and replace it by its effect on the remaining part to which it was attached. The potential on the neighboring sites are renormalized and so is the coupling between the remaining two parts

6.5.4   Comparison between Gaussian and Lorentzian distributions

Before we start to assume a Lorentzian distribution to describe the fluctuation of transport coefficients, it deserves to say something about why we switched to Lorentzian distribution and what is its relation to the Gaussian distribution. We know that for large $N \times N$ matrices ($N \to \infty$), and for fixed mean level spacing, the two distributions are equivalent [89]. To prove this we need just to compare the n-level cluster functions [80] [89] and one finds they are the same for both ensembles. We will show here an easiest proof which do not need complex arguments. Because for both ensembles, the distribution of the eigenvectors is uniform, we need just to compare the eigenenergies distributions. We will modify a little the Lorentzian distribution defined in (6.42) by introducing the mean level spacing Δ which verifies :

$$\Delta = \pi\lambda/N, \qquad N, \lambda \to \infty. \tag{6.46}$$

we can thus write:

$$P^{\mathcal{L}}(\{E_i\}) \quad \propto \quad \prod_{i<j} |E_i - E_j|^\beta \prod_{i=1}^{N} \frac{1}{[\pi^{-2} N^2 \Delta^2 + (E_i - \epsilon)^2]^{\beta(N-1)/2+1}} \tag{6.47}$$

$$\propto \quad \prod_{i<j} |E_i - E_j|^\beta \prod_{i=1}^{N} \frac{1}{[1 + \frac{(E_i - \epsilon)^2}{\pi^{-2} N^2 \Delta^2}]^{\beta(N-1)/2+1}} \tag{6.48}$$

$$\tag{6.49}$$

Using the relation $[1 + \frac{x}{n}]^n \to e^x$ we obtain:

$$P^{\mathcal{L}}(E_1 \dots E_N) \quad \propto \quad \prod_{i<j} |E_i - E_j|^\beta \prod_{i=1}^{N} e^{-\beta \frac{(E_i-\epsilon)^2}{2N\pi^{-2}\Delta^2}} \tag{6.50}$$

If we introduce again λ, the result becomes:

$$P^{\mathcal{L}}(E_1 \dots E_N) \quad \propto \quad \prod_{i<j} |E_i - E_j|^\beta \prod_{i=1}^{N} e^{-\beta N \frac{(E_i-\epsilon)^2}{2\lambda^2}} \tag{6.51}$$

After normalization we recover the Gaussian distribution and therefore we can claim that for large number N the two distributions are equivalent:

$$P^{\mathcal{L}}(\{E_i\}) = P^G(\{E_i\}) \tag{6.52}$$

This means that for large degrees of freedom, we can switch from Gaussian to Lorentzian distribution in order to benefit from the interesting properties of the Lorentzian ensembles.

6.5.5   Simple model solution
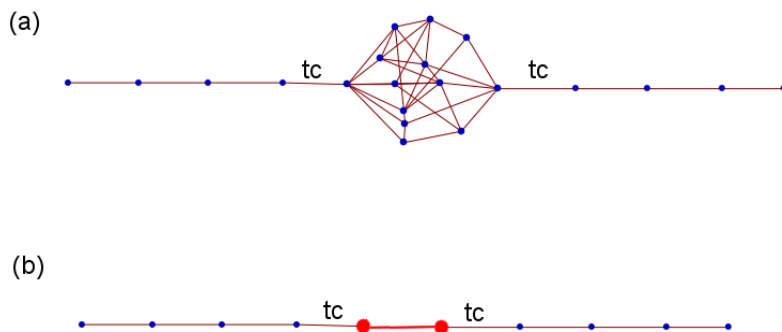
Figure 6.8: Decimation and renormalization procedure of the original model. We obtain a simpler model with only two random sites (red system).the coupling the two sites is also random. t_c is the coupling to the perfect 1D leads.

Now that we introduced the Lorentzian ensembles and the decimation-renormalization procedure, we want to study the fluctuation of quantum transport coefficients of a chaotic cavity sketched between two 1D perfect leads. The approach we want to follow is to first simplify the problem without doing approximations and propose the minimal model which mimics the behaviour of the chaotic cavity. First, we start by adopting the lattice picture of a cavity as shown in Fig. (6.8 (a)). We assume uniform leads with perfect coupling to the cavity (the coupling coefficient $t_c = 1$). We also assume symmetric conduction band $E \in [-2t_h, 2t_h]$ where the hopping term of the leads will be taken equal to one ($t_h = 1$) in all what follows. The self energy of the 1D lead is :

$$\Sigma(E) = \frac{E}{2} - i\sqrt{1 - \left(\frac{E}{2}\right)^2} \tag{6.53}$$

The Hamiltonian of the cavity is an $N \times N$ matrix. The sites are indexed from 1 to N where we choose to have the indexes 1 and N for the sites of the cavity which are connected to the leads. Now, if we use the decimation procedure and remove all the sites of the chaotic cavity, we need to renormalize the first sites connected to the cavity [87, 88].

$$\tilde{H}^r = H_0 + \tau \frac{1}{E - H} \tau^\dagger \tag{6.54}$$

where H^r is the renormalized Hamiltonian of the two sites which were connected to the cavity. H_0 is the Hamiltonian of the same two sites before renormalization (Here $H_0 = 0$ since the potential on these sites is 0 and they are not directly coupled). H is the Hamiltonian of the cavity and τ is the coupling matrix between the two sites and the cavity:

$$\tau = \begin{pmatrix} t_c, & 0, & 0, & \dots \\ \dots, & 0, & 0, & t_c \end{pmatrix} \tag{6.55}$$

Now let us understand the following arguments: We start by taking H from Gaussian ensembles. Then we can switch to Lorentzian distribution since they both are equivalent at large N. After doing the decimation procedure, we obtain a simpler system composed of two sites. Using the first property of the Lorentzian ensembles, we can claim that $\frac{1}{E-H}$ is also Lorentzian. The matrix $\tau \frac{1}{E-H} \tau^{\dagger}$ is no more than the mathematical operation taking a submatrix from $\frac{1}{E-H}$ and multiplying the result by the factor t_c^2 (τ is a sparse matrix) and according to the second property of Lorentzian ensembles this matrix is also Lorentzian. Finally, we deduce that the new small Hamiltonian $\tilde{H}^r$ (Fig 6.8(b))is distributed according to Lorentzian ensembles. From now on, we assume this Hamiltonian (we will drop the tilde and the index r) and use it to obtain the distribution of quantum transport coefficient since it is equivalent to the original system.(equivalent in the sense it gives the same coefficients). Now, we can write this Hamiltonian as follows:

$$H = \begin{pmatrix} v_1 & v_{12} \\ v_{21} & v_2 \end{pmatrix} \tag{6.56}$$

v_1, v_2 are the potentials on the sites and v_{12}, v_{21} are the coupling between them. We will look at a system under time-reversal symmetry and therefore we sample Hamiltonians from Lorentzian orthogonal ensembles $\mathcal{LOE}$. Within this symmetry, we have $v_{12} = v_{21}$.
This Hamiltonian is symmetric and therefore can be diagonalized by an orthogonal matrix:

$$P = \begin{pmatrix} \cos(\theta) & -\sin(\theta) \\ \sin(\theta) & \cos(\theta) \end{pmatrix} \tag{6.57}$$

The columns of this matrix are the eigenvectors of the Hamiltonian.
The eigenenergies of the Hamiltonian are easy to obtain and read:

$$E_1 = \frac{v_1 + v_2}{2} + \sqrt{\left(\frac{v_1 - v_2}{2}\right)^2 + 4v_{12}^2} \tag{6.58}$$

$$E_2 = \frac{v_1 + v_2}{2} - \sqrt{\left(\frac{v_1 - v_2}{2}\right)^2 + 4v_{12}^2} \tag{6.59}$$

The only possibility to have a degenerate eigenvalue is to have $v_{12} = 0$ (sites not coupled) and $v_1 = v_2$. we can also write the inverse relations:

$$v_1 = E_1 \cos^2(\theta) + E_2 \sin^2(\theta) \tag{6.60}$$
$$v_2 = E_2 \cos^2(\theta) + E_1 \sin^2(\theta) \tag{6.61}$$
$$v_{12} = (E_1 - E_2) \cos(\theta) \sin(\theta) \tag{6.62}$$

We come back now to the scattering approach to compute the transmission and the Seebeck coefficient S_k of the system [87, 102]. The scattering matrix of this system is:

$$S = 1 - 2\pi i W^{\dagger} \frac{1}{E - H - \Delta(E) + i\pi W W^{\dagger}} W \tag{6.63}$$

The matrix W which contains the coupling coefficients reads:

$$W = \begin{pmatrix} v(k) & 0 \\ 0 & v(k) \end{pmatrix} \tag{6.64}$$

Where $v^2(k) = \frac{1}{\pi}\sin(k) = \frac{1}{\pi}\sqrt{1 - \left(\frac{E}{2}\right)^2} = \frac{\Gamma}{2\pi}$, k is the Fermi wavenumber. we have also:

$$\Delta = \begin{pmatrix} \frac{E}{2} & 0 \\ 0 & \frac{E}{2} \end{pmatrix} \tag{6.65}$$

We notice that these two matrices are diagonal and moreover, proportional to the identity matrix, because the two leads are symmetric. The whole leads self energy reads:

$$\Sigma = \Delta(E) - i\pi W W^{\dagger} = \begin{pmatrix} \Sigma^l & 0 \\ 0 & \Sigma^r \end{pmatrix} \tag{6.66}$$

l and r refer respectively to left and right self energies which are the same in our case ($\Sigma^l = \Sigma^r$). Therefore, this self energy is also proportional to the identity matrix.

We continue and write the scattering matrix in a more convenient way:

$$S = \frac{1 - i\pi W^\dagger \frac{1}{E - \Delta(E) - H} W}{1 + i\pi W^\dagger \frac{1}{E - \Delta(E) - H} W} \tag{6.67}$$

We have already shown that in order to obtain a scattering matrix S distributed according to circular ensembles (Here it is COE), we need the matrix $\tilde{H} = \pi W^\dagger \frac{1}{E - \Delta(E) - H} W$ to be distributed according to Lorentzian ensembles with center $\epsilon = 0$ and width $\lambda = 1$. We can write this in the following way:

$$S \in COE \Rightarrow \tilde{H} \in \mathcal{L}OE(\epsilon = 0, \lambda = 1) \tag{6.68}$$

We quickly recall that $\tilde{H} = \frac{\Gamma}{2} \frac{1}{E - \Delta(E) - H}$ and give the following successive results based on the characteristics of Lorentzian distributions [87, 103] :

$$S \in COE \Rightarrow \qquad \tilde{H} \qquad \in \mathcal{L}OE(\epsilon = 0, \lambda = 1) \tag{6.69}$$

$$\Rightarrow \quad \frac{1}{E - \Delta(E) - H} \quad \in \mathcal{L}OE(\epsilon = 0, \lambda = \frac{2}{\Gamma}) \tag{6.70}$$

$$\Rightarrow \quad E - \Delta(E) - H \quad \in \mathcal{L}OE(\epsilon = 0, \lambda = \frac{\Gamma}{2}) \tag{6.71}$$

$$\Rightarrow \qquad H \qquad \in \mathcal{L}OE(\epsilon = E - \Delta(E), \lambda = \frac{\Gamma}{2}) \tag{6.72}$$

We deduce from this that the Hamiltonian matrix should belong to Lorentzian orthogonal ensembles with center $\epsilon = E - \Delta(E)$ and width $\lambda = \frac{\Gamma}{2}$. We summarize this and write [86, 87, 89]:

$$P(H) \propto \frac{1}{\det[\left(\frac{\Gamma}{2}\right)^2 + (E - \Delta(E) - H)^2]^{\beta(N-1)/2+1}} \tag{6.73}$$

(In our case $\beta = 1$ and $N = 2$)

We can express this distribution in a better way if we notice that:

$$P(H) \propto \frac{1}{|\det(E - H - \Sigma)|^{\beta(N-1)+2}} \tag{6.74}$$

This means that in order to obtain a uniform distribution for the scattering matrix S, the Hamiltonian should be distributed according to Lorentzian ensembles with a center and a width determined by the self energy of its environment. This constraint shows that we can not qualify a system as completely random just by choosing the Hamiltonian random. The "adaptation" of the scattering system distribution and its environment is crucial to completely randomize the system in the sens of circular ensembles.

We made the last proof assuming ideal leads (perfect coupling). It is not hard to generalize this result to the case of non-ideal leads (coupling $t_c \neq 1$) and the final result remains unchanged since we include the coupling in the self energy of the leads.

6.5.6   Poisson kernel distribution

Which distribution of the scattering matrix do we obtain if we choose a Hamiltonian from Lorentzian ensembles with a center and width different from what was stated above?

If we choose $H \in \mathcal{L}OE(\epsilon, \lambda)$, λ and ϵ being arbitrary, we do not obtain, in general, uniformly distributed scattering matrix (circular ensembles). Indeed, circular ensembles are characterized by a mean scattering $\bar{S}$ matrix which is zero.

$$\bar{S} = \int S P(S) d\mu(S) \tag{6.75}$$

$P(S)$ belongs to circular ensembles $\Rightarrow \bar{S} = 0$.

For arbitrary λ and ϵ, the mean scattering matrix do not vanish in general and the distribution of S becomes a Poisson Kernel distribution:

$$P(S) \propto |\det(1 - \bar{S}^\dagger S)|^{-(\beta(N-1)+2)} \tag{6.76}$$

the mean scattering matrix is given by the parameters $\tilde{\epsilon}$, $\tilde{\lambda}$ of the matrix $\tilde{H} = -\pi W^\dagger \frac{1}{E - \Delta(E) - H} W$ [89]:

$$\bar{S} = \sigma I, \text{ with } \quad \sigma = \frac{1 - \tilde{\lambda} - i\tilde{\epsilon}}{1 + \tilde{\lambda} + i\tilde{\epsilon}} \tag{6.77}$$

we recover the result saying that if $\tilde{H}$ is centered ($\tilde{\epsilon} = 0$) and has a width $\tilde{\lambda} = 1$, the distribution of the scattering matrix will belong to circular ensembles ($\bar{S} = 0$). We can also give the distribution of the eigenphases of the Poisson kernel distribution:

$$P\{\phi_i\} \propto \prod_{i<j} |e^{i\phi_i} - e^{i\phi_j}|^\beta \prod_j |1 - \sigma^* e^{i\phi_j}|^{-(\beta(N-1)+2)} \tag{6.78}$$

$\beta = 1$, 2 and 4 respectively for orthogonal, unitary and symplectic ensembles.
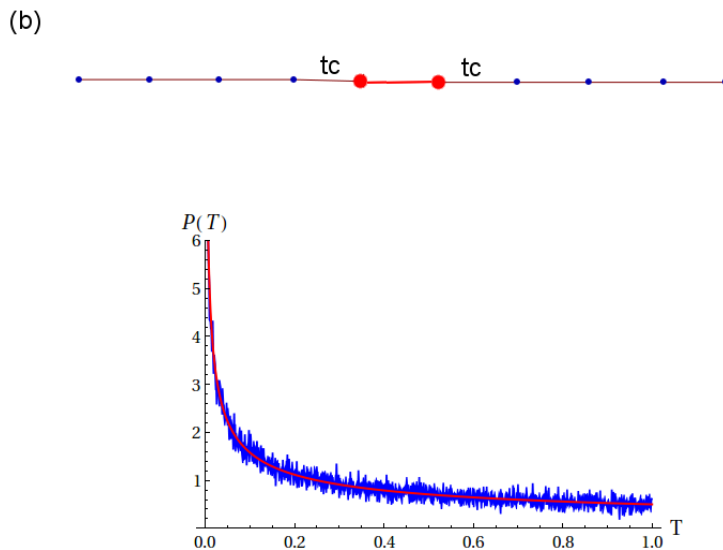
(b)

Figure 6.9: Transmission probability distribution: The transmission is distributed according to the law $\frac{1}{2\sqrt{T}}$ (red color). The system considered in simulation is shown in top figure. The Hamiltonian is taken from Lorentzian orthogonal ensembles with mean $(E - \Delta(E))$ and width $\Gamma/2$.

6.5.7   Transmission and Seebeck coefficient distribution

We shall start with the simple case of the transmission coefficient. The minimal model we already introduced, has a simple formula which gives its transmission:

$$T = \Gamma G_{12} \Gamma G_{12}^{\dagger} \tag{6.79}$$

where G defined as the Green's function of the system.

If we take a Hamiltonian distributed according to Lorentzian ensembles with mean $\epsilon = E - \Delta(E)$ and width $\lambda = \Gamma/2$ we should recover the result obtained in literature [95, 96] using circular ensembles. we find:

$$P(T) = \frac{1}{2\sqrt{T}} \tag{6.80}$$

As we can see in Fig. (6.9), the numerical simulation result is well fitted by the expected law $1/2\sqrt{T}$

Distribution of the Seebeck coefficient S_k

Generally, people look less to the Seebeck coefficient and most of works concern transmission coefficient although they are both similar linear response theory coefficients: One describes the response to a voltage difference between electrons reservoirs (this is T) and the other describes the response to a difference in temperature between the two reservoirs(This is Seebeck S_k). This is due, maybe, to the fact that handling temperature is more complex than handling voltage. Nonetheless, there exist some interesting experimental works looking at the statistics of Seebeck coefficient in chaotic cavities. Indeed, the group of Molenkamp [91] studied the thermovoltage of a quantum dot, precisely, the fluctuations in the thermopower as a function of a magnetic field and dot shape. The system is managed to be open for two modes of conduction and the thermopower is obtained by the technique of current heating: One of the electronic reservoirs (Leads) sketching the quantum dot, is heated with a low frequency current, while the 2DEG in the QD remains at equilibrium. The measurements of thermopower display a non-Gaussian distribution which is in agreement with simulations using random matrix theory. For the theoretical work, Van Langen et al [92] studied the zero-temperature limit of the distribution of thermopower S_k in a disordered 1D wire in the localized regime. The distribution is found to be Lorentzian:

$$P(\sigma) \propto \frac{1}{1 + \sigma^2}$$

where σ is the thermopower normalized over the mean level spacing. Here also the agreement was good with the numerical simulation. We can mention also the work by Brouwer et al [93] on the statistics of the Seebeck of a quantum dot with two single channel ballistic point contacts. The analytical work allowed them to express the system of equations giving the Seebeck statistics but the final result was obtained by simulation after doing numerically a very complex integral. They found a distribution exhibiting a cusp at the origin $S_k = 0$ with a logarithmic tale for large value of the thermopower.

All the up-to-date results give numerical solution for the problem of thermopower statistics in a chaotic cavity connected to one mode conducting leads. Here in this sections, we succeed to bring an easiest approach to provide the analytical solution giving the distribution of thermopower in the presence of time reversal symmetry. We try to stay very close to the subject of this thesis, focusing on the Green's function and self energy treatment of the problem of electrons transport.

Seebeck Statistics and the minimal model

We need first to recall that the minimal system is equivalent to the original (Large number of sites) in the calculation of the transmission probability. Since this is true at all Fermi energy, the Seebeck of the two systems are the same. In the following, we will assume very low temperatures, for which the Seebeck can be given by the Mott formula:

$$S_k = -\frac{\pi^2}{3}\frac{k_b^2 \mathcal{T}}{e}\frac{\partial \ln(T)}{\partial E} \tag{6.81}$$

In what follows, we will drop the sign(-), impertinent for the statistics and drop also the factor $\frac{\pi^2}{3}\frac{k_b^2 \mathcal{T}}{e}$ which will be considered as a unit of measure. We need to express the Seebeck coefficient S_k using the Hamiltonian parameters v_1, v_2, and v_{12}. To do this task, we start with the expression of the transmission that we can deduce and simplify from [12] Eq. (6.79) [102]:

$$T = \Gamma^2 \frac{v_{12}^2}{|(E - v_1 - \Sigma)(E - v_2 - \Sigma) - v_{12}^2|^2} \tag{6.82}$$

This expression, based on the Green's function of the system, is pretty simple. It can not be the case if we kept the original system, with very large number of sites. This shows the advantage of taking an equivalent minimal model.

Expression (6.82) can be written in another form, based on the Hamiltonian eigenenergies, E_1 and E_2 [102]:

$$T = \Gamma^2 \frac{v_{12}^2}{|(E - E_1 - \Sigma)(E - E_2 - \Sigma)|^2} \tag{6.83}$$

Now the Seebeck coefficient comes straightforward ($S_k = \frac{\partial \ln(T)}{\partial E}$):

$$S_k = \frac{\partial \ln \Gamma^2}{\partial E} - \frac{1 - \dot{\Sigma}}{E - E_1 - \Sigma} - \frac{1 - \dot{\Sigma}^*}{E - E_1 - \Sigma^*} - \frac{1 - \dot{\Sigma}}{E - E_2 - \Sigma} - \frac{1 - \dot{\Sigma}^*}{E - E_2 - \Sigma^*} \tag{6.84}$$

This expression is valid for all Fermi energies. The dot refers to the derivative over energy and the star refers to complex conjugate. Before we look at the statistics of the Seebeck coefficient at an arbitrary Fermi energy, we will start to investigate the simple case of the half filling limit in the middle of the band of conduction ($E_F = 0$). [13] To see the simplifications we get in this limit, we need just to recall that: $\Sigma = \frac{E}{2} - i\sqrt{1 - \left(\frac{E}{2}\right)}$ and therefore:

$$\frac{\partial \ln \Gamma^2}{\partial E} = 0, \quad \dot{\Sigma} = \frac{1}{2}, \quad \text{and} \quad \Sigma = -i \tag{6.85}$$

---

12. Σ, represents here the self energy of one lead. It is a scalar quantity.
13. We remind that for 1D semi-infinite leads, the conduction band is: $E_F \in [-2t_h, 2t_h]$. t_h is the hopping term in the leads. $E_F = 0$ is the half-filling limit.

With these simplifications, the expression of the Seebeck coefficient becomes much more simpler and contains solely the eigenenergies of the Hamiltonian matrix of the scattering region:

$$S_k = \frac{E_1}{1 + E_1^2} \frac{E_2}{1 + E_2^2} \qquad (6.86)$$

The distribution of S_k can be written in an integral form the following way:

$$P(S_k) \propto \int |E_1 - E_2| \frac{dE_1 dE_2}{[(1 + E_1^2)(1 + E_2^2)]^{3/2}} \delta(S_k - \frac{E_1}{1 + E_1^2} - \frac{E_2}{1 + E_2^2}) \qquad (6.87)$$

The weight in the integral corresponds to the Lorentzian weight(The width and center are adapted to have a completely chaotic cavity in the sens of circular ensembles). We can express this probability density function using the circular orthogonal ensembles rather than the $\mathcal{LOE}$. This can be easily done just by using the variable change :

$$E_i = \tan(\frac{\phi_i}{2})$$

After simple trigonometric manipulations, we obtain the following expression for the Seebeck coefficient:

$$S_k = \sin(\frac{\phi_1 + \phi_2}{2}) \cos(\frac{\phi_1 - \phi_2}{2}) \qquad (6.88)$$

The weight of circular orthogonal ensembles is proportional to the factor:

$$|e^{i\phi_1} - e^{i\phi_2}| = 2|\sin(\frac{\phi_1 - \phi_2}{2})|.$$

The probability density function of S_k becomes:

$$P(S_k) \propto \int_{-\pi}^{\pi} |\sin(\frac{\phi_1 - \phi_2}{2})| \delta(S_k - \sin(\frac{\phi_1 + \phi_2}{2}) \cos(\frac{\phi_1 - \phi_2}{2})) d\phi_1 d\phi_2. \qquad (6.89)$$

We can guess that it is better to use the new variables u and v defined as follows:

$$u = \frac{\phi_1 - \phi_2}{2}, \qquad v = \frac{\phi_1 + \phi_2}{2}$$

with this new variables the expression becomes [14]:

$$P(S_k) \propto \int_{-\pi}^{\pi} |\sin(u)| \delta(S_k - \sin(v) \cos(u)) du dv. \qquad (6.90)$$

We are omitting a lot of factors after each transformation. This is not a problem because we know that the final result should be normalized.

Now, we will try to shorten the interval of integration in order to have a biunivoque relation between the variables of the new change we will make soon. So, we can write [87, 102]:

$$P(S_k) \propto \int_{0}^{\pi} \sin(u)[\delta(S_k + \sin(v) \cos(u)) + \delta(S_k - \sin(v) \cos(u))] du dv. \qquad (6.91)$$

Next, we do the following shifts $u \to u - \frac{\pi}{2}$ and $v \to v - \frac{\pi}{2}$ and melt the two delta functions:

$$P(S_k) \propto \int_{-\frac{\pi}{2}}^{+\frac{\pi}{2}} \cos(u) \delta(|S_k| - \cos(v) \sin(u)) du dv. \qquad (6.92)$$

Because the expression we integrate is even (for both u and v), we restrict the integration on $[0, \frac{\pi}{2}]$ and then perform the last variable substitution:
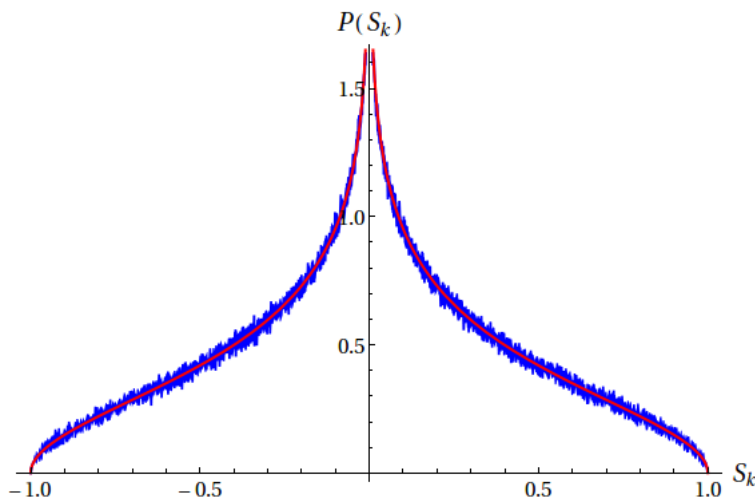
$$p = \sin(u) \qquad q = \cos(v)$$

Figure 6.10: The distribution of the Seebeck coefficient S_k at half filling limit (E=0). S_k is bounded and the distribution is singular at the origin. The numerical simulation is well fitted with the function obtained analytically. This Seebeck is for a chaotic cavity connected to two 1D leads(one conducting mode in each one).

The integral becomes:

$$P(S_k) \propto \int_0^1 \frac{dpdq}{\sqrt{1-q^2}} \delta(|S_k| - pq) \tag{6.93}$$

After a first simple integration over the variable q, we obtain:

$$P(S_k) \propto \int_{|S_k|}^1 \frac{dp}{\sqrt{p^2 - S_k^2}}. \tag{6.94}$$

This last integral is easy to do. We obtain after normalization the following probability density function [87, 102]:

$$\boxed{P(S_k) = -\frac{1}{\pi} \log \frac{|S_k|}{1 + \sqrt{1 - S_k^2}}} \tag{6.95}$$

We can extract two very important things from this result:
  – The Seebeck is bounded: we can not have Seebeck coefficients bigger than 1 in absolute value. This characteristic seems to be generalized to all energies as we can see it later(the bound changes).
  – At the origin, the distribution is singular and do not have a cusp as it may seen in some numerical simulations.

Now that we finished with the analytical result, we need to verify this distribution numerically. The first, problem we face, is how to generate the Lorentzian orthogonal ensembles. The difficulty comes from the fact that the elements of the Hamiltonian matrix are not independent variables [15]. We will show later, in the coming sections how to generate them, but here, I would like to use the usual law of probability. This method is based on the integral form Eq. (6.87). First we separate the integrals on two intervals: $|E_i < 1|$ and $|E_i > 1|$. In the last one, we perform the substitution $E_i \to 1/E_i$. Out of thin air, we recover the same expression as for $|E_i < 1|$. Therefore, we can

---

14. After changing to the variables u and v, the range of integration becomes different from $[-\pi, \pi]$. Thus, the integrated expression is invariant under the translations $u \to u \pm \pi$ and $v \to v \pm \pi$ and therefore we recover the whole interval $[-\pi, \pi]$

15. We remind that the Gaussian distribution is the only distribution whose elements are independent See [79] [80]

write:

$$P(S_k) \propto \int_{-1}^{1} |E_1 - E_2| \frac{dE_1 dE_2}{[(1 + E_1^2)(1 + E_2^2)]^{3/2}} \delta(S_k - \frac{E_1}{1 + E_1^2} - \frac{E_2}{1 + E_2^2}) \tag{6.96}$$

Notice that the integral is from -1 to 1. To do this numerically, we proceed as follows:

- I divide the interval of S_k over 1000 small intervals.
- I take E_1, E_2 randomly with a uniform law from $[-1, 1]$.
- I calculate S_k with these values.
- I sum the weights of the corresponding values of S_k.
- I do it again and again with adding each time the corresponding weight.
- I normalize and plot the result to obtain the wanted distribution.

The result of numerical simulation is shown in Fig. (6.10) . We can see how the analytical result fits well the data obtained from simulation. The values of the Seebeck coefficient are bounded and range between -1 and 1. It is also important to see that the distribution is singular at the origin and do not have a cusp as may appear in numerical data (The cusp may appear because of the discretization of the Seebeck range in simulation).

At $E = 0$, the lattice effect on the dispersion relation may cause unexpected results. For this reason, it is important to obtain the density function distribution of Seebeck at the continuum limit, for energies in the bottom of the conduction band.

The distribution of the Seebeck coefficient at arbitrary energy

As may someone guess, the calculation of the probability density function of Seebeck coefficient S_k at energy $E \neq 0$ is much more difficult and necessitate more care and tricks. To start, let us rewrite the S_k at arbitrary energy [102]:

$$S_k = \frac{\partial \ln \Gamma^2}{\partial E} - \frac{1 - \dot{\Sigma}}{E - E_1 - \Sigma} - \frac{1 - \dot{\Sigma}^*}{E - E_1 - \Sigma^*} - \frac{1 - \dot{\Sigma}}{E - E_2 - \Sigma} - \frac{1 - \dot{\Sigma}^*}{E - E_2 - \Sigma^*}. \tag{6.97}$$

After simple manipulations we can express this result in a more convenient form as follows:

$$S_K = K - \frac{2}{\Gamma}[\frac{x - b}{1 + x^2} + \frac{y - b}{1 + y^2}] \tag{6.98}$$

where the new variables used above are defined the following way:

$$K = \frac{\partial \ln(\Gamma^2)}{\partial E} \tag{6.99}$$

$$b = \frac{2\Re(\Sigma)}{\Gamma} \tag{6.100}$$

$$x = \frac{2(E - E_1 - \Re(\Sigma))}{\Gamma} \tag{6.101}$$

$$y = \frac{2(E - E_2 - \Re(\Sigma))}{\Gamma} \tag{6.102}$$

If we want our Scattering matrix to belong to COE, the Hamiltonian should have the following Lorentzian distribution [16] [17]:

$$P(H)dH \propto \frac{dH}{|\det(E - H - \Sigma)|^3} \propto \frac{|E_1 - E_2|dE_1 dE_2}{[((\frac{E - E_1 - \Re(\Sigma)}{\Gamma/2})^2 + 1)((\frac{E - E_1 - \Re(\Sigma)}{\Gamma/2})^2 + 1)]^{3/2}}$$

This means that in terms of the reduced variables x and y:

$$P(H)dH \propto \frac{|x - y|dxdy}{[(1 + x^2)(1 + y^2)]^{3/2}} \tag{6.103}$$

---

16. Based on the remarks of the sections of this chapter: The Hamiltonian distribution needs to have a center and a width according to its self energy in order to obtain a uniform distribution for the scattering matrix.

17. Here Σ is the matrix self energy of the two leads

which is similar to the one we used for the case $E = 0$. For this reason, we will perform the same substitution:

$$x = \tan(\frac{\phi_1}{2}), \qquad y = \tan(\frac{\phi_2}{2})$$

and try now to find the Seebeck distribution:

$$
\begin{aligned}
P(S_k) &\propto \int p(x,y)\delta(S_K - K + \frac{2}{\Gamma}[\frac{x-b}{1+x^2} + \frac{y-b}{1+y^2}])dxdy \\
&\propto \int |\sin(\frac{\phi_1 - \phi_2}{2})|\delta(S_k - k + \frac{2}{\Gamma}[\sin(\frac{\phi_1 + \phi_2}{2})\cos(\frac{\phi_1 - \phi_2}{2}) \\
&\quad -b\cos(\frac{\phi_1 + \phi_2}{2})\cos(\frac{\phi_1 - \phi_2}{2})])d\phi_1 d\phi_2
\end{aligned}
$$

Again, we put $u = \frac{\phi_1 - \phi_2}{2}$ and $v = \frac{\phi_1 + \phi_2}{2}$ to obtain:

$$P(S_k) \propto \int_{-\pi}^{+\pi} |\sin(u)|\delta(\tilde{S}_k + \frac{2}{\Gamma}[\sin(v)\cos(u) - b\cos(u)\cos(v)])dudv \tag{6.104}$$

Here, we put $\tilde{S}_k = S_k - K - 2b/\Gamma$

The main trick to simplify the calculations, is to write :

$$\sin(v)\cos(u) - b\cos(u)\cos(v) = \sqrt{1+b^2}\cos(u)[\frac{1}{\sqrt{1+b^2}}\sin(v) - \frac{b}{\sqrt{1+b^2}}\cos(v)]$$

and define after that $\cos(\Omega) = \frac{1}{\sqrt{1+b^2}}$. We then obtain:

$$\sin(v)\cos(u) - b\cos(u)\cos(v) = \sqrt{1+b^2}\cos(u)\sin(v - \Omega) \tag{6.105}$$

The integral form of the distribution becomes, after taking into account those simplifications:

$$
\begin{aligned}
P(S_k) &\propto \int_{-\pi}^{+\pi} |\sin(u)|\delta(\tilde{S}_k + \frac{2}{\Gamma}\sqrt{1+b^2}\cos(u)\sin(v-\Omega)dudv \tag{6.106} \\
&\propto \int_{-\pi}^{+\pi} |\sin(u)|\delta(\frac{2\sqrt{1+b^2}}{\Gamma}\tilde{S}_k + \cos(u)\sin v)dudv \tag{6.107}
\end{aligned}
$$

In the last step we used the fact that sin is a periodic function and thus a shift by Ω do not change the result when we integrate from $-\pi$ to π. We used also the basic relation for distributions : $\delta(\alpha f(x)) = \frac{1}{|\alpha|}\delta(f(x))$.

We do not need to go further in calculations: the last expression is the same as Eq. (6.90) obtain at half filling limit ($E = 0$). Therefore, we can directly give the resul of this integral:

$$P(S_k) \propto P_{E=0}(\frac{\Gamma}{2\sqrt{1+b^2}}\tilde{S}_k) \tag{6.108}$$

What is amazing is that things could be more simplified if one notices that:

$$K + \frac{2b}{\Gamma} = 0 \tag{6.109}$$

This implies that $S_k = \tilde{S}_k$. From the form of the self energy of a 1D lead [18], we can deduce the following result:

$$\left(\frac{\Gamma}{2}\right)^2 (1 + b^2) = 1 \tag{6.110}$$

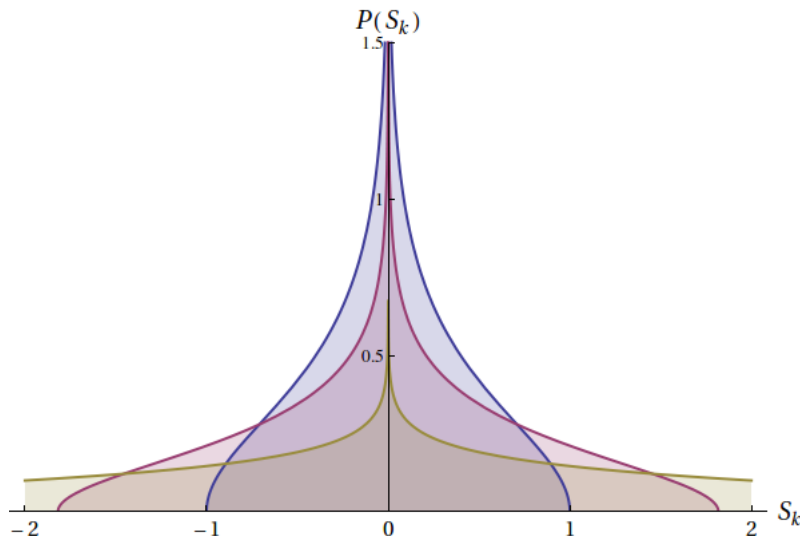18. $\Sigma = \Re(\Sigma) - i\frac{\Gamma}{2} = \frac{E}{2} - i\sqrt{1 - \left(\frac{E}{2}\right)^2}$

Figure 6.11: The distribution of Seebeck coefficient at different values of Fermi energies: E=0 (Blue), E=-1.3 (Purple) and E=-1.8 (Green).

Taking into account these results, we can write:

$$P(S_k) \propto P_{E=0}\left((\frac{\Gamma}{2})^2 S_k\right) \tag{6.111}$$

Finally, if we put $a = \left(\frac{\Gamma}{2}\right)^2$ we obtain after normalization [87, 102, 88]:

$$\boxed{P(S_k) = -\frac{a}{\pi} \log \frac{a|S_k|}{1 + \sqrt{1 - a^2 S_k^2}}.} \tag{6.112}$$

At $E = 0$ we have $a = 1$ and we recover the previous result obtained at half filling limit.
We wish to make some remarks on this result:

- At a given Fermi energy, the Seebeck is bounded: The system can have Seebeck coefficients only in the range $[-\left(\frac{2}{\Gamma}\right)^2, \left(\frac{2}{\Gamma}\right)^2]$
- The range of Seebeck values becomes wider when we approach the continuum limit, in the bottom of the conduction band ($E \sim -2$).
- Numerical simulations could be sometimes misleading: Indeed, the figure we obtain with simulation may show a cusp at the origin (because of the discretization in simulation) whereas the analytical result shows a singularity. The divergence at this point is $P(S_k) \sim -\frac{a}{\pi} \log(a|S_k|)$.

We insisted in the previous sections on the fact that our result is exact and that we did not do any approximation. Indeed, we took the correct form of the self energy and did not assume like in most works on quantum transport, the wide band limit, where the self energy is taken energy-independent. It is easy to see that neglecting the real part of the self energy will have consequences on the final result: In our case, the calculation assuming $\Re\Sigma = 0$ gives the following result:

$$P(S_k) \propto P_{E=0}(\frac{\Gamma}{4} S_k), \qquad \text{If } \Re\Sigma(E) \text{ neglected} \tag{6.113}$$

which means that the bounds of the Seebeck coefficient change: The range of the Seebeck coefficient scales like $\frac{1}{\Gamma}$ an not like $\frac{1}{\Gamma^2}$ as we found when we took the correct form of the self energy.

6.6   Generating Lorentzian ensembles

Random matrix theory implies, in general, calculations of high complexity and it is not easy for someone to always be sure there is no mistake. When the length of calculations is very long,

the process becomes like a blind walk: At each step the probability to make mistakes becomes bigger. For this reason, doing numerical simulation to verify the results is very important and helps a lot to have the intuition in the steps we should follow in the analytical procedure. Nevertheless, simulation is not always easy and it is important to master the operations which generate the different ensembles we introduced in this chapter. In this section, we want to explain the way we obtain those ensembles. Most of libraries give the Gaussian ensembles. Indeed, the elements of a Gaussian matrix distribution are independent [79] [80] (Look also to my first sections) which makes this distribution easy to generate. The Lorentzian ensembles do not have this property [19] and generating them becomes difficult. To show how to surpass this problem we need first to show how to generate circular ensembles which is by the way tricky.

Generating circular unitary ensembles CUE

We will start with the method which generates a matrix from CUE. Of course, the elements of this matrix are not independent and therefore this complicates the operation. It is also known that obtaining a random unitary matrix from CUE by exponentiating Hermitian ones taken from Gaussian ensembles do not work unfortunately. Indeed, the properties of the matrix $U = e^{iH}$ with H taken from Gaussian ensembles are different from the properties of CUE matrices. This is due to multiple wrapping around the unit circle after exponentiation [105]. Anther example which shows the difficulty of generating random unitary matrices is the QR decomposition [20]. Indeed, if we apply the Gram-Schmidt orthonormalization to the columns of a matrix Z, the resulting matrix is unitary. This means that is the entries of the matrix Z are i.i.d standard normal complex variables then Q is distributed according to the Haar measure. Unfortunately, the algorithm doing this is unstable and we do not obtain the characteristics of a matrix belonging to CUE. The reader can refer to the very good references Edelman and Rao [81] and Mezzadri [106] to see how to fix this problem. The correct algorithm giving a matrix from CUE reads (Python language):

```python
# A random matrix distributed with Haar measure        (CUE)        #

from scipy import*
def CUE(n):
          z = (randn(n,n) + 1j*randn(n,n))/sqrt(2.0)
          q,r = linalg.qr(z)
          d = diagonal(r)
          ph = d/absolute(d)
          q = multiply(q,ph,q)
          return q
```

This routine calls the function named CUE which returns a matrix randomly distributed from the circular unitary ensembles.

Generating circular orthogonal ensembles COE

Now that we introduced how to generate a matrix from the circular unitary ensembles, it is easy to use this result to generate matrices from circular orthogonal ensembles: Indeed, we know that a symmetric unitary matrix can be written as a product of a unitary matrix and its transpose. Thus if we define the matrix $S = U^T U$ where U is a matrix from CUE, the matrix S will be distributed according to circular orthogonal ensembles COE. The algorithm which makes this procedure(written in Python) reads:

```python
#A Random matrix distributed according to circular orthogonal ensembles#
```

---

19. The Gaussian distribution is the only one whose elements are independent [79]
20. The QR decomposition is decomposing a matrix A into a product $A = QR$ of an orthogonal matrix Q and an upper triangular matrix R.

```
from scipy import*
def COE(n):
        U=CUE(n)
        S = dot(transpose(U),U)
        return S
```

This routine calls the function COE which returns a matrix distributed according to circular orthogonal ensembles. You notice that this routine uses the function CUE defined previously. This means that the first routine should be present in the program if we want to use the second routine.

Generation Lorentzian ensembles

The algorithms we presented so far concern the distribution of the scattering matrix. Now, we come to our aim, which is to generate Lorentzian randomly distributed matrices. This algorithm we present here is based on the theoretical analysis we introduced when we compared the scattering and the Hamiltonian approaches. We showed that if a matrix S is parameterized as follows:

$$S = \frac{1 - iH}{1 + iH} \tag{6.114}$$

and the matrix H is Lorentzian with center zero and width $\lambda = 1$, this implies that S has a uniform distribution according to circular ensembles. Now that we know how to generate circular ensembles, we use this property to generate Lorentzian ensembles: If S is CUE (or COE), the matrix H defined as :

$$H = -i\frac{1 - S}{1 + S} \tag{6.115}$$

belongs to Lorentzian unitary ensemble $\mathcal{L}UE$ (or Lorentzian orthogonal ensemble $\mathcal{L}OE$). These matrices has center zero and width $\lambda = 1$. The algorithm which uses this property and generates these two ensembles looks like what follows (in Python Language):

```
#A Random matrix distributed according to circular orthogonal ensembles#

from scipy import*
def LUE(n):
        S=CUE(n)
        H=-1j * dot((eye(n)-S),linalg.inv(eye(n)+S))
        return H

def LOE(n):
        S=COE(n)
        H=-1j * dot((eye(n)-S),linalg.inv(eye(n)+S))
        return real(H)
```

In this programs we call the functions LUE and LOE which returns a matrix chosen randomly from respectively, $\mathcal{L}UE$ and $\mathcal{L}OE$. Again, we used in this algorithm, the previous routines generating COE and CUE ensembles, and therefore they all need to be present in the same programs. The algorithms exhibited above generates Lorentzian matrices with center zero and width $\lambda = 1$. To obtain different center and different width, we use the following property:

$$H \in \mathcal{L}OE(\text{Center} = 0, \text{width} = 1) \Rightarrow \lambda H + \epsilon \in \mathcal{L}OE(\text{Center} = \epsilon, \text{width} = \lambda)$$

All these algorithms are very useful and simplify a lot the numerical simulation. For instance, we will explain here how to use them in order to obtain the distribution of the Seebeck coefficient S_k
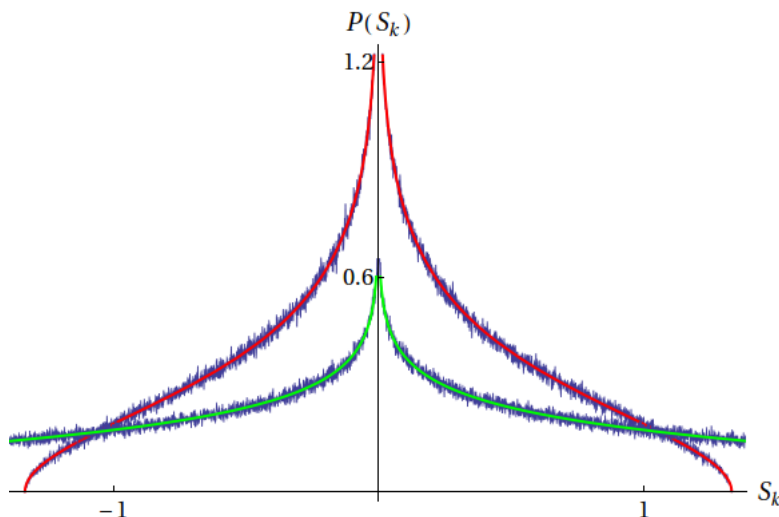
Figure 6.12: Verification of the Seebeck coefficient density function at arbitrary Fermi energy: E=-1.7 (Green curve) and $E = -1$ (Red curve). The agreement between simulation and the analytical expression is excellent. The density function has a singularity at the origin. The density function is non-zero over a range $\frac{8}{\Gamma^2}$.

directly by sampling Hamiltonians from Lorentzian orthogonal ensemble $\mathcal{LOE}$. We start first, with the simple case of the half filling limit ($E = 0$). We need to remind that the coefficient S_k reads:

$$S_k = -\frac{E_1}{1 + E_1^2} - \frac{E_2}{1 + E_2^2} \tag{6.116}$$

It needs no effort to see that this result is more simple if we rewrite it down the following way [21]:

$$S_k = -\text{Tr}\frac{H}{I + H^2} \tag{6.117}$$

This very simple expression is very practical: We sample Hamiltonians from $\mathcal{LOE}$ and uses this formula to directly obtain the Seebeck coefficient. Then, doing statistics on the data, gives the distribution of S_k. The program doing this has a few lines !

We can generalize this and try to apply it at an arbitrary Fermi energy. Indeed, the general expression of Seebeck in terms of the variables x and y defined previously Eq. (6.98) is :

$$S_K = K - \frac{2}{\Gamma}[\frac{x - b}{1 + x^2} + \frac{y - b}{1 + y^2}] \tag{6.118}$$

Where x, y are the eigenlevels of a Lorentzian matrix, let us call it M. The expression of Seebeck coefficient S_k in a matrix form reads:

$$S_k = K - \frac{2}{\Gamma}\text{Tr}\frac{M - bI}{I + M^2} \tag{6.119}$$

With this expression, we can easily verify the analytical result we obtained at arbitrary Fermi energy (We could not do it before). Fig. (6.12) shows the results of numerical simulation of Seebeck coefficient probability density function at two different energies ($E = -1$ and $E = -1.7$). The agreement with analytical result is excellent. The Seebeck S_k of the chaotic cavity can not take any value: the range of Seebeck is $[- \left(\frac{2}{\Gamma}\right)^2, \left(\frac{2}{\Gamma}\right)^2]$. The probability density function has a logarithmic singularity (and not a cusp) at the origin. It is evident that the mean value of the Seebeck coefficient is zero. It is also easy to find the mean value $\langle S_k^2 \rangle$ defined as:

$$\langle S_k^2 \rangle = \int S_k^2 P(S_k)dS_k \tag{6.120}$$

---

21. We remind that we already omitted a sign (-) in the definition we adopted for the Seebeck coefficient S_k. This sign is irrelevant for the statistics

we find that $\langle S_k^2 \rangle = \frac{2}{3\Gamma^2}$

Seebeck coefficient and the scattering matrix formula

We succeeded to write the Seebeck coefficient in a matrix form based on the Hamiltonian. What we want to do here, is to use the Scattering matrix S rather than the Hamiltonian H to express the Seebeck in a matrix form. We start by reminding the following important formula:

$$S = \frac{1 - i\pi W^\dagger \frac{1}{E - \Delta(E) - H} W}{1 + i\pi W^\dagger \frac{1}{E - \Delta(E) - H} W} \tag{6.121}$$

If we put

$$M^{-1} = \pi W^\dagger \frac{1}{E - \Delta(E) - H} W = \frac{\Gamma}{2} \frac{1}{E - \Delta(E) - H}$$

then we can write M as a function of the scattering matrix as follows:

$$M = i\frac{1 + S}{1 - S} \tag{6.122}$$

Now, we want to replace this formula in the following expression giving the Seebeck coefficient:

$$S_k = K - \frac{2}{\Gamma} \text{Tr} \frac{M - bI}{I + M^2} \tag{6.123}$$

After doing this substitution, we obtain the following result:

$$S_k = K + \frac{1}{\Gamma} \text{Tr} \frac{S - S^\dagger}{2i} - \frac{b}{\Gamma} \text{Tr} \frac{S + S^\dagger}{2} + \frac{2b}{\Gamma} \tag{6.124}$$

Simpler result can be achieved if we recall that the coefficient K and b, defined for a 1D perfect lead(See Eq. (6.99)), verify:

$$K + \frac{2b}{\Gamma} = 0$$

All in All, the final result reads [102, 88]:

$$S_k = \frac{1}{\Gamma} \text{Tr} \frac{S - S^\dagger}{2i} - \frac{b}{\Gamma} \text{Tr} \frac{S + S^\dagger}{2} \tag{6.125}$$

This is a very interesting expression which gives the Seebeck coefficient solely in terms of the scattering matrix S. We can start and investigate the simple case of the half-filling limit (E=0). The expression of the Seebeck coefficient in this limit becomes:

$$S_k = \frac{1}{2} \text{Tr} \frac{S - S^\dagger}{2i} \tag{6.126}$$

It follows that the imaginary part of the scattering matrix trace $\text{Tr} \frac{S - S^\dagger}{2i}$ fulfills the same distribution law as the Seebeck. It is easy to show, the same way we did it for the imaginary part (using the eigenphases and the circular law), that the distribution of the real part of scattering matrix trace $\text{Tr} \frac{S + S^\dagger}{2}$ is the same as the law of S_k. If we look at expression (6.125), we see that the sum of the real and the imaginary part of the scattering matrix trace (up to some factors) has also the same law. In fact, we know that the Gaussian, Lorentzian and Levy law are stable by additivity. How about the distribution of the Seebeck coefficient. Of course, we can notice that in (6.125) the real and the imaginary parts are not independent, but it is a good exercise to use the invariance properties of circular ensemble to see how can this expression be modified and simplified.
We start with the following formula:

$$x = \frac{1}{2} \text{Tr} \frac{S + S^\dagger}{2} \tag{6.127}$$

We know that the distribution of x is $P(x) = -\frac{1}{\pi} \log \frac{|x|}{1 + \sqrt{1 - x^2}}$ We can write this result as follows:

$$P(x) \propto \int \delta(x - \frac{1}{2} \text{Tr} \frac{S + S^\dagger}{2}) d\mu(S) \tag{6.128}$$

Let U be any unitary but fixed matrix. It is well known that the Haar measure $d\mu(S)$ is invariant under the transformation $S \to USU^T$ [89, 102, 88]:

$$d\mu(S) = d\mu(USU^T) \tag{6.129}$$

We apply this property with a matrix $U = e^{i\theta/2}I$. This gives:

$$
\begin{aligned}
P(x) &\propto \int \delta(x - \frac{1}{2}\mathrm{Tr}\frac{e^{i\theta}S + e^{-i\theta}S^\dagger}{2})d\mu(S) \\
&\propto \int \delta(x - \frac{1}{2}[\cos(\theta)\mathrm{Tr}[\frac{S + S^\dagger}{2}] + \sin(\theta)\mathrm{Tr}[\frac{S - S^\dagger}{2}]])d\mu(S)
\end{aligned}
$$

The angle theta is arbitrary. If we choose it as follows:

$$
\begin{aligned}
\cos(\theta) &= -\frac{b}{\sqrt{1 + b^2}} \\
\sin(\theta) &= \frac{1}{\sqrt{1 + b^2}}
\end{aligned}
$$

and remind that the constant b and K, related to the lead self energy, verify:

$$\frac{\Gamma}{2}\sqrt{1 + b^2} = 1$$

we can recover the expression of the Seebeck at an arbitrary energy Eq. (6.125) and claim again:

$$P(S_k) \propto P_{E=0}\left(\left(\frac{\Gamma}{2}\right)^2 S_k\right)$$

This is, by the way, another demonstration of the probability density function of the Seebeck coefficient at arbitrary Fermi energy.

It becomes clear now how important and useful is the expression of the Seebeck coefficient in a matrix form based on the scattering matrix S. The use of the symmetries and the conservation laws of the circular ensembles (in particular the Haar measure) makes the calculation more intuitive and much simpler.

6.7 Time delay matrix

Before we start to introduce the time delay matrix, we would like to show how this matrix comes naturally and have his place in the problem of the probability density function of the Seebeck coefficient. In the previous section, we saw how important is the distribution of $\mathrm{Tr}\frac{S+S^\dagger}{2}$ and $\mathrm{Tr}\frac{S-S^\dagger}{2i}$. In this section, we will not be interested in the distribution of the trace, but in the matrix $\frac{S+S^\dagger}{2}$ itself, or precisely, in the probability density function of its eigenvalues. Let us start, as usual, with the case of the half-filling limit ($E = 0$) at the middle of the band of conduction. The scattering matrix in this limits reads:

$$S = \frac{iH - 1}{iH + 1} \tag{6.130}$$

We want to study the eigenvalues of the matrix Q^+ defined as follows:

$$Q^+ = \frac{S + S^\dagger}{2} \tag{6.131}$$

We will consider the case where the scattering matrix is uniformly distributed according to circular orthogonal ensembles. This implies a Lorentzian distribution for the Hamiltonian H, from the orthogonal ensembles: $H \in \mathcal{LOE}$. The eigenvalues of the matrix Q^+ are noted (τ_1, τ_2). The joint probability density function of these eigenvalues are obtained as follows:

$$
\begin{aligned}
p(\tau_1, \tau_2) &\propto \int \delta(\tau_1 - \frac{1 - E_1^2}{1 + E_1^2})\delta(\tau_2 - \frac{1 - E_2^2}{1 + E_2^2})\frac{|E_1 - E_2|}{[(1 + E_1^2)(1 + E_2^2)]^{3/2}}dE_1dE_2 \\
&\propto \int \sum_{\alpha,\beta\in\{+,-\}} \frac{\delta(E_1 - \alpha f(\tau_1))\delta(E_2 - \beta f(\tau_2))}{[(1 + E_1^2)(1 + E_2^2)]^{-1/2}}\frac{|E_1 - E_2|}{|E_1 E_2|}dE_1dE_2
\end{aligned}
$$

where the function f is defined as follows:

$$f(x) = \sqrt{\frac{1-x}{1+x}}$$

we can notice that :

$$[1 + f(x)^2]^{-1/2} f(x) \propto \sqrt{1-x}.$$

Using this relation after doing the integrals over the delta functions, we can write:

$$p(\tau_1, \tau_2) \quad \propto \quad \frac{1}{\sqrt{1-\tau_1}\sqrt{1-\tau_2}}[|f(\tau_1) - f(\tau_2)| + |f(\tau_1) + f(\tau_2)|] \qquad (6.132)$$

To drop the absolute value, we just highlight that:

$$f(\tau_1) > f(\tau_2) \Leftrightarrow \tau_1 < \tau_2$$

and therefore, we can finally write:

$$p(\tau_1, \tau_2) \quad \propto \quad \frac{\Theta(\tau_2 - \tau_1)}{\sqrt{1+\tau_1}\sqrt{1-\tau_2}} + \frac{\Theta(\tau_1 - \tau_2)}{\sqrt{1+\tau_2}\sqrt{1-\tau_1}} \qquad (6.133)$$

After normalization, we can write the joint probability distribution of the eigenvalues of the real part of the scattering matrix S, noted $Q^+ = \frac{S+S^\dagger}{2}$, in the final form [88]:

$$\boxed{p(\tau_1, \tau_2) = \frac{1}{4\pi}\Big[\frac{\Theta(\tau_2 - \tau_1)}{\sqrt{1+\tau_1}\sqrt{1-\tau_2}} + \frac{\Theta(\tau_1 - \tau_2)}{\sqrt{1+\tau_2}\sqrt{1-\tau_1}}\Big]} \qquad (6.134)$$

Now that we finished, with the real part of the scattering matrix, we continue and look at the imaginary part, noted Q^-:

$$Q^- = \frac{S - S^\dagger}{2i} \qquad (6.135)$$

Of course, we can proceed the same way we did for the real part Q^+, nevertheless, we prefer to do it otherwise in order to use the symmetries and the invariance laws we already discussed. The first step is very simple: we rewrite Q^- as follows:

$$Q^- = -\frac{iS + (iS)^\dagger}{2} = \frac{\tilde{S} + \tilde{S}^\dagger}{2} \qquad (6.136)$$

where we defined $\tilde{S} = -iS$.
Now, since S belongs to COE, $\tilde{S}$ has also the same distribution and therefore belongs to COE. Because of this and the expression form Eq. (6.136), we can apply the results obtained for the real part of the scattering matrix and claim that Q^- eigenvalues fulfill the same distribution as those of Q^+.
In fact, this result can be more generalized if we remind that the Haar measure is invariant under some transformations: For the COE ensemble, the Haar measure is invariant under

$$S \to USU^T$$

that is to say:

$$d\mu(S) = d\mu(USU^T)$$

applying this result, we can claim the general results:

$$P(\frac{S + S^\dagger}{2}) = P(\frac{USU^T + (USU^T)^\dagger}{2})$$

To test these results, in particular the joint probability distribution of the eigenvalues of Q^+, we can compute the probability density function of the variable $x = \frac{\tau_1 - \tau_2}{2}$, or the variable $y = \frac{\tau_1 + \tau_2}{2}$ using $P(\tau_1, \tau_2)$. Indeed we should find for example : $P(x) = -\frac{1}{\pi}\log\frac{|x|}{1+\sqrt{1-x^2}}$. This result is obvious because the variable x as it was defined, is the expression of the Seebeck coefficient at $E = 0$.

6.7.1 Time delay matrix

The time delay matrix was introduced by Eisenbud[107], Wigner[108] and expressed later in a matrix form using the scattering matrix by Smith[109]. The matrix of interest, which is related to the time delay in a quantum system, reads:

$$Q_E = -i\hbar S^\dagger \frac{\partial S}{\partial E}$$

The eigenvalues of this matrix are the proper delay times.
It is interesting to express this matrix in the case of the minimal model we are studying. To do this, our starting equation is, as usual, the scattering matrix form:

$$S = \frac{1 - i\frac{\Gamma}{2}\frac{1}{E - \Delta(E) - H}}{1 + i\frac{\Gamma}{2}\frac{1}{E - \Delta(E) - H}} \tag{6.137}$$

If we put

$$M = \frac{2}{\Gamma}(E - \Delta(E) - H)$$

Then we can write

$$M = i\frac{1 + S}{1 - S}$$

This relation can easily be deduced from the Hamiltonian approach to express the scattering matrix. $\Delta(E) = \frac{E}{2}$ is the lead self energy and $\Gamma = \sqrt{4 - E^2}$ is the broadening element.
It is easy to find the derivative over energy:

$$\partial_E S = i\partial_E M \frac{1}{iM - 1} - \frac{iM + 1}{iM - 1}i\partial_E M \frac{1}{iM - 1} \tag{6.138}$$

$$= -\frac{\Gamma'}{\Gamma}(1 - S^2) - i\frac{1}{2\Gamma}(1 - S)^2 \tag{6.139}$$

After straightforward manipulations, we can express the time delay matrix $Q_E = -iS^\dagger \partial_E S$ ($\hbar = 1$) as follows:

$$Q_E = \frac{\Gamma'}{\Gamma}\frac{S - S^\dagger}{2i} - \frac{1}{\Gamma}\frac{S + S^\dagger}{2} + \frac{1}{\Gamma} \tag{6.140}$$

It is easy to verify that this matrix written this way using solely the scattering matrix is Hermitian.

$$Q_E = Q_E^\dagger$$

This means that the eigenvalues of Q_E are real. This is important since these eigenvalues have the dimension of time.
Notice that this relation can also be written as follows [88]:

$$Q_E = \frac{\Gamma'}{\Gamma}Q^- - \frac{1}{\Gamma}Q^+ + \frac{1}{\Gamma}. \tag{6.141}$$

We want to find the joint probability distribution for the eigenvalues of the time delay matrix. To do this, we shall start with the half filling limit $E = 0$.
In this limit, the time delay matrix reads:

$$Q_E = \frac{1}{2}(1 - Q^+) \tag{6.142}$$

Using the previous result obtained for Q^+, we can write the j.p.d.f for the eigenvalues of Q_E notes $\{\tilde{\tau}_1, \tilde{\tau}_2\}$:

$$\boxed{P(\tilde{\tau}_1, \tilde{\tau}_2) = \frac{1}{2\pi}[\frac{\Theta(\tilde{\tau}_1 - \tilde{\tau}_2)}{\sqrt{\tilde{\tau}_2(1 - \tilde{\tau}_1)}} + \frac{\Theta(\tilde{\tau}_2 - \tilde{\tau}_1)}{\sqrt{\tilde{\tau}_1(1 - \tilde{\tau}_2)}}]} \tag{6.143}$$

This result shows clearly that the proper delay times $\tilde{\tau}_1$ and $\tilde{\tau}_2$ are positive.
The expression of the time delay matrix as a function of the early defined matrices Q^+ and Q^- shows how closely is this matrix related to the Seebeck coefficient. The distribution of the proper times delay is easily generalized to arbitrary Fermi energy using the invariance of the Haar measure defined for circular orthogonal ensembles.
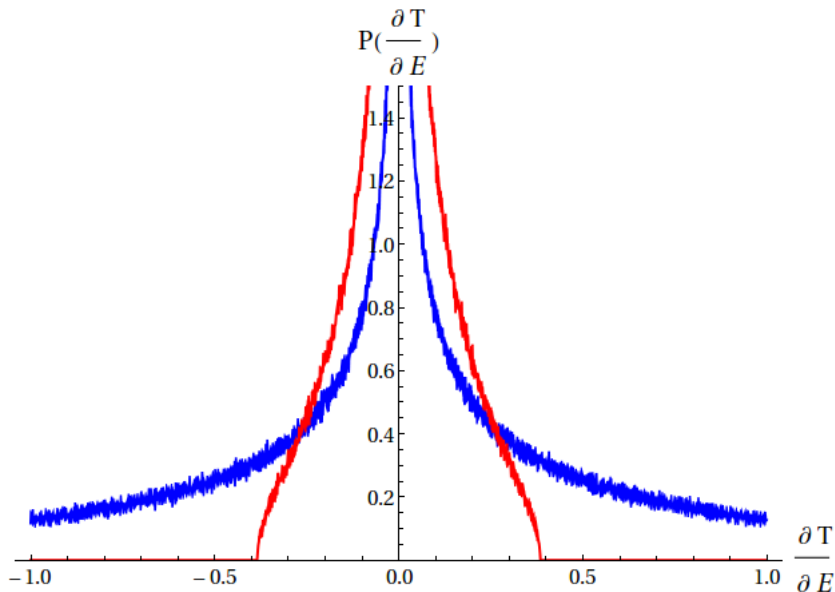
Figure 6.13: Numerical simulation of the probability density function of the transmission derivative of a chaotic cavity at two different Fermi energies: $E = 0$(Red curve) and $E = -1.8$ (Blue curve).

6.8   Distribution of the Transmission derivative

We investigated the transmission probability density function and found that the chaotic cavity with a scattering matrix distributed according to circular orthogonal ensemble has the following law; $P(T) = \frac{1}{2\sqrt{T}}$. This means that the system is most of the time, nearly closed. We later looked at the distribution of the Seebeck coefficient and found the following law:

$$P(S_k) = -\frac{a}{\pi} \log \frac{|aS_k|}{1 + \sqrt{1 - a^2 S_k^2}}$$

with $a = (\frac{\Gamma}{2})^2$.

This law, shows that the distribution is singular at the origin. It has also another important implication: The Seebeck is bounded and can not take values outside the interval $[-(\frac{\Gamma}{2})^2, (\frac{\Gamma}{2})^2]$. This is a very important result since it highlights an interesting question: If the system can have all the possible transmission values between $[0, 1]$, and that the Seebeck definition $S_k \propto \frac{\partial T}{\partial E}/T$ implies that for small value of the transmission, the Seebeck should be very big and therefore not bounded, why do we obtain a bounded Seebeck?

Indeed the implication of this remark is that the transmission and its derivative are not independent. The same thing for the transmission T and the Seebeck S_k. In a mathematical form this gives a distribution $P(S_k, T)$ which do not factorize, and therefore, the distribution of the transmission derivative should be searched the following way:

$$P(x = \frac{\partial T}{\partial E}) = \int P(S_k, T)\delta(x - TS_k)dT dS_k \tag{6.144}$$

Here we defined $\frac{\partial T}{\partial E} = TS_k$ where we dropped the factors, irrelevant for the statistics, which exist in the correct definition.

Since we do not know the distribution $P(S_k, T)$, we will use the Lorentzian distribution of the Hamiltonian of the system and the expressions of S_k and T in terms of the levels E_1, E_2. This distribution is found numerically, using the algorithms generating circular and Lorentzian ensembles. Fig. (6.8) shows the result of numerical simulation, on the minimal model, of the probability density function of the transmission derivative of a chaotic cavity. The simulation shows that the probability to have large derivative of the transmission is small and sometimes exactly zero like the case of systems with a Fermi energy near to the half-filling limit (E=0). This means that the profile of the transmission do not exhibit sharp resonances and therefore expected to be smooth in general.

(b)

6.9   Decimation procedure implications

Here, in this section, we investigate the implication of the decimation renormalization procedure[101][104] and try to understand the simplification it can bring to the problem of quantum transport through a chaotic cavity. The first important thing it allowed us to achieve is to simplify the cavity and replace it with a minimal model, without approximation or loss of generality. This simplification allowed us to do analytical calculations and to make the numerical simulation very easy and very fast since we manipulate 2×2 matrices.

First, Let us recall what do we mean by the decimation renormalization procedure: We can take away a part of a system and replace it by its effect on the other parts it was connected to. This effect is contained in a quantity we call: Self energy.

The self energy of a decimated part of finite size is real whereas infinite size parts (like the leads) have a complex self energy. The self energy is related to the Greens function $\frac{1}{E-H_A}$, H_A is the Hamiltonian of the part we want to take away. This form, makes the Lorentzian ensembles special since they have the property saying: If A is a Lorentzian matrix $\frac{1}{A}$ is also Lorentzian [100][89]. The reader can find in section (6.5.5) how do we apply the decimation-renormalization procedure to go from the original model of chaotic cavity (large number of sites) to the minimal model (2 sites).

We start here with the minimal model: we assume the Hamiltonian of the 2×2 system(red sites in Fig. (6.9)) Lorentzian and the leads perfect and uniform (blue sites in Fig. (6.9)). We suppose that we don't know the self energy expression of the leads and try to find it using a procedure based on the decimation-renormalization. The Hamiltonian of the scattering system in Fig. (6.9) should have a Lorentzian distribution with a center $\epsilon = E - \Delta(E)$ and a width $\lambda = \frac{\Gamma}{2}$ in order to get a scattering matrix from the circular ensembles [86, 87, 88].

$$H \in \mathcal{L}OE(\epsilon = E - \Delta(E), \lambda = \frac{\Gamma}{2})$$

$\Delta(E)$, $-\Gamma/2$ are, respectively, the real and the imaginary part of self energy we want to obtain. [22] We do again the decimation procedure on this system: we take it away and renormalize the two neighboring sites. After normalization, we obtain a new system composed of the two sites with a Hamiltonian $\tilde{H} = \frac{1}{E-H}$ (the coupling matrices are identity matrices). It is easy to show, using the properties of the Lorentzian ensembles(section 6.5.2 or references[100][89]), that this new Hamiltonian is Lorentzian:

$$\begin{aligned}
H \in \mathcal{L}OE(E - \Delta(E), \Gamma/2) &\Rightarrow E - H \in \mathcal{L}OE(\Delta(E), \Gamma/2) \\
&\Rightarrow \tilde{H} \in \mathcal{L}OE(\frac{\Delta(E)}{(\Delta(E))^2 + (\Gamma/2)^2}, \frac{\Gamma/2}{(\Delta(E))^2 + (\Gamma/2)^2})
\end{aligned}$$

The decimation-renormalization procedure simplifies the degree of freedom but do not change the transport coefficient. This means that the new system we obtain should have the same scattering matrix with the same statistics: COE. But since the new Hamiltonian, is also a 2×2 matrix, it should have the same statistics as the one before(Because the S matrix is still uniformly distributed. [23]). Because, of this we can claim the following result:

$$\begin{cases} E - \Delta(E) &= \frac{\Delta(E)}{(\Delta(E))^2 + (\Gamma/2)^2} \\ \Gamma/2 &= \frac{\Gamma/2}{(\Delta(E))^2 + (\Gamma/2)^2} \end{cases}$$

---

22. I remind that we suppose here that we don't know the form of the self energy, although we can get is with several different methods

23. $S \in COE \Leftrightarrow \tilde{H} \in \mathcal{L}OE(E - \Delta(E), \Gamma/2)$

The solution of this system is

$$\begin{cases} \Delta(E) & = & E/2 \\ \Gamma/2 & = & \sqrt{1 - (E/2)^2} \end{cases}$$

which means that the self energy is :

$$\Sigma = \frac{E}{2} - i\sqrt{1 - \left(\frac{E}{2}\right)^2}$$

We obtained the self energy of a uniform 1D lead, as a consequence of the decimation-renormalization procedure. It seems that this procedure implies more than a simple simplification of the cavity and can even provide some interesting results. To give a better strong example, we try to study the quantum transport of electrons through two chaotic cavities in series as shown in Fig. (6.14). We first simplify the system, by changing the two cavities with two systems of 2 sites, using the procedure of decimation-renormalization. The length between these two minimal models is noted L. Then, we do again the decimation-renormalization procedure on one of the two systems. Since, after this procedure, the new Hamiltonian is composed of the two neighboring sites, the length between the two new scattering systems becomes shorter: $L - 1$. It is important to understand that the transport coefficients do not change after the decimation procedure and that decimating-renormalizing the 2×2 Hamiltonian gives a new 2×2 Hamiltonian with the same Lorentzian distribution [24]. So, we can do this procedure again and again, each time the length between the two scattering systems becomes shorter. We can claim now the following not obvious result: The probability density function of the transmission of two chaotic cavities whose scattering matrix of one of them is COE, is length independent:

$$\frac{dP_l}{dl}(T) = 0 \tag{6.145}$$

These interesting results do not necessitate calculations: Simple treatment with the decimation-renormalization procedure is enough.

Summary: In this chapter, we were interested in the statistics of the Seebeck coefficient of a chaotic cavity. Starting from a lattice model of a cavity with a Hamiltonian distributed according to Gaussian orthogonal ensembles, we proved that for a big number of degrees of freedom, this distribution is equivalent to a Lorentzian distribution. This last, has the interesting property of being stable by inversion and moreover, each submatrix of it is still Lorentzian. These properties allow to do a decimation -renormalization procedure to decrease the degrees of freedom of the cavity. The result of this procedure is a simple model exactly solvable. The analytical result giving the distribution of the Seebeck coefficient of the chaotic cavity is verified by numerical simulations. The form of the Seebeck distribution shows a singularity at the origin and bounds delimiting the values of the Seebeck in a range proportional to the square of the coupling parameter Γ. Different approaches based on the scattering matrix strengthen this result and make the numerical simulation easier since they use circular ensembles(easily generated). This work exhibits the powerful tool of decimation-renormalization procedure in the theory of random matrix theory. As an application, we showed that the distributions of the transmission or the Seebeck coefficient of two cavities in series, with appropriate distribution width and center, are independent of the length between the two chaotic cavities.

---

24. This only true if $H \in \mathcal{L}OE(\epsilon = E - \Delta(E), \lambda = \Gamma/2)$
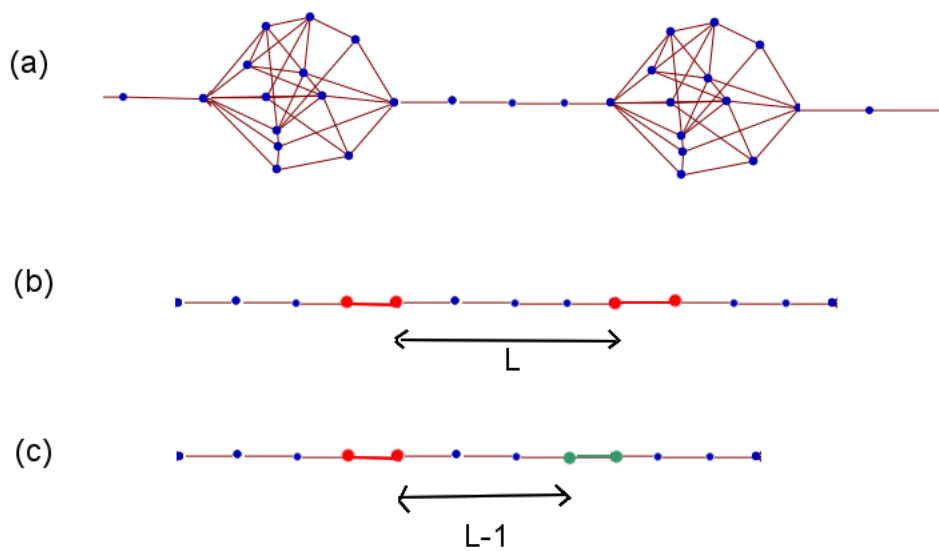
Figure 6.14: Decimation-renormalization procedure on a system composed of two chaotic cavities in series: First step, from (a) to (b), it replaces the two cavities with two minimal models distributed according to $\mathcal{L}OE$. The distance between the two scattering systems is noted L. The second step is to do again the decimation procedure on one of the two minimal systems, which shortens the length between the new scattering systems $(L-1)$.
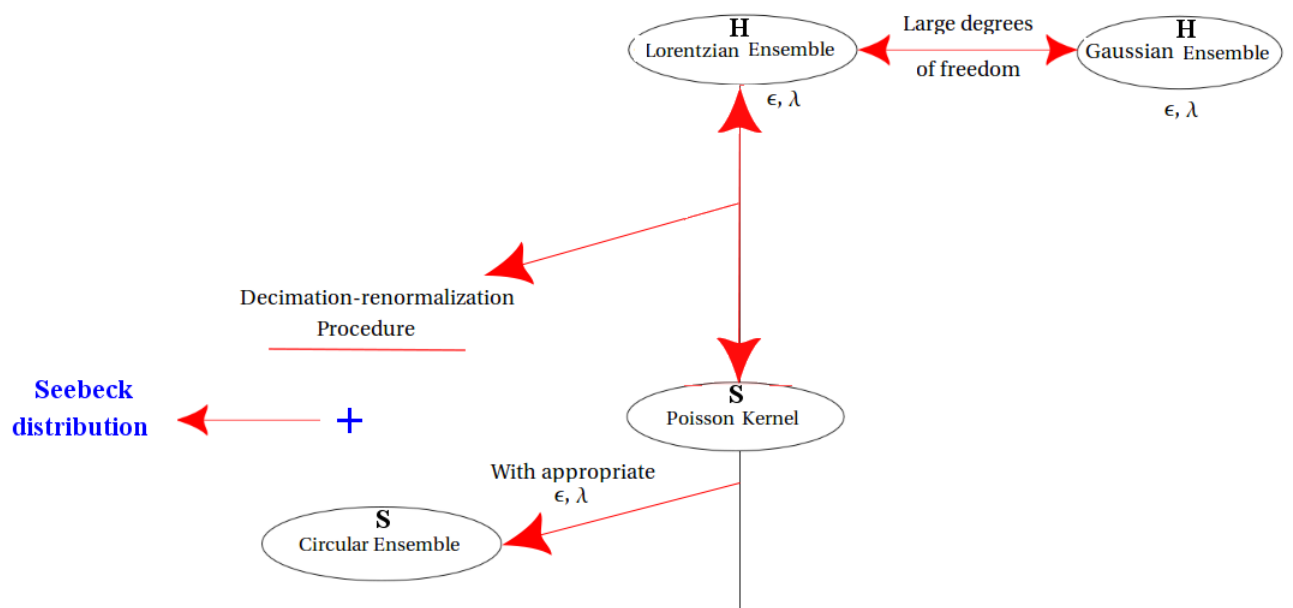
Figure 6.15: At large degrees of freedom the Gaussian and Lorentzian ensembles are equivalent. This kind of Hamiltonian distribution implies a scattering matrix S distributed , in general, according to Poisson Kernel. If the width and the center of the Lorentzian is appropriate (compatibles with the self energy of the lead), S becomes uniformly distributed according to circular ensembles. The Lorentzian distribution helps to lower the large degrees of freedom by means of the decimating-renormalization procedure

Appendix A

Hamiltonian of a slice and perfect leads

The perfect lead is a center piece of a lot of quantum transport problems. Its Hamiltonian representation in the Tight-binding picture is essential to implement numerical simulations and to understand the electronic transport in terms of the eigenmodes and channels. Naturally, the 1D chain which is the generating piece of uniform perfect leads is the key to explain their characteristics. In the following paragraphs, we try to study in details the Hamiltonian of 1D chain.
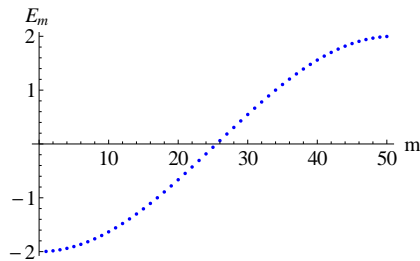
Hamiltonian of 1D chain

Figure A.1: Eigenvalues of 1D chain. The size is chosen N=5O sites and the parameters $\epsilon = 0$ and $t = 1$. All the eigenvalues are non degenerate

The Hamiltonian of a 1D chain in the Tight-binding representation can be written using the sites states $|i\rangle$ as follows:

$$H = \sum_i \epsilon_i |i\rangle\langle i| - \sum_i t_i[|i+1\rangle\langle i| + |i\rangle\langle i+1|] \tag{A.1}$$

Where the ϵ_i represents the potential on the site i and the t_i is the hoping term from and to the site i. This is the general 1D chain with general disorder (on the sites and in the hoping factors). In the absence of disorder (this is the case of perfect leads), we have $\epsilon_i = \epsilon$ and $t_i = t$ for all the sites i. Now, since we will be interested in the eigenvalues and eigenvectors of this Hamiltonian, it may be interesting to switch to a matrix representation. After all, the numerical implementation will use the matrix form. Because of the nearest neighbor approximation in the definition A.1, the

Hamiltonian is a sparse tridiagonal matrix:

$$H = \begin{pmatrix} \epsilon & -t & 0 & \cdots & 0 \\ -t & \epsilon & -t & & \vdots \\ 0 & -t & \ddots & \ddots & 0 \\ \vdots & & \ddots & & -t \\ 0 & \cdots & 0 & -t & \epsilon \end{pmatrix}$$

This $N \times N$ matrix (N is the number of sites) is real symmetric, thus it is diagonalizable by an orthogonal matrix P ($P = P^T$). Its eigenvalues are real (The matrix H is Hermitian) and non degenerate [29][31].

$$E_m = \epsilon - 2t \cos(\frac{m\pi}{N+1}) \tag{A.2}$$

The corresponding eigenfunction is a vector whose elements are:

$$V_i = \sqrt{\frac{2}{N+1}} \sin(\frac{m\pi}{N+1} i) \tag{A.3}$$

This set of eigenpair correspond to 1D chain with hard wall boundary conditions. Thus, the results obtained with cyclic boundary conditions (CBC) are quiet similar[30]. In fact, the Hamiltonian with the CBC is:

$$H = \begin{pmatrix} \epsilon & -t & 0 & \cdots & -t \\ -t & \epsilon & -t & & \vdots \\ 0 & -t & \ddots & \ddots & 0 \\ \vdots & & \ddots & & -t \\ -t & \cdots & 0 & -t & \epsilon \end{pmatrix}$$

Which means that the elements H_{1N} and H_{N1} are not zero anymore because the the first site and the last one are connected [1]. We do have $H_{1N} = H_{N1} = -t$ and the eigenvalues which follow are:

$$E_m = \epsilon - 2t \cos(\frac{2\pi m}{N}) \tag{A.4}$$

And the same way, the eigenvectors elements become:

$$V_i = \sqrt{\frac{2}{N}} \sin(\frac{2\pi m}{N} i) \tag{A.5}$$

The study of the eigenvalues and eigenvectors of a chain Hamiltonian is interesting to understand the conducting channels in a structure based on 1D-slices (Like a 2D perfect lead). Nevertheless, quantum transport relations usually use the Green's function as propagators, and so do the density of states. For this reason, it is very useful to know the different elements of the Green matrix. They are easily obtained in the case of a 1D-chain using the recursive procedure based on the Dyson equation: We start from the case of a unique site and add one by one to construct the whole chain, in each step the Green's function is updated. The results for this procedure, are given, in the case of a finite chain of N sites, as follows:

$$G_{11} = -\frac{\sin(N\theta)}{t \sin[(N+1)\theta]} \tag{A.6}$$

$$G_{1N} = -\frac{\sin(\theta)}{t \sin[(N+1)\theta]} \tag{A.7}$$

Where the angle θ is defined by the Fermi energy as follows:

$$\cos(\theta) = \frac{E - \epsilon}{-2t}. \tag{A.8}$$

---

1. In This case it is better to call it a 1D ring rather than 1D chain

We can also find the Green's functions for a semi-infinite chain extending from 1 to ∞:

$$G_{11} = -\frac{e^{i\theta}}{t} \tag{A.9}$$

$$G_{1l} = -\frac{e^{il\theta}}{t} \tag{A.10}$$

$$G_{ll} = -\frac{e^{il\theta}}{t}\frac{\sin(l\theta)}{\sin(\theta)} \tag{A.11}$$

The starting point to obtain these relations is the retarded propagator between site l and j of an infinite line. Then, the semi-infinite chain is obtained by cutting one link in this infinite line and then use the Dyson equation to get the quantities related to the semi-infinite chain. The propagator of the infinite line reads:

$$G_{lj} = -\frac{e^{i|l-j|\theta}}{2t\sin(\theta)} \tag{A.12}$$

We notice that the quantities given so far are complex oscillating function. This is because they correspond to propagating modes. When the Fermi energy is outside the band of conduction, the modes become become evanescent and the corresponding propagators are easily obtained by substituting $i\alpha$ for θ in the previous relations.

It is interesting to know that the case of a 2D semi-infinite lead is quite easy to study since the transverse mode do not mix in a lead of uniform width. Therefore, we need only to dress the quantities obtained in the case of 1D-lead with the transverse wave functions. Of course, for a given Fermi energy, the energy left for longitudinal motion is not the same for each mode and will depend on the transverse kinetic energy of the subband.

Appendix B

Green's function recursive procedure

In this appendix, I try to explain in details how do we use the formalism of Green's function and the recursive procedure to construct the scattering region when connected to semi-infinite leads. I prefer to start by reminding some basic but important rules:

- In each system, we can take off a part and replace it by its self energy. This self energy is added to the surface it is connected to.
- The self energy of an infinite part is in general complex whereas a finite part has a real self energy.
- The Green's function of a system to which we attached a part is calculated using the effective Hamiltonian: $G = \frac{1}{E - H_{eff}}$ and $H_{eff} = H_0 + \Sigma$.

We start computing the Green's function needed to express the conductance as follows: The first slide is connected to the left lead. Therefore, the Green's function reads:

$$G_{11} = \frac{1}{E - H_1 - \Sigma_l} \tag{B.1}$$

We attach now the second slide to the first one and compute the new surface Green's function G_{22}:

$$G_{22} = \frac{1}{E - H_2 - V_{21}G_{11}V_{12}}$$

We notice that the perfect lead plus the first slide act like a self energy on the second slide(that is why $V_{21}G_{11}V_{12}$ is added to the Hamiltonian H_2 The Surface Green's function on the ith surface is
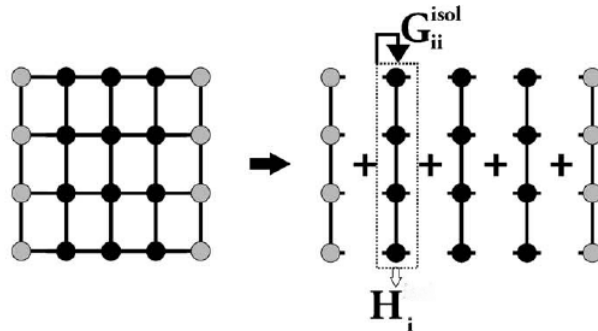

Figure B.1: The recursive procedure to get the Green's function of the system.The scattering region is constructed slide by slide. The gray color refers to the effect of the semi-infinite leads on the system via their self energy.

now straightforward [1]:

$$G_{ii} = \frac{1}{E - H_i - V_{i,i-1}G_{i-1,i-1}V_{i-1,i}} \tag{B.2}$$

we continue this procedure the same way until the last slide where we should not forget to take into account the right lead via its self energy Σ_r. The Green's function reads:

$$G_{nn} = \frac{1}{E - H_n - V_{n,n-1}G_{n-1,n-1}V_{n-1,n} - \Sigma_r} \tag{B.3}$$

In the Landauer-Buttiker formula expressing the quantum conductance, we need the submatrix G_{1n}:

$$\mathcal{G}(E) = \frac{2e^2}{h}\text{Tr}[\Gamma_l G_{1n}\Gamma_r G_{1n}^\dagger] \tag{B.4}$$

The left and right broadeninig matrices are defined as follows: $\Gamma_{l,r} = i(\Sigma_{l,r} - \Sigma_{l,r}^\dagger)$.
The important submatrix G_{1n} is obtained the following way:

$$G_{1n} = \prod_{i=1}^{i=n} G_{ii}V_{i,i+1} \tag{B.5}$$

Where by convention, the matrix $V_{n,n+1} = I$ (the identity matrix).

---

1. G_{ii} is the submatrix containing all the Green's function elements between two sites of the ith slide

Appendix C

The self Energy of a semi-infinite leads

This thesis and in general the studies on quantum transport of electrons through constrictions owe too much to the contraction of the semi-infinite leads to the self energies. In deed, these open systems are defined with an infinite size Hamiltonian, and thus the contraction of the leads using the concept of self energies reduces this size and defines an effective Hamiltonian which allows a simpler manipulation and an easy extraction of the resonant states. In this appendix, I will provide two simple and interesting ways to get this self energy for the two most studies cases : 1D and 2D. The first method is based on the concept of Green's function and how do we obtain the new Green's function elements of two parts after they became connected. I recall that the self energy is related to the surface Greens function as follows:

$$\Sigma = \tau^\dagger G \tau \tag{C.1}$$

Where the τ matrix defines how the lead is connected to the leads.
From this, we notice that if the τ matrix is equal to the identity matrix, then the self energy will be identified to the surface Green's function. that is why we need only to study * this case, from which we deduce the general case just by multiplying the final results with the coupling matrix as shown in C.1.
When we add a new perfect slice to a 2D semi-infinite perfect lead, we obtain again the same semi-infinite lead! using this property when expressing the new self energy using [] we can write the following closed equation:

$$\Sigma = \frac{1}{E - H_0 - \Sigma} \tag{C.2}$$

It can also be written in a different way:

$$-\Sigma^2 + (E - H_0)\Sigma = 1 \tag{C.3}$$

Now, let us note (ρ_k, X_k) the eigenpairs of H. This means

$$H X_k = \rho_k X_k \tag{C.4}$$

If we note the eigenpairs of Σ, (λ_k, Y_k) and apply Eq. (C.3) to an eigenvector Y_k we get:

$$-\Sigma^2 Y_k + (E - H_0)\Sigma Y_k = Y_k \tag{C.5}$$

This equation becomes:

$$H_0 Y_k = -\frac{\lambda_k^2 - E\lambda_k + 1}{\lambda_k} Y_k \tag{C.6}$$

This means that Y_k is also an eigenvector of H_0 i.e., Σ and H_0 have the same set of eigenvectors with different eigenvalues. From Eq. (C.6), we can deduce the relation between the eigenvalues of Σ and H_0 which reads:

$$\lambda_k^2 - (E - \rho_k)\lambda_k + 1 = 0 \tag{C.7}$$

This equation of second order gives twice the number of solutions we want. In fact, this relation is valid for the retarded and advanced self energies. It is therefore normal to find double solutions. To ensure the convergence of the physical quantities and for causal considerations, we need to keep the for the retarded self energy Σ^r the solutions with negative imaginary part when they are complex and smaller than one when they are real. The eigenvalues λ_k of the retarded self energy read:

$$
\lambda_k = \begin{cases} \frac{(E-\rho_k)}{2} - i\sqrt{1 - (\frac{E-\rho_k}{2})^2} & |E - \rho_k| < 2 \\[2mm] \frac{(E-\rho_k)}{2} - s\sqrt{(\frac{E-\rho_k}{2})^2 - 1} & |E - \rho_k| \geq 2 \end{cases}
$$

$s = \text{sign}(E - \rho_k)$ The self energy is therefore given by the eigenvectors and the eigenvalues as follows:

$$
\Sigma(p, q) = \sum_{k=1}^{N} Y_k(p) \lambda_k Y_k(q) \tag{C.8}
$$

This formula can be applied for any uniform lead with any potential in the transverse direction.

Appendix D

Fresnel inegral

One way, which is the most used in physics, to define the Fresnel integrals is:

$$f(u) = C(u) + iS(i) = \int_0^u e^{i\frac{\pi}{2}t^2} dt \tag{D.1}$$

where we defined:

$$C(u) = \int_0^u \cos(\frac{\pi}{2}t^2)dt \tag{D.2}$$

and

$$S(u) = \int_0^u \sin(\frac{\pi}{2}t^2)dt \tag{D.3}$$

the two functions are both even.
The expansion of the two functions $C(u)$ and $S(u)$ for $u \gg 1$ gives:

$$C(u) \sim \frac{1}{2} + \frac{\cos(\frac{\pi}{2}u^2)}{\pi u} \tag{D.4}$$

$$S(u) \sim \frac{1}{2} - \frac{\sin(\frac{\pi}{2}u^2)}{\pi u} \tag{D.5}$$

this expansion helps us to give and understand the following result:

$$\int_a^b e^{i\frac{\pi}{2}t^2} dt \sim \begin{cases} (1+i) + O(\frac{1}{s}) & ab < 0 \\ 0 + O(\frac{1}{s}) & ab > 0 \end{cases} \tag{D.6}$$

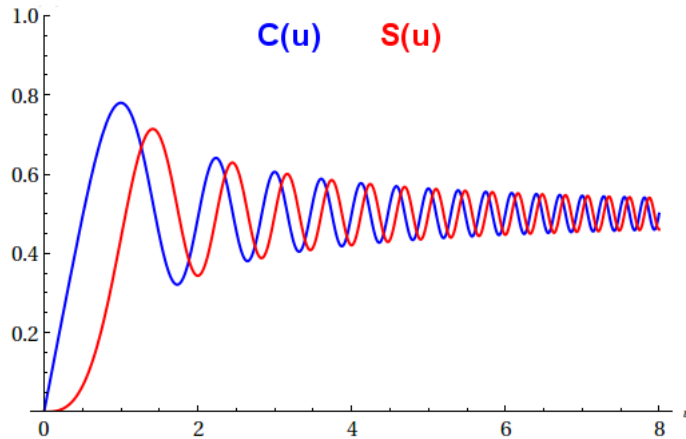Where we defined $s = min(|a|, |b|)$.

Figure D.1: Plot of the Fresnel integrals $C(u)$ (blue curve) and $S(u)$ (red curve).

Appendix E

The wave number expressions

To express the Green's function in a form using simple quantities, it is important to know that the Fermi wave number k_F can be expressed in different ways:

$$
k_F = \begin{cases}
\frac{M\pi}{N+1} & (a) \\
\sqrt{E+4} & (b) \\
\pi - \arccos(\frac{E+2}{2}) & (c) \\
\sqrt{1 - (\frac{E+2}{2})^2} & (d)
\end{cases}
\tag{E.1}
$$

Expression (a) is easy to understand: Since the wavenumber is quantized, (multiple of $\frac{\pi}{N+1}$) and that the highest conducting mode, M, corresponds to the Fermi wavenumber, it comes immediately that $k_F = \frac{M\pi}{N+1}$.

Expression (b) also is straightforward: In the continuum, the dispersion relation is simply $E = k_F^2$ ($t_h = \frac{\hbar^2}{2ma^2} = 1$). The shift of the bottom of the conduction band to -4 makes that in our treatment we should write $E + 4 = k_F^2$.

To get expression (c), we start by reminding that θ_m verifies:

$$
\cos(\theta_m) = \frac{E}{2} + \cos(\frac{m\pi}{N+1})
\tag{E.2}
$$

So, for a conducting channel, θ_m should be real which means:

$$
-1 \leq \frac{E}{2} + \cos(\frac{m\pi}{N+1}) \leq 1
\tag{E.3}
$$

At low energy, near the bottom of the conduction band ,we should verify the left side of the inequality (the right is always verified) which becomes, for the highest conducting mode, M,an equality:

$$
\frac{E}{2} + \cos(\frac{M\pi}{N+1}) = -1 \Rightarrow k_F = \frac{M\pi}{N+1} = \pi - \arccos(\frac{E+2}{2}).
\tag{E.4}
$$

For expression (d), an easy expansion near the bottom of the conduction band ($E = -4$) gives:

$$
\sqrt{1 - (\frac{E+2}{2})^2} = \sqrt{\frac{-E}{4}(E+4)} \sim \sqrt{E+4}
\tag{E.5}
$$

These different formulas, expressing the Fermi wavenumber, can be considered as a concrete way to define the continuum limit: The region of energies giving very close curves with the three different formulas (b), (c) and (d) Eq. (E.1) is the continuum limit (See Fig. (E.1)).
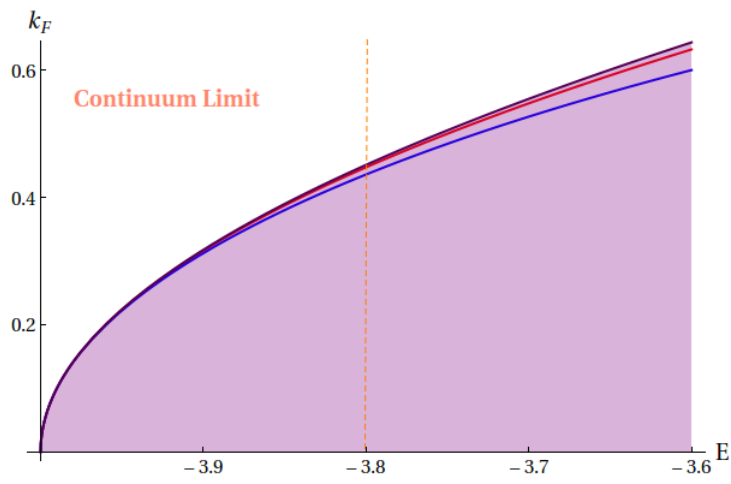
Figure E.1: different formulas of k_F near the bottom of the conduction band. Formula (b): Red curve, formula (c): Purple curve, formula (d): Blue curve. The continuum limit is the region of energies where the three curves are very close.

Appendix F

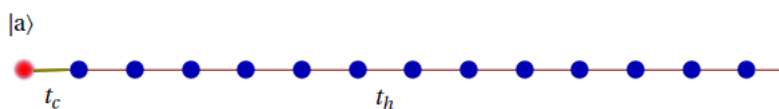# Bloch and Wannier representations of a one dimensional semi-infinite lead

Figure F.1: Schematic of an impurity site $|a\rangle$ connected to a semi-infinite 1D lead. The coupling between the impurity site and the lead is t_c. The hopping term in the lead is t_h.

    Here in this chapter, we want to show how do we obtain the Hamiltonian form and the coupling matrix W we used in the chapter dealing with random matrix theory. Let us start with the simple example of one impurity site connected to one semi-infinite perfect 1D lead. The Hamiltonian of this system in a tight binding form using the localized Wannier states on a lattice $|n\rangle$ reads:

$$H = \underbrace{-t_h \sum_{n=1}^{\infty}(|n\rangle\langle n+1| + |n+1\rangle\langle n|)}_{\text{the lead}} + \underbrace{E_a|a\rangle\langle a|}_{\text{the impurity site}} \quad \underbrace{-t_c(|a\rangle\langle 1| + |1\rangle\langle a|)}_{\text{The coupling}} \tag{F.1}$$

$|a\rangle$ is the Wannier state on the impurity site with energy E_a. t_h is the hopping term in the lead and t_c is the coupling between the impurity site and the lead. We want now to write down this Hamiltonian using the block states $|k\rangle$ defined as follows:

$$|k\rangle = \sqrt{\frac{2}{\pi}}\sum_{n=1}^{\infty}\sin(nk)|n\rangle \tag{F.2}$$

the inverse relation is also easy to obtain:

$$|n\rangle = \sqrt{\frac{2}{\pi}}\int_0^\pi dk\,\sin(nk)|k\rangle \tag{F.3}$$

$n = 1, 2, 3 \ldots$
To go from one representation to another, we need to remind that the localized Wannier stated are orthonormal: $\langle n|m\rangle = \delta_{nm}$. We may also need the following useful formula:

$$\int_0^\pi dk\,\sin(nk)\sin(mk) = \frac{\pi}{2}\delta_{nm} \tag{F.4}$$

We can now write down the Hamiltonian in the Bloch representation. We first start with the lead:

$$\int dk E(k)|k\rangle\langle k| = -t_h\sum_{n=1}^{\infty}(|n\rangle\langle n+1| + |n+1\rangle\langle n|) \tag{F.5}$$

this transformation gives the energy dispersion $E(k)$:

$$E(k) = -2t_h \cos(k) \tag{F.6}$$

This also defines the conduction band since the lead is considered as the electrons reservoirs.

$$E \in [-2t_h, 2th]$$

For the coupling Hamiltonian, we obtain:

$$-t_c(|a\rangle\langle 1| + |1\rangle\langle a|) = \int dk[v(k)|a\rangle\langle k| + v^*(k)|k\rangle\langle a|] \tag{F.7}$$

$v(k) = -\sqrt{\frac{2}{\pi}}t_c \sin(k)$. With all this, we can write down the Hamiltonian in the Bloch representation as follows:

$$H = E_a|a\rangle\langle a| + \int dk E(k)|k\rangle\langle k| + \int dk[v(k)|a\rangle\langle k| + v^*(k)|k\rangle\langle a|] \tag{F.8}$$

We can deduce from this form the self energy of the lead. First we need the density of states:

$$\rho(E) = \left(\frac{\partial E}{\partial k}\right)^{-1} \tag{F.9}$$

We define also: $V(E) = \rho(E)|v(E)|^2$. The self energy is therefore obtained as follows: The imaginary part of the retarded self energy is $\Im\Sigma = -\pi V(E)$ and the real part is obtained by the Kramers-Kronig relation:

$$\Re\Sigma = P \int \frac{V(E')}{E - E'} dE'$$

Finally, we can write:

$$\Sigma^r(E) = \frac{E}{2} - i\sqrt{1 - \left(\frac{E}{2}\right)^2} \tag{F.10}$$

Bibliography

[1] A. Topinka et al , Coherent branched flow in a two-dimensional electron gas, Nature London 410,183 2001.

[2] H. Van Houten C. Beenakker, Quantum Point Contact Physics today 1996.

[3] T. R. Lenka, A. K. Panda Characteristics Study of 2DEG Transport Properties of Al-GaN/GaN and AlGaAs/GaAs-based HEMT.

[4] T. J. Thornton, M. Pepper, H. Ahmed, D. Andrews, G. J. Davies, Phys. Rev. Lett. 56, 1198 (1986)

[5] H. Z. Zheng, H. P. Wei, D. C. Tsui, G. Weimann, Phys. Rev. B 34, 5635 (1986).

[6] L. I. Glazman, G. B. Lesovik, D. E. Khmel'nitskii, R. I. Shekhter, JETP Lett. 48, 238 (1988)

[7] C. W. J. Beenakker, H. van Houten, Sol. State Phys. 44, 1 (1991).

[8] S. M. Cronenwett et al, Phys. Rev. Lett. 88, 226805 (2002)

[9] Y.Meir, J. Phys.: Condens. Matter 20 (2008) 164208 (4pp)

[10] D. K. Ferry, S. M. Goodnick, Transport in nanostructures

[11] M. Buttiker, Quantized transmission of a saddle-point constriction, Phys. Rev. B 41, 7906-7909 (1990)

[12] M. S. Chung,J.S. Choi, Ji Mo Park, K. S. Lee, Shape effects of the conductance of a quantum ballistic constriction in a two-dimensional electron gaz, Material science and engineering, B35(1995) 440-445

[13] A. Szafer, A. D. Stone, Phys. Rev. Lett. 62, 300–303 (1989)

[14] Hackens B, Martins F, Ouisse T, Sellier H, Bollaert S, Wallart X, Cappy A, Chevrier J, Bayot V and Huant S 2006 Nat. Phys

[15] Ihn T, Rychen J, Cilento T, Held R, Ensslin K, Wegscheider W and Bichler M 2002 Physica E 12 691

[16] Schnez S, Guettinger J, Huefner M, Stampfer C, Ensslin K and Ihn T 2010 Phys. Rev. B 82, 165445 (2010).

[17] B. J. LeRoy thesis,Imaging Coherent Electron Flow Through Semiconductor Nanostructures

[18] M. P. Jura et al, Electron interferometer formed with a scanning probe tip and quantum point contact, PRB 80,041303 (2009)

[19] L. Burgi et al, Quantum coherence and lifetimes of surface-state electrons. Journal of Electron Spectroscopy and Related Phenomena vol. 109, num. 1-2, p. 33-49

[20] Y. Meir, N. S. Wingreen, Landauer Formula for the Current through an Interacting Electron Region, Phys. Rev. Lett. 68, 2512-2515 (1992)

[21] D. S. Fisher, P. A. Lee, Relation between conductivity and transmission matrix, Phys. Rev. B 23, 6851-6854 (1981)

[22] K. A. Muttalib, J. L. Pichard and A. D. Stone Random matrix theory and universal statistics for disordered quantum conductors. Phys. Rev. Lett. 59, 2475–2478 (1987)

[23] P. A. Mello, P. Pereyra and N. Kumar, Ann. Phys. (N.Y.) 181, 290 (1988).

[24] Georgo Metalidis thesis , Electronic Transport in Mesoscopic System

[25] K. Kazymyrenko and X. Waintal, Knitting algorithm for calculating Green functions in quantum systems, Phys. Rev. B 77, 115119 (2008)

[26] P. Darancet, V. Olevano, D. Mayou, Phys. Rev. B 81, 155422 (2010)

[27] Y. Asada, Numerical calculation of the Landauer conductance through an interacting electron system in the Hartree-Fock approximation, arXiv:cond-mat/0603147v1

[28] K. Sasada, N. Hatano, Calculation of the Self-Energy of Open Quantum Systems, J. Phys. Soc. Jpn. 77 (2008) 025003

[29] S. L. Zhu, Z.D. Wang, L. Hu, J. Appl. Phys. 91, 6545 (2002)

[30] P. Markos, J. Phys. C: Solid State Phys. 21 L317

[31] A. Siber, American Journal of Physics (2006) Volume: 74, Issue: 8, Pages: 692-698

[32] Scot Elmer James Shaw, Propagation in Smooth Random Potentials, Phd thesis

[33] M. A. Topinka et al, Imaging Coherent Electron Flow from a Quantum Point Contact, Science289, 2323, 29 September 2000.

[34] M. G. Pala et al, Scanning gate microscopy of quantum ring: effects of an external magnetic field and of charged defects. Nanotechnology 20 (2009) 264021.

[35] M. G. Palla et al, Local density of states in mesoscopic samples from scanning gate microscopy, Physical Review B 77, 125310 (2008).

[36] A. Bachtold et al, Scanned Probe Microscopy of Electronic Transport in Carbon Nanotubes, Physical Review Letters. 84, 6082-6085(2000).

[37] M. A. Topinka, Imaging coherent electron wave flow through 2D electron gas nanostructures, Phd Thesis, Harvard university.

[38] B. J. Leroy et al, Imaging Electron Interferometer, PRL 94, 126801, (2005).

[39] B. J. Leroy et al, Imaging coherent wave flow in a two-dimensional electron gas, Physica E18 (2003).

[40] M. A. Eriksson et al, Cryogenic scan probe characterization of semiconductor nanostructures. Applied Physics Letters 69, 671 (1996).

[41] F. Martins et al, Imaging Electron Wave Functions Inside Open Quantum Rings, PRL 99, 136807 (2007).

[42] A. Abbout, G. Lemarie, J. L. Pichard, Thermal Enhancement of Interference Effects in Quantum Point Contacts, Phys. Rev. Lett. 106, 156810 (2011).

[43] G. Metalidis et al, Green's function technique for studying electron flow in two-dimensional mesoscopic samples. PRB 72,235304(2005).

[44] M. Ya. Azbel', Phys. Rev. Lett. 46, 675 (1981).

[45] M. Ya. Azbel', Phys. Rev. Lett. 47, 1015 (1981).

[46] M. Ya. Azbel', Phys. Rev. B 26, 4735 (1982)

[47] Er'el Granot, Graded transmission in a bent orifice, Phys. Rev. B. 60 Number 20, (1999).

[48] Er'el Granot, Near-threshold-energy conductance of a thin wire, Phys. Rev. B. 60 Number 15, (1999)

[49] Er'el Granot, Phys. Rev. B. 71, 035407 (2005).

[50] S. A. Gruvitz, Y. B. Levinson, Phys. Rev. B 47, Number 16 (1993).

[51] Y. B. Levinson, M. I. Lubin, E. V. Sukhorukov, Short-range impurity in a saddle-point potential: Conductance of microjunction, Phys. Rev. B 45, Number 20 (1992).

[52] U. Fano, Effects of Configuration Interaction on Intensities and Phase Shifts, Phys. Rev. 124, 1866–1878 (1961)

[53] Mario I. Molina, Nonlinear surface impurity in a semi-infinite two dimensional square lattice: Green function approach. PRB 74, 045412 (2006).

[54] T. Morita, T. Horiguchi, Analytic properties of the lattice Green function. J. of Phys A: Gen. Phys., Vol 5, 1972.

[55] T. Morita, Useful procedure for computing the lattice Green's function square, tetragonal and bcc lattices. Journal of mathematical physics Volume 12.

[56] Wolfram Mathematica program.

[57] A. Casuli, W. Li, J. Llibre and Z. Zhang, Chebyshev property of complete elliptic integrals and its application to Abelian integrals, Pacific Journal of Mathematics, Vol. 202, No. 2, 2002.

[58] Eleftherios N. Economou, Green's Functions in Quantum Physics (Springer Series in Solid-State Sciences).

[59] Rodolfo A. Jalabert, Wojciech Szewc, Steven Tomsovic, and Dietmar Weinmann, What Is Measured in the Scanning Gate Microscopy of a Quantum Point Contact? PRL 105, 166802 (2010).

[60] Alessandro Cresti, Microscopic current imaging in quantum point contact devices, JOURNAL OF APPLIED PHYSICS 100, 053711 (2006).

[61] Neil W. Ashcroft,N. David Mermin, Physique des solides

[62] S. E. J. Shaw, R. Fleischmann, E. J. Heller, Quantum Coherence Beyond the Thermal Length arXiv:cond-mat/0105354v1.

[63] Safa Kasap, Thermoelectric effects in metals: Thermocouples

[64] M. Jonson and G. D. Mahan, Mott's formula for thermopower and the Wiedemann-Franz law, Phys. Rev. B 21, 4223–4229 (1980).

[65] Anders Mathias Lunde and Karsten Flensberg, On the Mott formula for the thermopower of non-interacting electrons in quantum point contacts. J. Phys.: Condens. Matter 17 (2005) 3879–3884

[66] Appleyard N J et al 1998 Phys. Rev. Lett. 81 3491

[67] Appleyard N J et al 2000 Phys. Rev. B 62 16275(R)

[68] O. Bohigas, M. J. Giannoni, and C. Schmit, Phys. Rev. Lett. 52, 1-4 (1984)

[69] J.P. Bouchaud, M. Potters, Financial Applications of Random Matrix Theory: a short review

[70] Antonia M. Tulino, Sergio Verdú, Random Matrix Theory and Wireless Communications

[71] L.A. Pastur, Theor. Math. Phys. 10, 67 (1972).

[72] N. Dupuis and G. Montambaux, Phys. Rev. B 43, 14390 (1991)

[73] Bohigas, Haq and Pandey, Nuclear Data for Science and Technology (1983)

[74] Claude Mahaux, Hans A. Weidenmüller, Shell-model approach to nuclear reactions, North-Holland Pub. Co., 1969

[75] H. Tureci, Y. Alhassid, Physical Review B 74, 165333, 2006.

[76] Y. Alhassid, The statistical theory of quantum dots. Rev. Mod. Phys. 72, 895-968(2000)

[77] R. Balian, Random matrices and information theory, Nuovo cimento, B57, 183-193

[78] Peter J. Forrester, Log-Gases and Random Matrices

[79] C. E. Porter, N. Rosensweig, Statistical properties of atomic and nuclear spectra. Ann, Acad. Sci. Fennicae, Ser. A. VI Physica 44, 1-66

[80] M. L. Mehta, Random matrices.(Hardcover)

[81] A. Edelman, N. R. Rao, Random matrix theory. Acta Num. 14, 233-297 (2005).

[82] P. W. Brouwer, K. M. Frahm, and C. W. J. Beenakker, Quantum mechanical time-delay matrix in chaotic scattering, Phys. Rev. Lett. 78, 4737-4740 (1997).

[83] Fritz Haake, Quantum signature of chaos. (Springer)

[84] T. A. Brody et al, Random matrix physics: spectrum and strength fluctuations. Rev. Mod. Phys. 53, 385–479 (1981).

[85] C. W. J. Beenakker, Random-matrix theory of quantum transport, Rev. Mod. Phys. 69, 731–808 (1997)

[86] P. W. Brouwer.Generalized circular ensemble of scattering matrices for a chaotic cavity with non-ideal leads. Phys. Rev. B 51, 16878-16884 (1995)

[87] A. Abbout, G. Fleury, J. L. Pichard and K. Muttalib. Delay-Time and Thermopower Distributions at the Spectrum Edges of a Chaotic Scatterer. arXiv:1210.8170

[88] A. Abbout. Time delay matrix at the spectrum edge and the minimal chaotic cavities.arXiv:1211.4602

[89] P. W. Brouwer, On the random matrix theory of quantum transport, Phd thesis.

[90] F. Dyson, Statistical theory of the energy levels of complex systems I, J. Math. Phys. 3, 140 (1962).

[91] S. F. Godijn, S. Möller, H. Buhmann, and L. W. Molenkamp and S.Van Langen, Thermopower of a Chaotic Quantum Dot. Phys. Rev. Lett. 82, 2927-2930 (1999).

[92] S. A. van Langen, P. G. Silvestrov†, C. W. J. Beenakker, Thermopower of single-channel disordered and chaotic conductors. Superlattices and Microstructures, Vol. 23, No. 3/4, 1998.

[93] P. W. Brouwer, S. A. van Langen, K. M. Frahm, M. Büttiker, and C. W. J. Beenakker, Distribution of Parametric Conductance Derivatives of a Quantum Dot, Phys. Rev. Lett. 79, 913–916 (1997)

[94] F. Dyson, Statistical theory of the energy levels of complex systems II, J. Math. Phys. 3, 157 (1962).

[95] H. Baranger, P. Mello, Mesoscopic Transport Through Chaotic Cavities: A Random S-Matrix Theory Approach, Phys. Rev. Lett. 73, 142-145 (1994).

[96] R. Jalabert, J. L. Pichard, C. W. J. Beenaker, Universal quantum signature of Chaos in Ballistic Transport. Europhys.Lett. 27 (1994) 255.

[97] Stephano Longhi, Spectral singularities in a non-Hermitian Friedrichs-Fano-Anderson model. Phys. Rev. B 80, 165125 (2009).

[98] S. Datta, Electronic Transport in Mesoscopic Systems

[99] A. M. Mathai, R. K. Saxena and H. J. Haubold, The H-function: theory and applications (Springer).

[100] L. K. Hua, Harmonic Analysis of Functions of Several Complex Variables in the Classical Domains (Amer. Math. Soc., Providence, 1963).

[101] G. Grosso, S. Moroni, G. P. Parravicini, Electroninc structure of the InAs-GaSb superlattice studied by the renormalization method, Phys. Rev. B 40, 12328–12337 (1989).

[102] A. Abbout, H. Ouerdane, C. Goupil. Statistical analysis of the figure of merit of a two-level thermoelectric system: a random matrix approach. (in preparation)

[103] A. Abbout. Level spacing distribution of a Lorentzian matrix at the spectrum edge. arXiv:1211.5169.

[104] P. Giannozzi et al, The ordinary and matrix continued fractions in the theoretical analysis of Hermitian and relaxation operators. Applied Numerical Mathematics 4 (1985) 273-295.

[105] Karol Zyczkowski and Marek Kus, Random unitary matrices, J. Phys. A: Math. Gen. 27 (1994) 4235-4245.

[106] Francesco Mezzadri, How to generate random matrices from the classical compact groups.

[107] L. Eisenbud, PhD thesis (Princeton, 1948).

[108] E. P. Wigner, Phys. Rev. 98, 145 (1955).

[109] F. T. Smith, Phys. Rev. 118, 349 (1960).